Quantum Dot Based Aptasensors for the Detection of Biomolecules with Related Raman/SERS Spectral Analysis

BY

SHREYA GHOSH
B. Tech., West Bengal University of Technology, 2012
M.E., Jadavpur University, 2014

THESIS

Submitted as partial fulfillment of the requirements
for the degree of Doctor of Philosophy in Bioengineering
in the Graduate College of the
University of Illinois at Chicago, 2019

Chicago, Illinois

Defense Committee:

Michael Stroscio, Chair and Advisor
Mitra Dutta, Electrical and Computer Engineering
Thomas Royston
Dieter Klatt
Anne George, Oral Biology

I dedicate this dissertation to my parents,

Mr. Sabyasachi Ghosh and Mrs. Bithika Ghosh….

without your love and blessings, this day wouldn't have arrived,

And

My husband Shreyan…

For being the rock behind me and the good chef that he is.

Acknowledgements

I would like to thank my advisor Dr. Michael Stroscio for his constant guidance and support during my graduate studies. I am extremely grateful to him for his words of encouragement and also giving me an opportunity to be a part of his research group. Working under him has been one of the most enriching experiences for my scientific career and has provided me a direction for my future endeavors.

I would also like to thank Dr. Mitra Dutta for being a part of my thesis committee. She has always been a source of inspiration for me. I am highly thankful to her for her constant support in the lab and also agreeing to recommend me whenever I reached out to her.

I am really grateful to Dr. Thomas Royston for agreeing to be a part of my committee as well as for recommending me in several instances. I also extend my sincere gratitude to Dr. Dieter Klatt for serving on my committee and for being so helpful.

I would also like to acknowledge Dr. Anne George and Dr. Yinghua Chen for conducting the cell culture experiments on our sensors and also providing us with the cell penetrating peptide. I am extremely thankful to Dr. Anne George for being a part of my committee and being so helpful with the research results and papers.

I would like to thank Dr. Yiping Zhao and his graduate student Layne Hyer Bradley at University of Georgia at Athens for providing us with the silver nanorod substrates. I am extremely grateful to Dr. Joel Schwartz at UIC for providing us with Furin and PepO for Raman experiments. My sincerest acknowledgements Dr. Alan Nicholls and Dr. Fengyuan Shi for helping me out with my Raman experiments at the Research Resources Centre

I would like to thank all my group members at the Nano Engineering Research Laboratory for being so helpful. A special thanks to Dr. Debopam Datta for being so supportive

Acknowledgements (continued)

during the initial part of my research work. I would like to acknowledge Jesvin Sebastian, Anna Metlushko, Mehar Cheema and Shreya Chaudhry for being such wonderful interns.

I am extremely grateful to all the funding sources of my research. A special mention to all the members of the Graduate College and the Departments of Bioengineering and Electrical and Computer Engineering for all your support.

Contribution of authors

The experimental methods, results and discussions in this thesis are copied both from my published papers and submitted manuscripts with provided permission from the journal (see appendix). The contributions of all the co-authors are listed as follows:

Authors' contribution in chapter 2: Dr. Michael Stroscio and Dr. Mitra. Dutta led the project and helped with the development of main ideas including revision of the paper. Shreya Ghosh performed the experiments and wrote the manuscript. Dr. Debopam Datta and Mehar Cheema helped with the experiments and contributed to writing the paper.

Authors' contribution in chapter 3: Dr. Michael Stroscio and Dr. Mitra. Dutta led the project and helped with the development of main ideas including revision of the paper. Shreya Ghosh performed the experiments and wrote the manuscript. Dr. Debopam Datta and Shreya Chaudhry helped with the experiments and contributed to writing the paper.

Authors' contribution in chapter 4: Dr. Michael Stroscio and Dr. Mitra. Dutta led the project and helped with the development of main ideas including revision of the paper. Shreya Ghosh performed the experiments and wrote the manuscript. Anna Metlushko and Shreya Chaudhry helped with the experiments and contributed to writing the paper.

Authors' contribution in chapter 5: Dr. Michael Stroscio and Dr. Mitra Dutta conceived and advised on the overall project idea. Shreya Ghosh performed the experiments and wrote the manuscript.

Authors' contribution in chapter 6: Dr. Michael Stroscio and Dr. Mitra Dutta conceived and advised on the overall project idea. Shreya Ghosh performed the experiments and wrote the manuscript. Dr. Anne George conceived the cell culture experiments. Dr. Yinghua Chen performed the cell culture experiments. Jesvin Sebastian helped with the experiments and contributed to editing some parts of the manuscript.

Authors' contribution in chapter 8: Dr. Michael Stroscio and Dr. Mitra Dutta conceived and advised on the overall project idea. Shreya Ghosh performed the experiments and wrote the manuscript.

Table of contents

Table of contents (continued)

List of Tables

List of Tables (continued)

List of Figures

List of Figures (continued)

List of Figures (continued)

List of Figures (continued)

List of Figures (continued)

List of abbreviations

Au	Gold
Ca	Calcium
CRP	C – Reactive Protein
DNA	Deoxyribonucleic Acid
EDC	1-Ethyl-3-(3-dimethylaminopropyl)carbodiimide
EDTA	Ethylenediaminetetraacetic Acid
FRET	Fluorescence Resonance Energy Transfer
GA	Glycated Albumin
GO	Graphene Oxide
HS	Human serum
HSA	Human serum albumin
IFN - γ	Interferon - gamma
IgG	Immunoglobulin-G
IL - 6	Interleukin - 6
MB	Molecular Beacon
Mg	Magnesium
MWCO	Molecular Weight Cut-Off
Na	Sodium
NSET	Nanoparticle Surface-Energy Transfer
PBS	Phosphate Buffered Saline
PCR	Polymerase Chain Reaction
PCT	Procalcitonin

List of abbreviations (continued)

PDMS	Polydimethylsiloxane
PEG	Polyethylene Glycol
PepO	Peptide O
PL	Photoluminescence
K	Potassium
QD	Quantum Dot
RNA	Ribonucleic Acid
SELEX	Systematic Evolution of Ligands by Exponential Enrichment
SERS	Surface-Enhanced Raman Spectroscopy
Sulfo - NHS	N-hydroxysulfosuccinimide
TBA	Thrombin Binding Aptamer
TCEP	Tris(2-carboxyethyl)phosphine
TFE	Transferrin
TG	Thapsigargin
TNF-α / TNF-alpha	Tumor Necrosis Factor – alpha

Summary

This work presents the findings on the optical detection of biomarker proteins and metal ions using quantum dot based aptasensors along with the Raman / Surface Enhanced Raman Spectroscopy (SERS) of a wide range of biomolecules.

Optical aptasensors were designed for the detection Glycated Albumin, Tumor Necrosis Factor-alpha, C – Reactive Protein and calcium ions. These molecular beacons were composed of a quantum dot connected to a gold nanoparticle via a DNA aptamer. The DNA aptamers were chosen based on the affinity towards the target analyte. The sensor operated on the principle of Fluorescent Resonant Energy Transfer (FRET) with the quantum dot – gold nanoparticle functioning as the donor – quencher pair. The molecular beacons successfully detected the biomarker proteins not only in the physiologically relevant concentrations but also showed an error free performance in lower concentrations as well.

The response of the optical aptasensors was then studied in an intracellular environment. During this experiment, the molecular beacons were conjugated with a cell penetrating peptide called DSS, which assisted the molecular beacons in crossing the biological cell membrane. A preliminary study on the conjugation of the DSS peptide with the Glycated Albumin detecting molecular beacons was conducted to determine the right concentration of the DSS to be used in future experiments. The Tumor Necrosis Factor – alpha detecting molecular beacons were also conjugated with the DSS peptide to study the functionality of the sensor. A successful intracellular FRET phenomenon was observed in the presence of the target protein. A similar response was also observed when the DSS conjugated calcium ion detecting molecular beacons were studied in osteoblast cell lines.

Summary (continued)

A preliminary study was conducted on the design of an aptasensor comprised of the molecular beacon anchored onto a graphene oxide for the detection of C – Reactive Protein. The sensor successfully detected the protein with a specific range of concentration and had a limit of detection in the range of 0.5 pM to 1.6 pM. This design opened up a new direction in theranostic studies in bioengineering because of its applicability in drug delivery and disease diagnostics.

Finally, Raman spectral signature of various biomolecules such as biomarker proteins, peptides, enzymes and bio fluids were analyzed to obtain a signature spectrum with possible assignments from literature. While the Raman spectra for most of the biomolecules were obtained, some complex molecules like Tumor Necrosis Factor – alpha and human serum required SERS to obtain a spectral signature with distinct peaks. A silver nanorod array based substrate was used for the SERS studies. The overall study primarily focused on studying the composition of the biomolecules and the secondary structure of the proteins.

1. Introduction

1.1. Proteins and amino acids

Proteins are large macromolecules, which are composed of smaller units called amino acids. They are fundamentally formed of elements such as carbon, hydrogen, nitrogen and sulfur. Amino acids are dipolar molecules, which contain an amine group and a carboxyl group as well. The structure of an amino acid has been shown in Figure 1 below. They form peptide bonds by linking the α-carbon of one amino acid with the α-amine group of another amino acid.

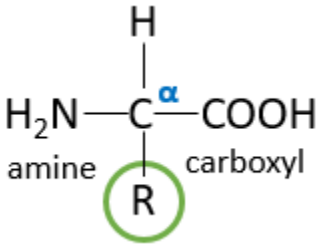

Figure 1. Basic structure of amino acid, which has an amine (NH_2) group on one end and a carboxyl (COOH) group on the other. 'R' indicates side chain / hydrocarbon group attached to the α-carbon.

Proteins have a complex structural hierarchy. The primary structure of proteins refers to the sequence of amino acids, which forms the protein. The structure facilitated by the folding of the primary amino acid sequence using hydrogen bonds is known as the secondary structure (α - helix / β - sheet / β - turns). Tertiary structure of proteins refers to a higher order of folding in a polypeptide chain stabilized by hydrogen bonds / van der Waals bonds / hydrophobic bonds / disulfide bonds. The bonding between multiple polypeptide chains is known as the quaternary structure.

Proteins play a very significant role in the human physiology and are an indispensable molecular machine for the cellular functioning of all life forms. Several diseases have established a direct correlation with protein structure. Additionally, healthcare diagnostics have become hugely dependent on biomarker proteins. These are proteins, which are either up-regulated or down-

regulated in the presence of certain disease pathology. For instance, proteins such as Tumor Necrosis Factor – alpha (TNF-α), Interleukin – 6 (IL-6), Procalcitonin (PCT) etc. are excellent indicators of acute infectious conditions (example sepsis) [1]. C – Reactive Protein (CRP), on the other hand, is a biomarker for a wide range of diseases [2].

1.2. Quantum Dots

Quantum dots are semiconductor nanocrystals with diameters in the range of 2 – 10 nm. They are luminescent, an attribute, which is highly utilized in biosensors and drug delivery constructs etc. Quantum dots follow the principle of quantum confinement, where the semiconductor band gap increases with a decrease in the size of the nanocrystals. Consequently, the emission wavelength of the quantum dot can be controlled by tuning the size of the nanocrystals. The emission energy of semiconductor quantum dot nanocrystals can be expressed using Brus equation [3] (given below):

$$\Delta E = E_{gap} + \frac{h^2}{8m_e^* d^2} + \frac{h^2}{8m_h^* d^2} \quad (1.1)$$

In the equation (1.1), E_{gap} is the energy of the band gap, m_e^* represents the effective mass of the electron, m_h^* is the effective mass of the electron hole, d is the diameter of the quantum dot and h represents the Planck's constant. Commercially available quantum dots come with a core made of cadmium selenide (CdSe) along with a shell composed of zinc sulfide (ZnS – a wider band gap material) in order to increase the quantum yield by passivating the sites on the core surface where electrons might be trapped [4][5][6]. Additionally, a polymer layer (typically Polyethylene Glycol – PEG) is coated on the surface of these quantum dots to facilitate biocompatibility as well to add functional group for conjugation with other molecules. Other types of quantum dots available in the market are composed of indium gallium phosphide (InGaP). Quantum dots have

several advantages over traditional fluorophores. Some of them include broad excitation spectra in the UV range, narrow emission spectra, and resistance to photobleaching [6].

1.3. Aptamers

Aptamers are short single stranded DNA or RNA oligonucleotides, which display a binding affinity to specific target molecules. They are synthesized using a process called Systematic Evolution of Ligands by Exponential Enrichment (SELEX), in which a large nucleotide sequence (approximately 10^{15}) is subjected to the desired target molecule. Non-binding nucleotides are eliminated while amplifying the binding nucleotides using Polymerase Chain Reaction (PCR). This process is repeated until the highest number of target binding sequences are retained [4]. Aptamers are extensively used in biosensing as well as in therapeutic applications as they have several advantages over antibodies. Some of them include ease of functionalization, unlimited shelf life without having to worry about denaturation and cheaper in vitro production process etc.

1.4. Raman / Surface-Enhanced Raman Spectroscopy (SERS) of biomolecules

Raman spectroscopy has been successfully established as a powerful analytical tool for probing biological systems [7][8]. In Raman spectroscopy, a monochromatic laser beam illuminates the sample [9]. The interaction between the laser and the sample molecules gives rise to scattered light, which has a frequency different from that of the incident light [10]. When two atoms share a bond, they experience both attractive and repulsive forces. The magnitude of these forces varies based on the masses of the atoms. Raman spectra originate because of the inelastic collision between the incident laser beam and the vibrating molecules of the sample. Therefore, a large part of the scattered light has a frequency equal to that of the incident radiation. Only a

small portion of the scattered light exhibits a different frequency when compared to that of the incident laser beam. This makes the Raman signal inherently weak even though the vibrational frequencies are unique to the pair of atoms making it an effective tool in identifying the composition of the samples.

To improve the Raman signal, a technique called Surface Enhanced Raman Spectroscopy (SERS) is used. SERS is a type of Raman spectroscopy in which the Raman signal is highly enhanced [11]. This enhancement occurs because of a high Raman scattering cross-section when the sample molecules get adsorbed on the surface of the metallic nanostructured substrate [12]. Nanostructures from noble metals like gold, silver etc. show enhancement of Raman spectra because they generate surface plasmons in the presence of an incident laser light and hence exhibit SERS [13].

1.5. Overview

1.5.1. Specific aims

In this research thesis, two topics have been explored: 1. Quantum dot based optical aptasensor 2. Raman / SERS spectroscopy of biomolecules. Specifically, aptasensors for the detection of inflammatory disease biomarkers have been studied with greater depth while Raman / SERS spectra of these biomarker proteins have been investigated to study about their secondary structure and composition. The specific aims for this study have been summarized below:

Specific Aim 1: To design and test quantum dot and aptamer based nanosensors for the detection of biomolecules.

Specific Aim 2: To study the response of the quantum dot based optical aptasensors in a cellular environment using a cell penetrating peptide.

Specific Aim 3: To design and characterize a graphene oxide based aptasensor for the detection of C – Reactive Protein.

Specific Aim 4: To obtain spectral characterization of biomolecules by using Raman Spectroscopy / Surface-Enhanced Raman Spectroscopy.

1.5.2. Innovation

Aptamer based sensors have been evaluated to have excellent recognition capacity towards various types of target molecules [14]. These targets include metal ions such as lead [15][16], mercury [17][18], potassium [19][20][16], as well as biomolecules such as thrombin [21][22], interferon-γ [23], ATP [24] and AMP [25] etc. In this study, the sensor design consists of the DNA aptamer as the primary sensing element attached to a quantum dot (QD) on one end and gold (Au) nanoparticle quencher on the other end. This design utilizes Fluorescent Resonant Energy Transfer (FRET) for target detection. As has been seen in previously published studies and also to the best of our knowledge, the DNA aptamers chosen in this study for the detection studies of biomarker proteins like GA, TNF-α, CRP etc. have never been incorporated in such a molecular beacon design before, which makes the sensors novel. Also, this study further incorporates DSS peptide and graphene oxide (GO), respectively, into some of these sensors and investigate their responses. Since GO has already been proven to be biocompatible [26] and has also been successfully used as drug delivery agent [27], the optical sensor can potentially be used as a theranostic agent. Additionally, DSS peptide conjugated aptasensors can also be used for theranostic applications.

Both Raman spectroscopy and SERS are well established techniques in complex biomolecule analysis [7]. Though these techniques have been previously used to detect cytokines [28], there

are few studies which analyze inflammatory cytokines associated to sepsis. Therefore, here, we have obtained the Raman signature of CRP, which is an important inflammatory biomarker of sepsis. Having Raman signatures of these crucial biomarker proteins will make it more convenient for analyzing complex biofluids like septic serum or septic blood samples in future.

2. Detection of glycated albumin using quantum dot aptasensors for monitoring diabetes mellitus.

(This chapter is entirely copied from my published paper. Reprinted with permission from the following citation:

Ref [29] S. Ghosh, D. Datta, M. Cheema, M. Dutta, and M. A. Stroscio, "Aptasensor based optical detection of glycated albumin for diabetes mellitus diagnosis," *Nanotechnology*, vol. 28, no. 43, 2017.)

2.1. Overview

Glycated albumin (GA) has been reported as an important biomarker for diabetes mellitus. This study investigates an optical sensor comprised of deoxyribonucleic acid (DNA) aptamer, semiconductor quantum dot, and gold (Au) nanoparticle for the detection of GA. The system functions as a 'turn on' sensor because an increase in photoluminescence intensity is observed upon the addition of GA to the sensor. This is possibly because of the structure of the DNA aptamer, which folds to form a large hairpin loop before the addition of the analyte and is assumed to open up after the addition of target to the sensor in order to bind to GA. This pushes the quantum dot and the Au nanoparticle away causing an increase in photoluminescence. A linear increase in photoluminescence intensity and quenching efficiency of the sensor is observed as the GA concentration is varied between 0–14,500 nM. Time based photoluminescence studies with the sensor show the decrease in binding rate of the aptamer to the target within a specific time period. The sensor was found to have a higher selectivity towards GA than other control proteins. Further investigation of this simple sensor with greater number of clinical samples can open up avenues for an efficient diagnosis and monitoring of diabetes mellitus when used in conjunction with the traditional method of glucose level monitoring.

2.2. Background

Diabetes has been termed as one of the leading causes of global mortality. According to the World Health Organization, in 2014, approximately 422 million adults were found to have diabetes in comparison to 108 million people in 1980 [30]. Diabetes is a chronic state where the pancreas is unable to produce enough insulin and hence results in elevated glucose levels in bloodstream [31]. Such a condition is referred to as hyperglycemia [32]. It causes elevated concentrations of glycated proteins such as albumin and hemoglobin in the human system [33][34]. Diabetic nephropathy is a type of kidney failure caused by the incidence of diabetes. The most common clinical method adopted for monitoring diabetes, so far, is the combined measurement of blood glucose and glycated hemoglobin (HbA1c) levels. However, HbA1c levels can often be unreliable for patients with disorders such as hemolytic anemia, thalassemia etc. Fructosamine is also utilized for tracking glycemic index. However, fructosamine concentrations are highly dependent on concentrations of proteins, bilirubin, hemoglobin and various low molecular weight substances in the human system [34][35]. The half-lives for some of these proteins have not been estimated yet. Hence, fructosamine concentrations are often inaccurate. Therefore, glycated albumin (GA) has been determined to be a much more accurate marker for diabetes mellitus [34] especially for patients undergoing hemodialysis [36] or having hematologic disorders [37]. GA has come to the forefront as a tool for both the control and diagnosis for diabetic patients. GA begins with human serum albumin (HSA) and is developed into GA through a series of modifications and reactions. GA may be used as a glycemic control tool based on the extent of glycation depending on time allowed for glycation and amount of glucose available for reaction with HSA [38]. GA can also be used as an accurate marker in such pathologies including hemolytic anemia and deficiency anemia of diabetic patients [39]. While many markers exist that are currently used for diabetes management and predictive measures,

GA provides many advantages including earlier detection and prolonged circulation in the body. Measurement of glucose levels in the blood is the standard management method for diabetes management and detection. GA provides an alternative method to simple blood glucose detection and may offer an alternative diagnostic and prognostic marker for many diabetic patients. Using GA as a marker over long controlled periods of time (2–3 months) is made possible through the extended life span of hemoglobin levels in red blood cells [38]. Advantages of GA detection over typical blood glucose level measurement is also the ability to detect worsening glycemic control at an earlier stage compared to HbA1c detection [40]. It has also been seen that prolonged elevation of GA levels can lead to irreversible damage that is associated with diabetes mellitus, including neuropathy and coronary artery disease [41]. Therefore, to achieve a better diagnosis and management of diabetes, detection of glucose levels can be assisted by GA detection. The process of glycation of HSA is divided into several stages, first of which combines reduction of sugar (glucose) with primary amine groups to form a reversible Schiff base, which through further modification develops an Amadori product [42][43][44][45][46]. Many sugar molecules may be used to modify albumin, including galactose and fructose [47]. Following the Amadori product formation, the next stage involves the oxidation of glycated proteins that form reactive dicarbonyl compounds [38]. These reactive compounds further react with lysines and arginines to form AGE compounds, which include methylglyoxal-derived hydroimidazolone isomer 1 (MG-H1) and glyoxal-derived hydroimidazolone isomer 1 (G-H1) that have been seen in previous studies of GA [38]. Through these numerous steps of modification, HSA is glycated and goes through the transition to become GA. The primary functional groups of GA that are affected by glycation are lysine, arginine and cysteine [48]. The functional impact of GA has been shown to stabilize the tertiary and secondary structures and acquire a high life span [49].

The glycation process is often associated with oxidation processes as well, which are referred to as glycoxidation and affect early stages of the glycation process [50]. Previous studies show that higher levels of GA induce oxidative damage to cells [51][52]. Single stranded deoxyribonucleic acid (DNA) aptamers have been extensively studied by researchers previously for the detection of a wide range of targets such as metals ions including lead [15][16], mercury [17], potassium [16], as well as biomolecules such as ATP [24] and AMP [53], and proteins such as C-reactive protein (CRP) [54], interferon gamma (IFN-γ) [23], etc. DNA aptamers are defined as oligonucleotides, which contain a single, typically short, sequence of DNA that bind to specific antigens including molecules and ions. Using these short DNA sequences, targeting of specific molecules such as GA is facilitated through the aptamer binding sequences. One approach used frequently with aptamers involves using quantum dots; the resulting complexes are referred to as molecular beacons (MBs) [55]. MBs find a wide variety of applications in DNA binding protein detection [56][57], metal ions such as potassium [20][58], and have also been used as nucleic acid hybridization probes extensively [59]. Quantum dot technology is facilitated by aptamer and molecule binding via fluorescence resonant energy transfer (FRET). Dyes, quenchers, and metal nanoparticles can all serve as possible acceptors via FRET [60]. The mechanism of FRET transfer may be facilitated through quantum dot-gold nanoparticle interactions. When a quantum dot is brought into proximity of an Au nanoparticle once the aptamer binds the target molecule, the quantum dot fluorescence is then quenched via energy transference to the gold nanoparticle instead of the energy being emitted as a photon [16]. Since the absorption spectrum of gold nanoparticles is quite broad, they are quite effective as a quenching mechanism for quantum dot technology. Previous studies have established the quenching efficiency is proportional to $1/d_6$ for distances smaller than d_0 and $1/d_4$ for distances larger than d_0, defined as d being the distance of

the emitter from the quencher and d_0 is the characteristic distance where quenching and light emission are seen to be equal approximately 5 nm [16]. Nanosurface energy transfer is another phenomenon based on FRET for the case where a point-like object interacts with a local surface to promote quenching of light emission; in this case the change in light emission scales as $1/d_4$, and demonstrates the wide range of utility of FRET-based phenomena [16]. Gold nanoparticles have the capability to work through both FRET and NSET technology which demonstrates why they are typically used as quenchers in quantum dot systems. Previous works show that GA can be detected using enzymatic methods [34][61][62][63], affinity chromatography [35][64][65][66] immunochemistry [67][68]. While enzymatic sensors suffer various drawbacks such as high pH and temperature sensitivity [69], higher chances of denaturation and are therefore highly difficult to use enzymes in an in vitro environment [70][71], the other methods require longer processing times and exhibit poor precision [61]. Optical sensing of GA has been determined to be one of the most promising methods of detection since they do not require significant sample preparation and are relatively faster and cheaper [72]. Raman spectroscopy has been used to detect GA [73]. However, the limit of detection (LD) of the method was higher than that of the sensor proposed in our study. Other GA detection platforms includes fructosamine 6-kinase based electrochemical sensing [74][75], electrochemiluminescence sensing [76], surface plasmon resonance sensing [77] and aptamer based sensing [78]. In this study, we have synthesized a MB, where the DNA aptamer is attached to the quantum dot on one end and Au nanoparticle quencher to the other end for the detection of GA (Figure 2). Such a platform can be potentially used for monitoring diabetes.

2.3. Methods

2.3.1. Aptamer structure and modification

The GA binding aptamer used in this study was purchased from Biosearch Technologies (Petaluma, CA). It consists of 23 base pairs and has been modified on both ends with an amine group on the 5' and a Thiol group on the 3' (5′Amino C6/TGCGGTTGTAGTACTCGTGGCCG/Thiol C6 SS 3′). The aptamer was dissolved into Tris Ethylenediamine Tetraethyl Acetate buffer to obtain 100 μM aptamer solution.

2.3.2. Materials

GA, non-glycated HSA, transferrin and Immunoglobulin-G (IgG) were purchased from Sigma Aldrich (St. Louis, MO). CRP was obtained from EMD-Millipore (Temecula, CA) while recombinant human IFN-γ was purchased from BioLegend (San Diego, CA). Human serum (HS) was obtained from AB plasma of human male (Sigma Aldrich Inc., St. Louis, MO.) 1-ethyl-3-(3-dimethylaminopropyl) - carbodiimide (EDC) and tris (2-carboxyethyl) phosphine (TCEP) are obtained from Pierce Biotechnology (Rockford, IL). 20 nm carboxyl coated CdSe/ZnS QDs e-flour ITK 655NC with an average radius of 20 nm were purchased from Life Technologies (Carlsbad, CA). Monomaleimide functionalized nanogold (Au) particles having a diameter of 1.4 nm was obtained from Nanoprobes (Yaphank, NY). Nanosep molecular weight cutoff (MWCO) filters of 10 and 100 k pore sizes were purchased from Pall Lifesciences (Ann Arbor, MI).

2.3.3. Synthesis of MB

9 μl of TCEP was added to 20 μl of the 100 μM GA aptamer and incubated for 30 min at room temperature. This process facilitates the reduction of the dithiol groups in the aptamer. 100 μl of deionized water was added to one vial of Au nanoparticles. The entire volume of Au nanoparticle solution was added to the thiol activated GA aptamer-TCEP solution in a 3:1 ratio. The final solution was further incubated for 2 h at room temperature. After 2 h, the excess gold nanoparticles were filtered out by centrifuging the solution twice at 7000 rpm for 15 min each

using a 10 k MWCO filter. 13 μl of quantum dots were mixed with 87 μl of 10 mM borate buffer (pH 7.4). This quantum dot solution was further added to the GA aptamer/Au nanoparticle solution in the presence of 23 μl of 4 μg μl^{-1} EDC/Sulfo NHS solution. This solution was then allowed to stir gently for 2 h at room temperature. Subsequently, the samples are centrifuged at 7000 rpm for 5 min using a 100 k MWCO filter in 50 mM borate buffer (pH 8.3). This process is repeated 10 times to eliminate unbound aptamers and EDC from the sensor solution.

2.3.4. Analytical selection and prediction of secondary structure of GA aptamer

The secondary structure of the GA binding aptamer was determined using M-fold web server [79][80][81]. The parameters that were used to determine the structure was temperature and ionic concentration. Two temperature conditions were considered: (1) 25 °C, which is the room temperature and (2) 37 °C, which is the temperature under physiological conditions. For each of these temperatures, there were two different ionic condition considered: (1) 1.37 mM Na^+ and (2) 10 mM Na^+.

2.3.5. Optical detection of GA

The GA samples for the optical detection test were prepared by adding 0.005, 0.1, 1, 5, 10, 40 and 95 mg GA to 1 ml of 0.01 XPBS each. 5 μl of these GA samples were then added to 750 μl of sensor solution in a cuvette while keeping the cuvette undisturbed in the holder. The DNA aptamer in the sensor is allowed to bind to GA for 2 h before the photoluminescence intensity is recorded. The same conditions were repeated during the optical detection experiments with the control proteins and the clinical samples. The control proteins used for these experiments are non-glycated HSA, CRP, transferrin, IgG and IFN-γ. Their stock solutions were also made in 0.01 XPBS.

HS was used for preparation of clinical samples. 100 µl of HS solution is spiked with 0.1 mg named sample-S2 (see Results and discussion) and 0.95 mg of GA named sample S3 to simulate real life clinical sample and unspiked HS solution named sample S1 was used as the control counterpart for the clinical samples. The sample volume is used as 5 µl for the clinical samples to maintain uniformity with the pure samples.

2.3.6. Instruments

The photoluminescence measurements of the sensor were conducted using a USB4000 Ocean Optics (Dunedin, FL, USA) spectrophotometer with a continuous 375 nm LED excitation. The centrifuge used was Fisher Scientific Accuspin micro (Fisher Scientific, USA).

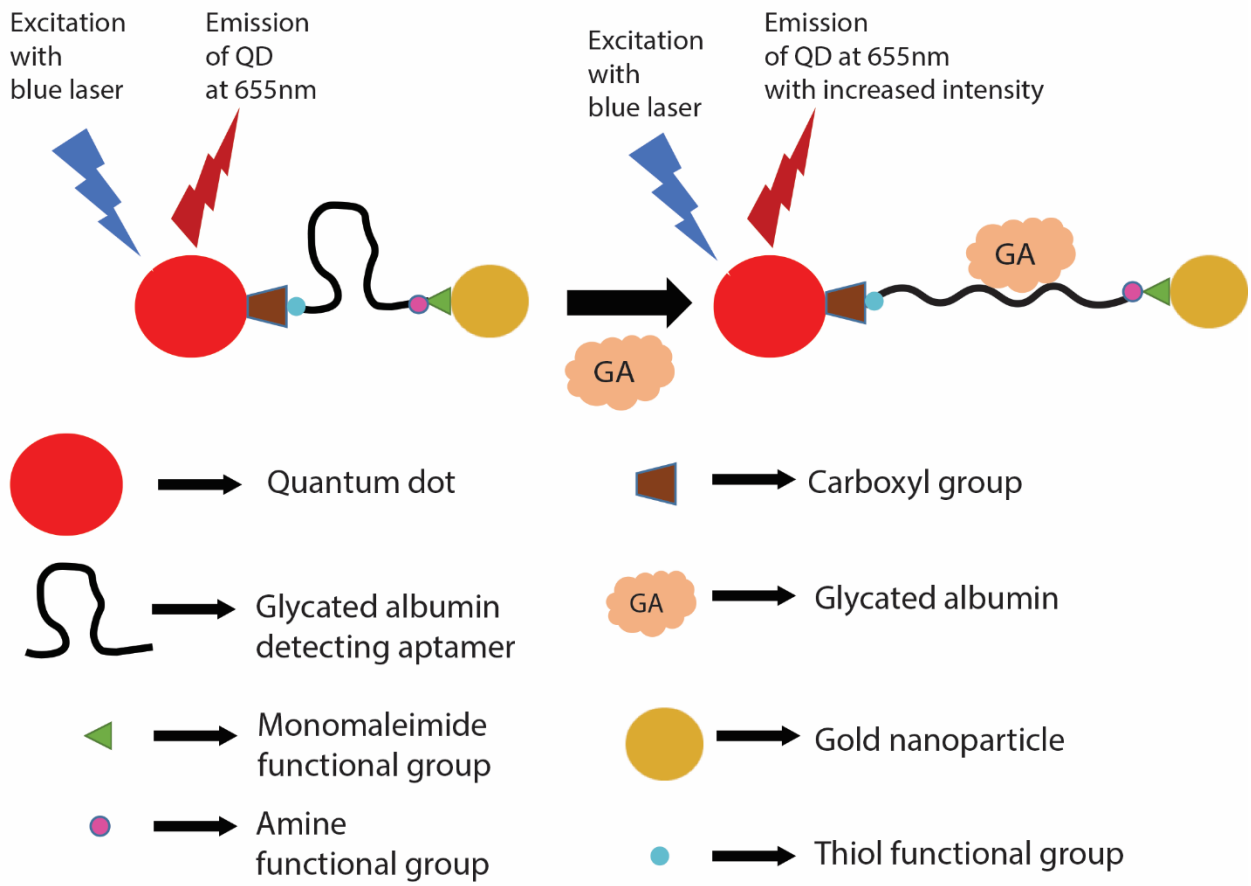

Figure 2. Molecular Beacon for the detection of Glycated Albumin. This figure illustrates the principle behind the detection of Glycated Albumin using Fluorescence Resonant Energy Transfer. An increase in PL intensity is observed after the addition of the addition of the target in the sensor

2.4. Results and discussion

2.4.1. Analytical selection and prediction of secondary structure of GA binding aptamer

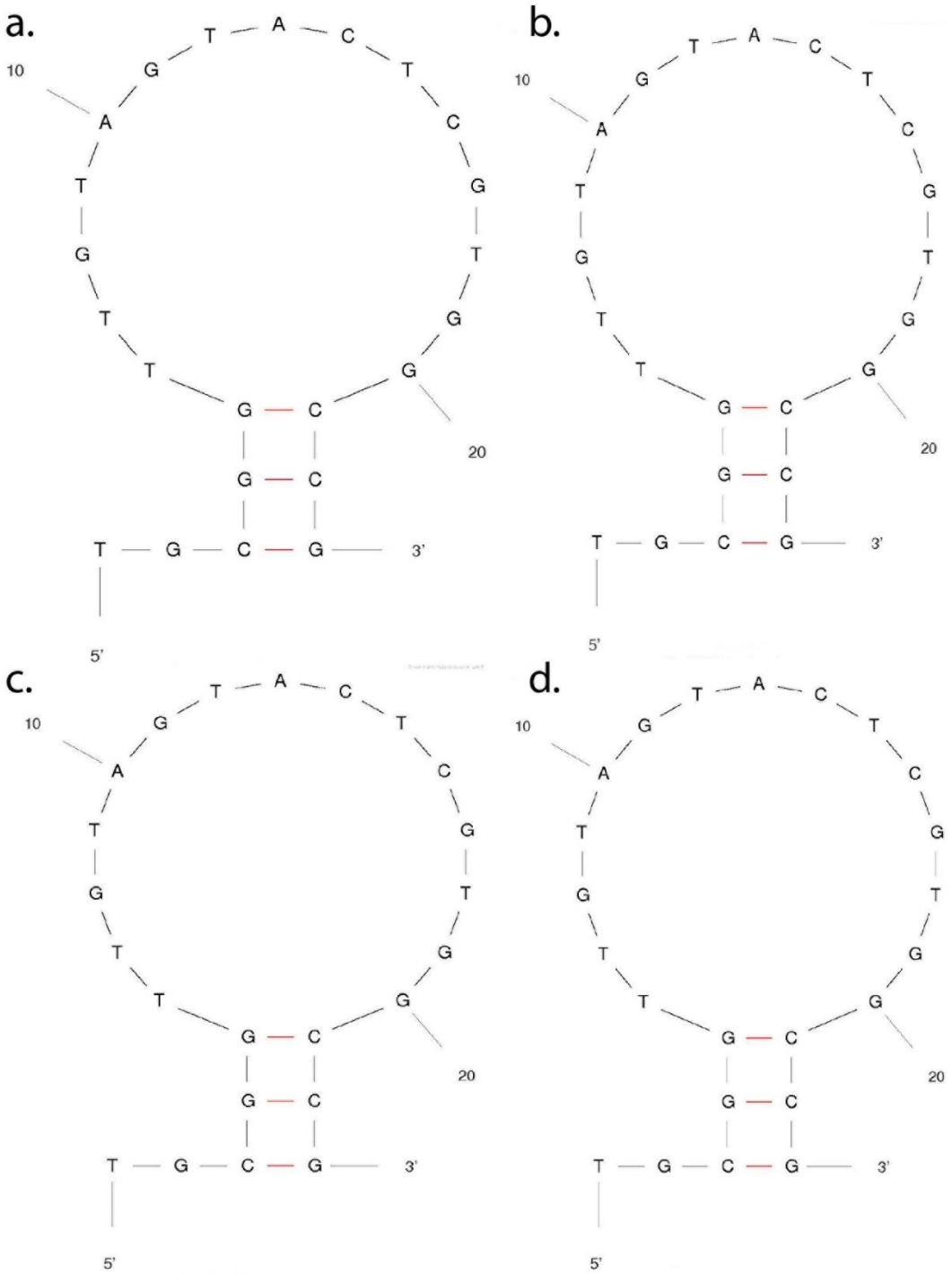

Figure 3. Secondary structure of the GA binding aptamer at (a) 1.37 mM Na^+ concentration and 25 ºC temperature, (b) 10 mM Na^+ concentration and 25 ºC temperature (c) 1.37 mM Na^+ concentration and 37 ºC temperature and (d) 10 mM Na^+ concentration and 37 ºC temperature.

The GA binding aptamer was chosen based on a previous study by Apiwat et al [78], where the DNA aptamer showed sensitivity towards GA. Apart from this, the choice was also based on the possibility of FRET between the quantum dot and the Au nanoparticle quencher. Since, the length of a single DNA base is 0.34 nm, the 23 base GA binding aptamer has a length of 7.82 nm. The presence of the Amino C6 modifier along with the Thiol C6 SS modifier will add another 1.2 nm approximately to the length of the DNA aptamer because of their combined 12 C–C bonds. This will result in an approximate distance of 9 nm between the quantum dot and the Au nanoparticle quencher.

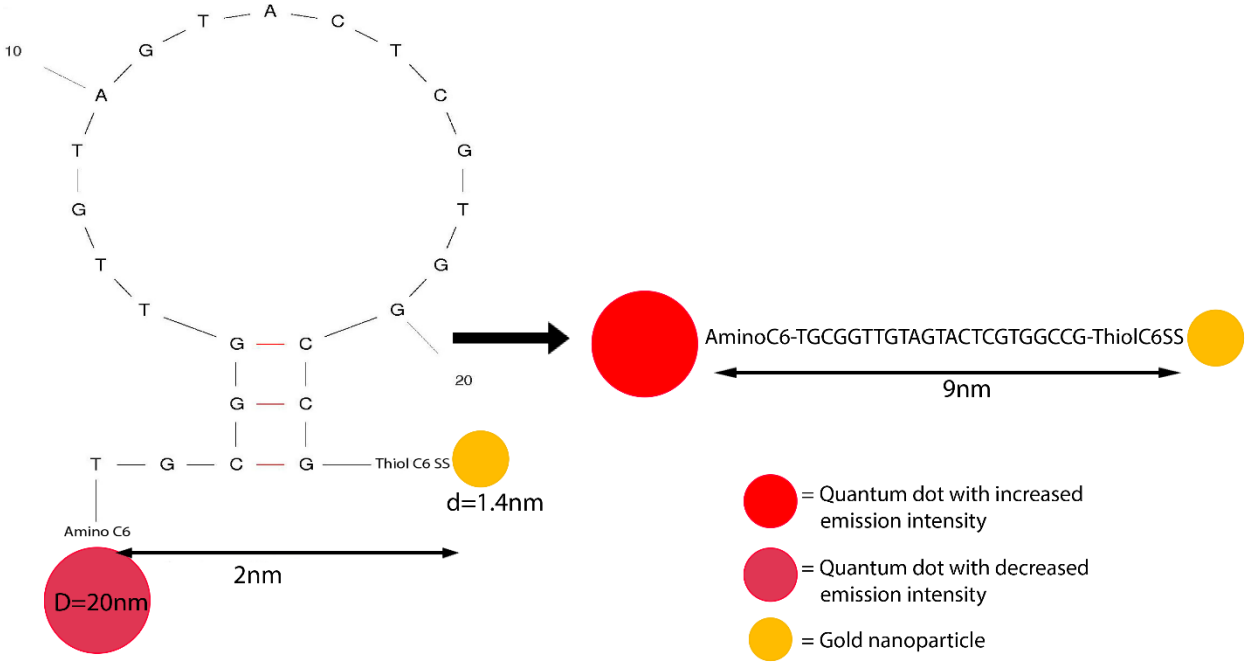

Figure 4. Schematic showing the change in the approximate distances between the Quantum dot and the Gold nanoparticle quencher before and after the addition of GA. The folded structure of the DNA aptamer before the addition of the analyte was predicted by M-fold webserver software

The M-fold webserver software predicted the secondary structures of the GA aptamer under the conditions mentioned in section 2.3.4. The aptamer was found to have a similar structure for all the conditions and is characterized by the formation of a hairpin loop at G5 and C21. This has

been clearly shown in Figures 3(a)–(d). The aptamer structures shown in Figures 3(a)–(d) have been chosen in such a way that they have the lowest ΔG. Table 1 represents the ΔG values of the aptamer under all the conditions mentioned in section 2.3.4. Based on the structure of the aptamer at 1.37 mM Na^+ concentration at a folding temperature of 25 °C (Figure 3(a)), it can be concluded that the GA binding aptamer remains in a hairpin loop structure before the addition of any analyte. This phenomenon results in bringing the quantum dot and the Au nanoparticle quencher closer to each other to an approximate distance of 2 nm (Figure 4). As discussed later in the thesis, an increase in photoluminescence is observed on the addition of the analyte, therefore it is assumed that the hairpin loop plays a significant role the binding of GA to the aptamer by opening up the hairpin loop and putting the quantum dot and Au nanoparticle quencher farther apart to a maximum distance of 9 nm approximately (Figure 4).

Table 1. Variation of Gibb's free energy values when the GA binding aptamer folds under different ionic and temperature conditions

Sl. No.	**Parameter**	**ΔG (kcal/mol)**
1.	1.37mM Na^+ concentration and 25ºC temperature	-0.18
2.	10mM Na^+ concentration and 25ºC temperature	-0.72
3.	1.37mM Na^+ concentration and 37ºC temperature	0.95
4.	10mM Na^+ concentration and 37ºC temperature	0.37

2.4.2. Optical detection of GA

2.4.2.1. Sensitivity and specificity of the aptasensor towards GA

The sensitivity of the aptamer based sensor towards GA was evaluated by adding the target progressively in concentrations ranging between 0 and 14,500 nM in the assay. As shown in Figure 5(a), the photoluminescence intensity increases with an increase in the concentration of

GA in the liquid sensor assay. This behavior is repeated when other sensor samples are tested with the same procedure and exhibits a steady linear increase in photoluminescence intensity over the same concentration range of GA (Figure 5(b)). This phenomenon can be attributed to the conformational change of the aptamer. In section 2.4.1, it has been mentioned that the DNA aptamer acquires a large hairpin loop like structure, which brings the quantum dot and the Au nanoparticle quencher closer. On the addition of GA, it is assumed that the aptamer unfolds from the hairpin loop like structure in order to bind to GA. This pushes the quantum dot and the Au nanoparticle quencher further apart, thus, causing an increase in the photoluminescence intensity. GA consists of a large number of arginine and lysine residues [82]. It has been previously studied that arginine and lysine exhibits a strong interaction with guanine while arginine also interacts with adenine and thymine [83]. The chosen DNA aptamer has 9 guanine bases and 7 thymine bases out of the entire 23 base structure and these bases comprise a major part of the hairpin loop as well as the external loop. Therefore, there is a high possibility that the hairpin loop plays a crucial role in the GA-aptamer complex formation. The quenching efficiency (Figure 6(a)) of the sensor was calculated by using the equation (2.1), where QE is the quenching efficiency, I is the photoluminescence intensity after the addition of target analyte at a specific concentration and I_0 is the photoluminescence intensity before the addition of target.

$$QE = \left(\frac{I - I_0}{I_0}\right) \times 100 \qquad (2.1)$$

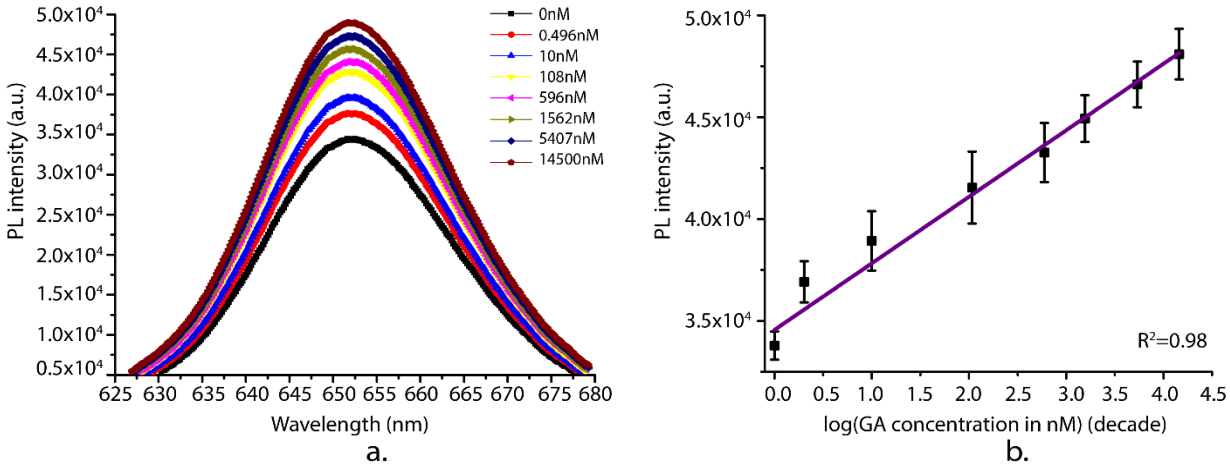

Figure 5. (a) Photoluminescence intensity of as a result of adding varied concentrations GA to 750 µl of the DNA aptamer based sensor solution. (b) Linear increase in the averaged photoluminescence intensity over the logarithm of the GA concentrations added to the sensor. The photoluminescence intensity was collected from six different sensor samples (n = 6) and the GA concentrations stated are its concentration in the assay.

Table 2. Comparison of the limit of detection of several GA detecting platforms with that of the proposed aptasensor in this study.

Sl. No.	Type of sensor	Limit of detection (LD)	Reference
1.	Enzymatic assay based electrochemiluminescence sensor	0.1 µM (6.6 µg/ml)	[76]
2.	Enzymatic assay based sensor	0.36 mg/ml	[84]
3.	Electrochemical aptasensor	3 µg/ml	[85]
4.	Raman spectroscopy based sensor	13.7 µM	[73]
5.	Graphene based optical aptasensor	50 µg/ml	[78]
6.	Enzymatic assay based colorimetric sensor	0.47 mg/ml	[86]
7.	HPLC based boronate immunoassay	>10.9 µM	[68]
8.	Hydrazine based colorimetric sensor	0.7 µM	[87]

9.	Affinity chromatography based immunoturbimetric sensor	0.81 mg/l	[35]
10.	**Optical aptasensor**	**1.08 nM (0.067 μg/ml)**	**This work** [29]

As can be seen in Figure 6(a), the sensor exhibited quenching efficiencies of 9.74 % ± 1.12% and 41.09% ± 0.81 % when the concentration of GA in the assay was 0.5 nM and 14,500 nM respectively. The concentration of GA (in nM) was converted to the corresponding logarithm value to show the linear behavior of the sensor ($R^2 = 0.99$). Figure 6(b) represents the behavior of the sensor when the original PL intensities are plotted w.r.t. the concentration of GA in nM.

The LD was calculated using equation (2.2), where SD_0 is standard deviation for blank sample, sensitivity is the slope of the quenching curve (shown in Figure 6(a)). LD is the limit of detection value of the GA concentration expressed in nM.

$$LD = \frac{3 \times SD_0}{Sensitivity} \qquad (2.2)$$

It was found that the average LD for the sensor was 1.008 nM. Considering the molecular weight of GA is 66.5 kDa, the LD (1.008 nM or 0.067 $\mu g ml^{-1}$) of this sensor is significantly lower than those reported in previous studies such as 0.47 mg ml^{-1} from the enzymatic assay [86] and 50 $\mu g ml^{-1}$ from the graphene based aptasensor [78]. Table 2 compares the LD of this aptasensor with various other GA sensing platforms. It clearly shows that the LD of the aptasensor proposed in this paper is superior to previously published platforms.

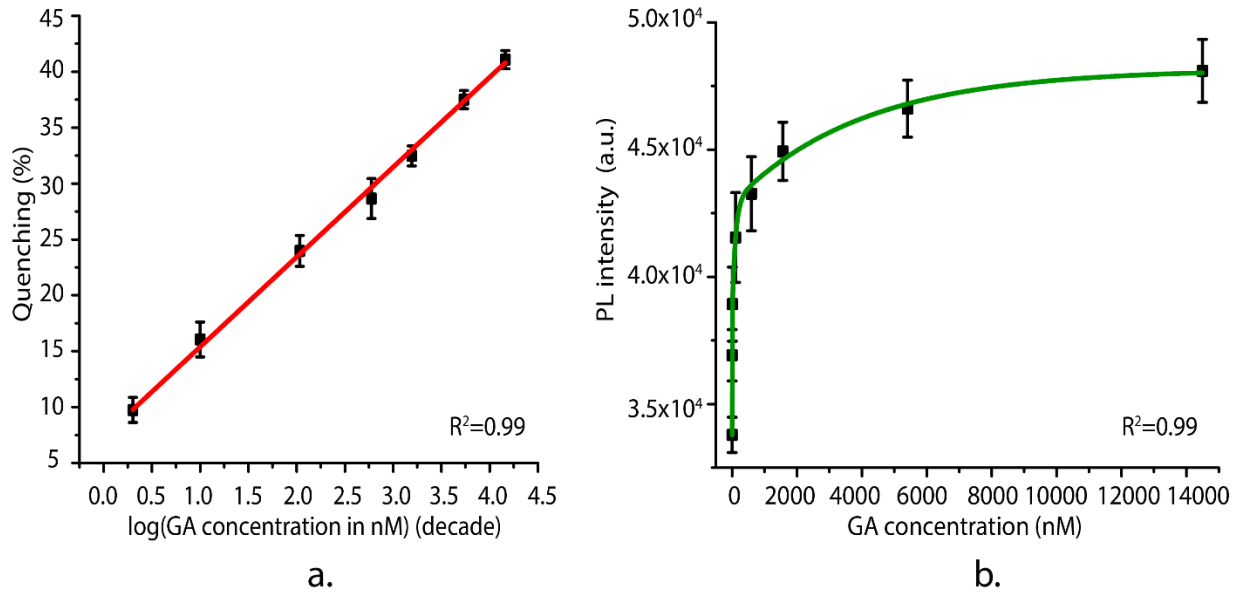

Figure 6. (a) Quenching efficiency demonstrated by the sensor on the addition of progressive addition of GA concentrations, the logarithm of which has been shown here. This represents the sensitivity of the sensor samples to the target GA. (b) Relationship between PL intensity and concentration of GA in nM. Experiments have been conducted with six different sensor samples in both cases (n = 6).

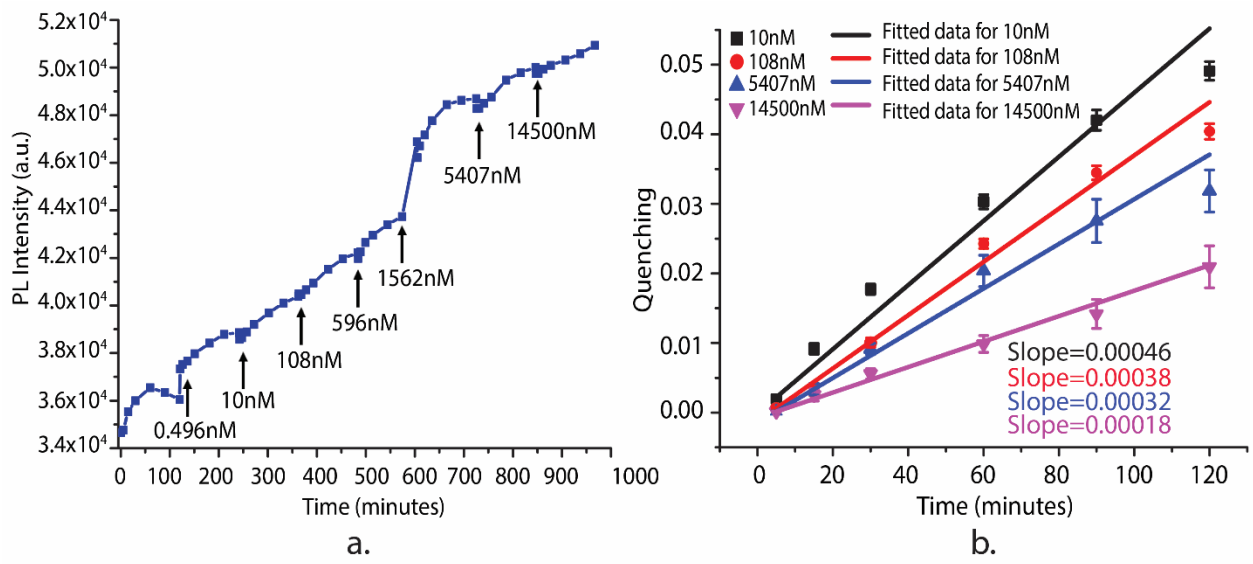

Figure 7. Time based change in (a) PL intensity of the aptasensor on successive addition of GA concentrations ranging between 0.496 nM-14500 nM (b) Quenching values of the sensor on addition of different concentrations of GA. Experiments have been conducted with six samples (n = 6).

Also, the concentration of GA in HS was found to be 3–105.3 μM (0.2–7.0 mg ml^{-1}) [78],[86]. Therefore, the aptasensor can potentially detect the presence of GA easily in diabetic serum.

In order to study the DNA-protein reaction behavior, a time based optical study was conducted. In this, once 5 μl of GA of a certain concentration was added, PL intensities were recorded after specific intervals of time (0–120 min). Figure 7(a) shows that the PL intensities increases almost linearly with the progression of time and concentration of GA. The time based quenching values (QE_T) represented Figure 7(b) have been calculated as the normalized difference between PL and PL_0 by using equation (2.3), where PL represents the PL intensity recorded after a specific period of time following the addition of target while PL_0 is the PL intensity before the addition of target.

$$QE_T = \frac{(PL - PL_0)}{PL_0} \qquad (2.3)$$

It was observed that the slopes of the quenching curves decrease with the increase in concentration of the target GA. This indicates that the reaction rate decreases with increase in concentration of GA. This behavior can be attributed to the fact that the DNA binding sites are getting occupied as more GA is introduced in the sensor.

The specificity test of the aptasensor was conducted by comparing its response to GA and some control proteins, HSA being the most important out of them. As can be seen in Figure 8, GA exhibited the maximum quenching of 41.09% ± 0.81% followed by HSA (9.93% ± 0.45%), Transferrin (6.97% ± 0.85%) and CRP (3.65% ± 0.45%). The cross reactivity of the aptamer with HSA is because HSA has a very similar structure to that GA. However, the control solutions for HSA, Transferrin, CRP and IgG were prepared in such a way that their concentration in assay was 15 μM except IFN-γ which was kept at a concentration of 142 nM. Since, GA shows a quenching efficiency significantly higher than that exhibited by the control proteins at the same concentration, it can be said that the aptamer chosen is fairly specific to GA.

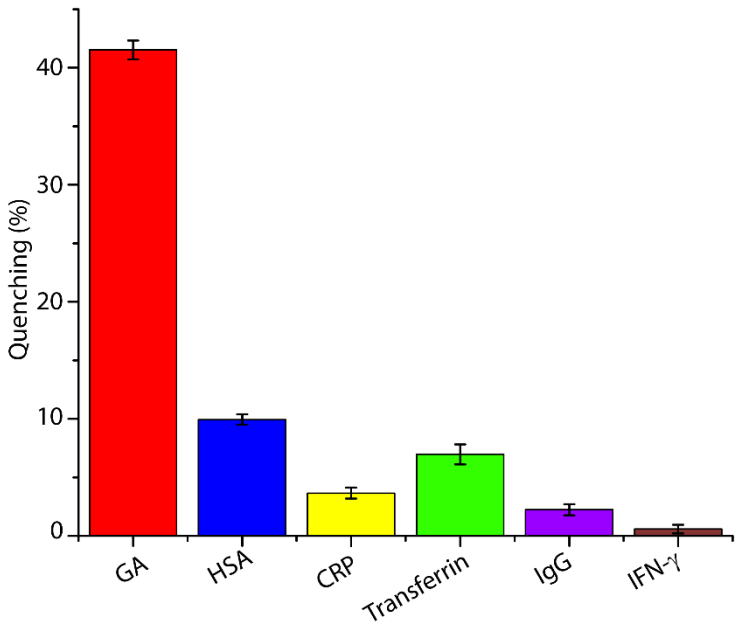

Figure 8. Response of the aptasensor towards control proteins. This graph compares the specificity of the sensor to GA and other control proteins, some of which have a high structural similarity with GA such as HSA. Experiments have been conducted in triplicates (n = 3).

2.4.2.2. Aptasensor response to clinical samples

Experiments with clinical samples were performed to evaluate the viability of this sensor to detect GA in human blood using glucose meters or continuous glucose monitoring method. The HS which contains most of the proteins, electrolytes, antibody and antigens except the fibrinogen, white blood cells and red blood cells which consists of 55% of the total volume of blood. Hence using HS as the background matrix for the clinical sample can be used to hypothesize the effect of real blood sample. Total protein content of the serum is 4–9 $gmdL^{-1}$ specified by the manufacturer [88], hence the percentage quenching of 10% for sample S1 shown in Figure 9(a) is assumed to be due to presence of proteins in the serum. Percentage quenching exhibited by the sample S2 is lower compared to that of sample S1 hence, pure HS sample can produce false positives for detection of 100 nM of GA. Whereas sample S3 shows a statistically significant higher quenching efficiency compared to control sample, hence sample S1 does not behave as a false positive target for detection of 1 μM GA concentration. The possible reason

behind high cross-reactivity towards HS is due to presence of different electrolytes and high concentration of albumin.

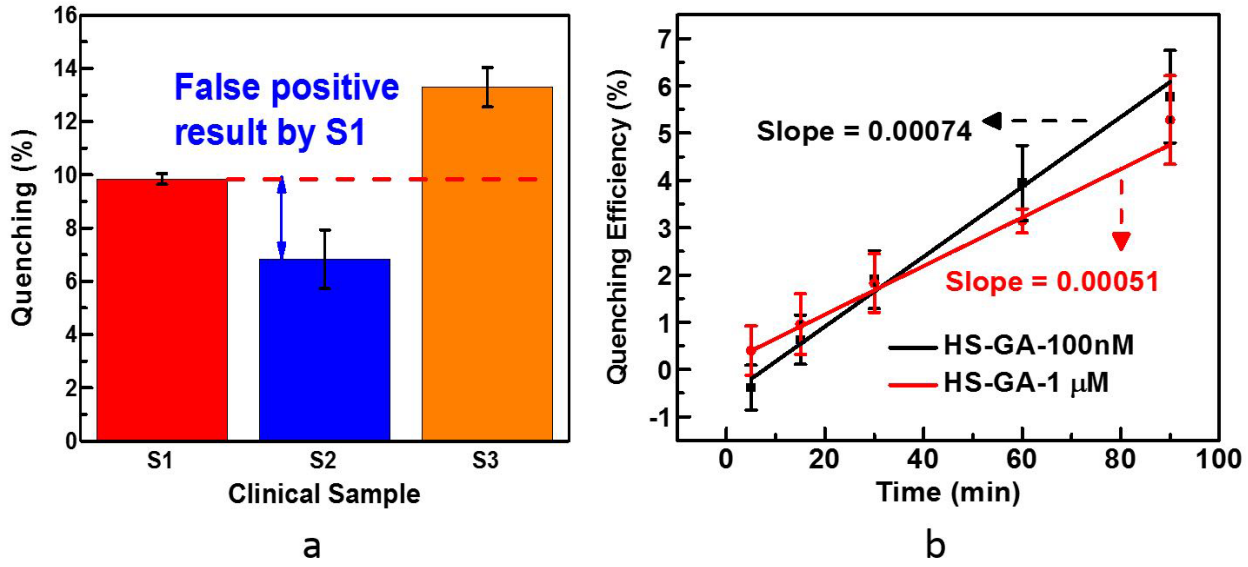

Figure 9. The percentage quenching is being presented in (a) which shows approximately 10% percentage quenching which can be co-related to quenching obtained for HSA in figure-7. Sample S1 behaves as a false positive for the concentration of 100 nM which almost 30 times higher compared to limit of detection obtained from characteristics curve. Figure (b) shows the change in quenching efficiency with time after addition of 5 μL of sample S2 and S3 to the sensor sample.

2.5. Conclusion

In this study, we have developed and characterized a simple DNA aptamer based sensor for the detection of GA. It functions on the principle of FRET rendering an increase in photoluminescence with the increase in GA concentration. This research demonstrates the capacity of the aptamer-based sensor to detect pure GA samples over a wide concentration range from 1.008–14,500 nM, where its LD is 1.008 nM and is specific to the target. Although, the sample demonstrates a certain range of cross reactivity in the clinical samples, it can still be used in diabetes diagnosis and monitoring more effectively if used in conjunction with the traditional method of glucose monitoring. This is because the photoluminescence signal will be higher for GA than any other protein at the same concentration level.

3. Detection of Tumor Necrosis Factor - alpha using optical aptasensors for detection of inflammation.

(This chapter is entirely copied from my published paper. Reprinted with permission from the following citation: Ref [89] S. Ghosh, D. Datta, S. Chaudhry, M. Dutta, and M. A. Stroscio, "Rapid detection of Tumor Necrosis Factor-alpha using quantum dot based optical aptasensor," *IEEE Trans. Nanobioscience*, vol. 17, no. 4, pp. 417–423, 2018.)

3.1. Overview

This study reports an optical 'turn off' aptasensor, which is comprised of a deoxyribonucleic acid aptamer attached to a quantum dot on the 5' terminus and gold nanoparticle on the 3' terminus. The photoluminescence intensity is observed to decrease upon progressive addition of the target protein tumor necrosis factor-alpha to the sensor. For PBS based TNF-alpha samples, the beacon exhibited 19 - 20% quenching at around 22 nM concentration. The photoluminescence intensity and the quenching efficiency showed a linear decrease and a linear increase respectively between 0 to 22.3 nM TNF-alpha. The detection limit of the sensor was found to be 97.2 pM. Specificity test results determined that the sensor has higher selectivity towards TNF-alpha than other control proteins like C - reactive protein, albumin, transferrin. The beacon successfully detected different concentrations of TNF-alpha in human serum based samples exhibiting around 10% quenching efficiency at 12.5 nM of the protein.

3.2. Background

Tumor necrosis factor-alpha (TNF-α) is a pro-inflammatory and pleiotropic cytokine mainly secreted by macrophages [90][91] and is used to determine immune responses to a disease for diagnostic purposes [92]. The soluble form of TNF-α appear to be involved in the inflammatory response [93]. It has also been shown to play a significant role in the regulation of tissue remodeling, gliosis, and scar formation by activating glial cells that surround and support

neurons [94]. There is growing evidence that TNF-α is linked to a range of inflammatory and autoimmune diseases. Chromosomes that are linked to late onset of Alzheimer's disease harbor and bind to TNF receptors [95]. Studies of rats with insulin resistance show that they produce higher levels of TNF mRNA and proteins that are also expressed in human obesity [96]. Agents that inhibit TNF-α can treat a range of inflammatory conditions such as rheumatoid arthritis, inflammatory bowel disease, sepsis and psoriasis [97]. Single stranded nucleic acid aptamers are typically short sequences of Deoxyribonucleic acid (DNA) or Ribonucleic acid (RNA), that bind to various target molecules with high sensitivity and specificity and are selected in vitro by a method called SELEX (Systematic Evolution of Ligands by EXponential enrichment) [98]. Aptamers have been utilized as the key sensing molecule in several biosensor assay platforms such as colorimetric [99], and chemiluminescent [100] platforms. Aptamers have been widely used to detect analytes such as cancer cells [101][102], metal ions like potassium [20][16][19], mercury [17][18], lead [15][16], cadmium [103], and proteins like thrombin [104][21], C-Reactive protein [105][106][54], glycated albumin [78][29], and interferon gamma (IFN-γ) [92][23].

Quantum dots (QDs) are semiconductor nanocrystals that are being extensively utilized in various biotechnological applications, including biological imaging and biosensing [107]. QDs manifest the phenomena of quantum confinement due to fact that the carrier wavefunctions must satisfy boundary conditions at the QD boundary [108]. QDs offer better brightness and photostability over more commonly used fluorescent dyes, which have low quantum yields and pH levels and hence are susceptible to chemical and photo degradation [109]. The absorption of photons that creates electron-hole pairs or excitons increases at higher energies in QDs, resulting in a broad absorption spectrum and longer fluorescence lifetime compared to fluorophores [110].

Recent efforts to utilize QDs have remarked on its ideal optical properties for light-emitting diodes [108], optical probes [107], solar cells [111], and lasers [112], as well as a transduction element in optical sensors. In fluorescence resonance energy transfer (FRET) based optical nanosensors, a linker molecule binds to the analyte and changes the distance between the QD and the quencher, causing a change in the QD's luminescence [113]. Gold (Au) nanoparticles in close proximity to a QD absorb the energy that would otherwise be emitted as a photon and are efficient quenchers for QDs due to their broad wavelength absorption spectrum of 300- 800 nm [16]. FRET is characterized by $1/d_6$ dependence for distances smaller than d_0, where d is the distance between the QD and the quencher and d0 is the distance between them at which 50 % quenching is achieved. Nanosurface energy transfer (NSET), characterized by $1/d_4$, can occur from a greater distance than FRET because it is not limited by dipole interactions between the donor and acceptor, instead relying on the donor's electromagnetic field and the conduction electrons on the acceptor. Au nanoparticles can serve as quenchers in both NSET and FRET for increased sensitivity at greater emitter-quencher distances compared to organic quenchers [114].

Enzyme Linked Immunosorbent Assays (ELISAs) have been traditionally used as a detection method of TNF-α but there are several disadvantages of ELISA such as high time consumption and false positive / false negative deviation [115]. To overcome the shortcomings of traditional ELISA immunoassays, researchers have mostly developed affinity based sensors with electrochemical transduction method [116][117][118][119], which are mostly voltammetric and impedimetric. Moreover, most of the work has utilized the traditional antibody based sandwich or direct sensing method for detection except Liu et.al. [92]. Liu et. al. has used TNF-α sensitive aptamer probe for detection. The former method requires immobilization of the antibody on a substrate, labelling the target with redox label hence the fabrication and operation of the sensor

becomes cumbersome. In addition to these sensing platforms, Weng et. al. have used an electrochemical immunosensor based on a $K_3[Fe(CN)_6]$- chitosan-glutaraldehyde system, where TNF-α was detected in PBS using cyclic voltammetry [120]. Several other electrochemical immunosensing platforms based on hydrogel prepared from ferrocene modified amino acid [121], fullerenefunctionalized carbon nanotubes and ionic liquid [122], alkaline phosphatase functionalized gold nanoparticle-poly (styreneacrylic acid) nanospheres [123] etc. have been used to detect TNF-α. An electrochemical impedance spectroscopy (EIS) based biosensor has been used by Pui et al to detect TNF-α in cell culture media [124]. Other sensing platforms for this biomarker include amperometry based immunosensing using magnetic beads [125] and hybridization chain reaction (HCR) based single molecule counting [126]. Previously reported optical sensor for detecting TNF-α utilizes fluorescence intensity change in ZnO nanorod [127], metal particle plasmon resonance assisted refractive index change in fiber-optic cable (fiber-optic particle plasmon resonance (FOPPR) sensor) [128] and resonance wavelength shift inside a silicon photonic ring-shaped microresonator [129]. Above mentioned optical biosensors use anti-TNF-α antibody for binding the target and senses change in optical property of the medium after binding event. There are very few optical biosensors reported with DNA [130] or RNA [131] based aptamer as biological active molecule with simple optical readout. To summarize, most of the reported optical biosensor with simple transduction methods either consists of complicated design strategies (antibody immobilization, antigen tagging) or sophisticated measurement techniques (FOPPR, evanescent wave based optical sensor).

In this manuscript, we are reporting a simple FRET based optical sensor using DNA aptamer as TNF-α detection probe with a very simple design and simple detection method (Figure 10) for the first time to the best of our knowledge. The simple transduction method of the sensor relies

upon change in fluorescence intensity of semiconductor nanocrystal based on the average distance between FRET pairs. Our group has extensively used this design strategies along with introduction of other active nanomaterials for detection of small sized metal ions like potassium [19], and mercury [18]. The sensing mechanism is heavily dependent on the folding capability of the DNA molecule to facilitate resonance energy transfer between QD and the quencher; hence detection of large sized protein and other bio molecules are of special interest specific to this sensor design and to overall sensor development community. We have successfully implemented this sensing strategy for detection of glycated albumin (molecular weight ~66 KDa) [29], hence TNF-α (~17.5 KDa) being much lighter molecule could be detected with this strategy.

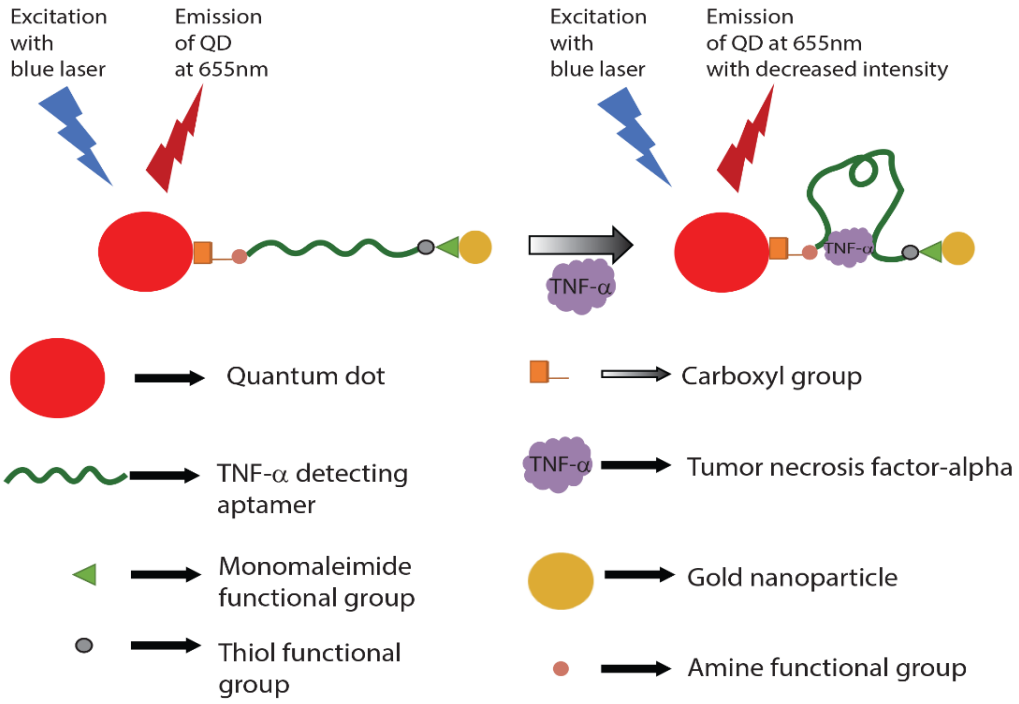

Figure 10. Schematic representation of the sensing strategy for the detection of TNF-α. This figure illustrates that as there is an increase in the target protein concentration, the PL intensity decreases. This phenomenon can be attributed to Fluorescence Resonant Energy Transfer, thereby making it the principle behind the detection of TNF-α. This figure is inspired from the illustrations provided by Ghosh et.al [29] and Datta et. al. [19].

3.3. Methods

3.3.1. Aptamer structure and modification

The TNF-α binding ssDNA aptamer used in this study consisted of 25 bases and was purchased from Biosearch Technologies (Petaluma, CA). It has been modified on both ends with an amine group on the 5' and a Thiol group on the 3' (5'AminoC6/TGGTGGATGGCGCAGTCGGCGACAA/Thiol C6 SS 3'). The aptamer was dissolved into 887 μl of Tris Ethylenediamine Tetraethyl Acetate (EDTA) buffer to obtain 100 μM aptamer solution in order to prevent cation induced degradation.

3.3.2. Materials

TNF-α, Human serum albumin (HSA) and Transferrin were purchased from Sigma Aldrich (St. Louis, MO). Human serum (HS) was obtained from AB plasma of human male and was also purchased from Sigma Aldrich (St. Louis, MO). C - reactive protein (CRP) was obtained from EMD-Millipore (Temecula, CA). 1-ethyl-3-(3-dimethylaminopropyl) - carbodiimide (EDC) and tris (2-carboxyethyl) phosphine (TCEP) are obtained from Pierce Biotechnology (Rockford, IL). 20 nm carboxyl coated CdSe/ZnS QDs e-flour ITK 655NC were purchased from Life Technologies (Carlsbad, CA). Monomaleimide functionalized nanogold particles having a diameter of 1.4 nm was obtained from Nanoprobes (Yaphank, NY). Nanosep molecular weight cutoff (MWCO) filters of 3k and 100k pore sizes were purchased from Pall Lifesciences (Ann Arbor, MI).

3.3.3. Synthesis of molecular beacon

20 μl of the 100 μM TNF-α aptamer was mixed with 9 μl of TCEP by allowing the mixture to incubate for 30 minutes at room temperature. This step results in the reduction of the dithiol groups in the aptamer. 100 μl of gold nanoparticle solution is formed by adding the same volume of de-ionized water to one vial of gold nanoparticles (6 nmoles). This was further added to the aptamer-TCEP mixture so that the resulting ratio between the quencher and the aptamer is 3:1.

The resulting solution was then incubated for 2 hours at room temperature following which it was centrifuged twice at 5000 rpm for 15 minutes each using a 3k MWCO filter in order to remove the excess unbound gold nanoparticles from the solution. After each centrifugation, the supernatant was washed with 50 μl of de-ionized water. The centrifuge used for all centrifugation steps was the Fisher Scientific Accuspin micro (Fisher Scientific, USA). A 100 μl QD solution was synthesized by adding 87 μl of 10 mM borate buffer (pH 7.4) to 13 μl of carboxylated CdSe/ZnS QD (0.1 nmoles). The QDs were bound to the DNA aptamer using the EDC/NHS coupling chemistry. 100 μl of the QD solution was added to the filtered TNF-α/gold nanoparticle solution in the presence of 23 μl of 4 μg/μl EDC/Sulpho NHS solution. The resulting solution was then allowed to shake gently for 2 hours at room temperature. Subsequently, the samples were centrifuged five times at 7000 rpm for 5 minutes each using a 100k MWCO filter in 50 mM borate buffer (pH 8.3). After each centrifugation, the supernatant was washed with 50 μl of the 50 mM borate buffer (pH 8.3). This step ensured the elimination of unbound aptamers and EDC from the sensor solution.

3.3.4. Structural characterization of TNF-α aptamer

Secondary structure prediction of aptamer In this study, the M-fold web server was used to determine the secondary structure of the TNF-α binding DNA aptamer [55][56][57][79],[81],[80]. The temperature and ionic concentrations were varied to compare the difference in secondary structure of the aptamer for each condition. Two temperature conditions were considered: 1.) 20 ^{o}C, which is the room temperature and in which the experiments were conducted 2.) 37 ^{o}C, which is the temperature under physiological conditions. For each of these temperatures, there were three different ionic conditions considered: 1.) 1.37 mM Na^{+}, 2.) 10 mM Na^{+} and 3.) 150 mM Na^{+}. These concentrations were particularly chosen because the Na^{+}

concentration for the designed sensor is 1.37 mM while the concentration of Na^+ in a mammalian cell and blood is around 12 mM and 145 mM respectively [132].

3.3.5. Optical detection of TNF-α

3.3.5.1. Sensitivity determination of sensor

The stock solutions of 5 μg/ml and 1 μg/ml TNF-α were prepared by serially diluting the 10 μg/ml protein in 0.01 XPBS solvent. 5 μl of these TNF-α samples were then added to 750 μl of sensor solution. The cuvette containing the aptasensor and the protein is then allowed to stand undisturbed for an hour to facilitate binding between the aptamer and the protein. Subsequently, the photoluminescence intensities were recorded using a USB4000 Ocean Optics (Dunedin, FL, USA) spectrophotometer with a continuous 375 nm LED excitation.

3.3.5.2. Specificity determination of sensor

The sensor was tested with control proteins using the same procedure as mentioned in section 2.5.1 to test its specificity towards TNF-α. The control proteins used for these experiments are human serum albumin, CRP, transferrin and thrombin. Their stock solutions were also made in 0.01 X PBS and the concentrations of all the proteins were kept at 65 nM or above in the sensor.

3.3.5.3. Sensitivity determination of sensor on clinical samples

The clinical samples were prepared by spiking commercially available human serum with several concentrations of the TNF- α protein. To prepare sample C1, 10 μl human serum was spiked with 5 μl of 10 μg/ml TNF-α. This rendered a final concentration of about 1 nM of TNF-α in the sensor solution. C2 was prepared by spiking 10 μl human serum with 10 μl of 10 μg/ml TNF-α so that the resulting final concentration of the protein in the sensor is 3 nM. Samples C3, C4 and C5 were prepared in a similar manner such that the final concentration of TNF-α in the sensor is 6 nM, 9 nM and 12 nM respectively.

3.4. Results

3.4.1. Structural characterization of TNF-α aptamer

Secondary structure prediction of aptamer According to the M-fold webserver software, the secondary structures of the TNF-α binding DNA aptamer was found to be similar under the conditions (a-d) mentioned in Figure 11. However, as can be seen in Figure 11 (e-f) when the Na+ concentration was increased to 150 mM, the secondary structure changed. For the first four conditions, the structure is characterized by 14 single strand bases and 1 closing helices. There are two stacks, one of which is formed by C^{11} -G^{21} while the other is formed by G^{12} -C^{20}. The structure also has a hairpin loop, the closing pair of which is C^{13} -G^{19}. Once the Na^{+} concentration is changed to 150 mM, the altered secondary structure primarily consists of an external loop with 8 single strand bases and 1 closing helices along with a total three stacks formed by T^{8} -A^{24}, C^{11} -G^{21} and G^{12} -C^{20} respectively. In this case, an interior loop is also observed with an external closing pair at G^{9} -C^{23}. The structure here retains the hairpin loop structure at C^{13} -G^{19} like the previous conditions.

Table 3. Variation of Gibbs free energy values of the TNF-α binding DNA aptamer with different temperature and ionic concentration.

Sl. No.	Na^{+} concentration (mM)	Temperature (°C)	ΔG(kcal/mole)
1.	1.37	20	-2.99
2.	1.37	37	-1.39
3.	10	20	-3.65
4.	10	37	-2.09
5.	150	20	-5.14
6.	150	37	-3.49

This DNA aptamer was chosen based on a previously published study by Orava et. al. [130]. As per this study, this aptamer was observed to specifically bind to TNF-α with dissociation constant of 7.0 ± 2.1 nM as measured by surface plasmon resonance (SPR). It also showed no binding affinity towards TNF-β, which is the closest known homologue to TNF- α and both have very similar structures [130]. Also, this aptamer was chosen in such a way that it facilitates FRET between the quantum dot and the gold nanoparticle quencher [19]. The length of this aptamer was found to be comparable to the characteristic distance required for FRET to happen. This aptamer has 25 bases, which accounts for a length of 8.5 nm while the functional groups in it accounts for an additional length of 0.12 nm. Hence, the total length of the functionalized aptamer is 8.62 nm. Table 3 shows the Gibb's free energy (ΔG) values of the aptamer when the temperature and Na+ concentrations are varied. It was observed that the ΔG values increased when the temperature was raised from 20 ºC to 37 ºC while keeping the ionic concentration constant. However, ΔG values decrease as the Na+ concentration is increased from 1.37 mM to 150 mM.

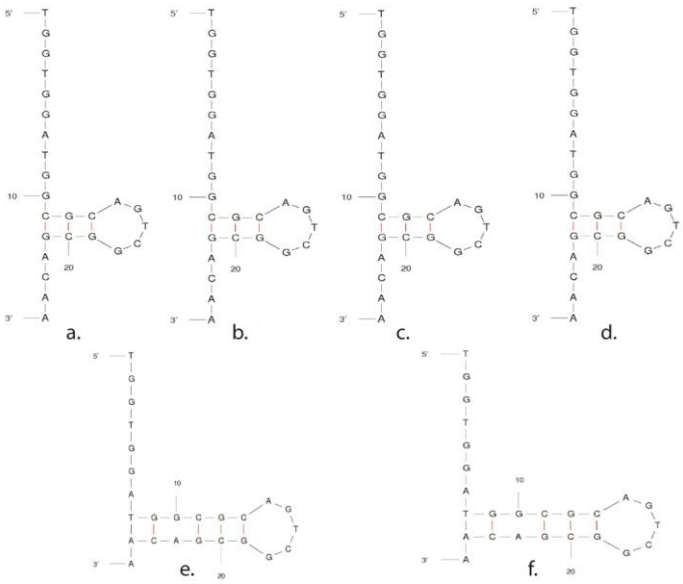

Figure 11. Secondary structures of the TNF-α binding aptamer as obtained from the M-fold server when the temperature and Na^+ concentrations are (a) 20 ºC and 1.37 mM, (b) 37 ºC and 1.37 mM, (c) 20 ºC and 10 mM, (d) 37 ºC and 10 mM, (e) 20 ºC and 150 mM and (f) 37 ºC and 150 mM respectively.

3.4.2. Optical detection of TNF-α

3.4.2.1. Sensitivity determination of sensor

Figure 12 (a) shows the photoluminescence spectra exhibited by the sensor when TNF-α is added progressively between 0 nM to 22.3 nM. A decrease in the photoluminescence intensity was observed as the concentration of the target increased. A repetition of this behavior in other sensor samples is represented in Figure 12 (b), which shows that the average photoluminescence intensity decreases linearly with the increase in the target protein concentration. The quenching efficiency has been calculated using equation (3.1), where qe (%) is the quenching efficiency expressed in percentage, I_0 is the peak photoluminescence intensity before the addition of target and I_{tnf} is the peak photoluminescence intensity after the addition of TNF-α.

$$qe(\%) = \left[\left(I_0 - I_{tnf} \right) / I_0 \right] \times 100 \qquad (3.1)$$

As seen in Figure 12 (c), the sensor shows quenching of 0.66 ± 0.17 % and 19.6 ± 1.77 % when the concentration of TNF- α is 0.344 nM and 22.3 nM, respectively. The quenching occurs because of FRET, which happens when the aptamer binds to TNF-α thus, bringing the QD and the gold nanoparticle quencher closer (Figure 10). As we continue increasing the concentration of the target protein in the sensor, the gold nanoparticle quenchers and the quantum dots are drawn closer as a result of the conformational change of the aptamer. During FRET, the gold nanoparticle quencher interacts with the quantum dot via dipole-dipole interaction, which results in an intersystem energy transfer from the quantum dot to the gold nanoparticle quencher. This is why a decrease in photoluminescence intensity and an increase in quenching is observed with the successive addition of TNF-α because greater number of quantum dots get involved in FRET [19].

The sequence of the TNF-α binding aptamer has 11 guanosine bases, out of which there are 4 sets of GG repeats. G-quadruplex structures are usually formed when three or more G bases are present consecutively in the sequence [133]. However, it has been observed that there are several aptamers, which have multiple GG repeats and have displayed the formation of G-quadruplex structure while binding to proteins like thrombin [83], nucleolin [86], HIV-1 nucleocapsid protein [84] and M. tuberculosis polyphosphate kinase 2 [85] etc. Therefore, it is assumed that this aptamer might also be taking up a G-quadruplex structure while binding to TNF-α.

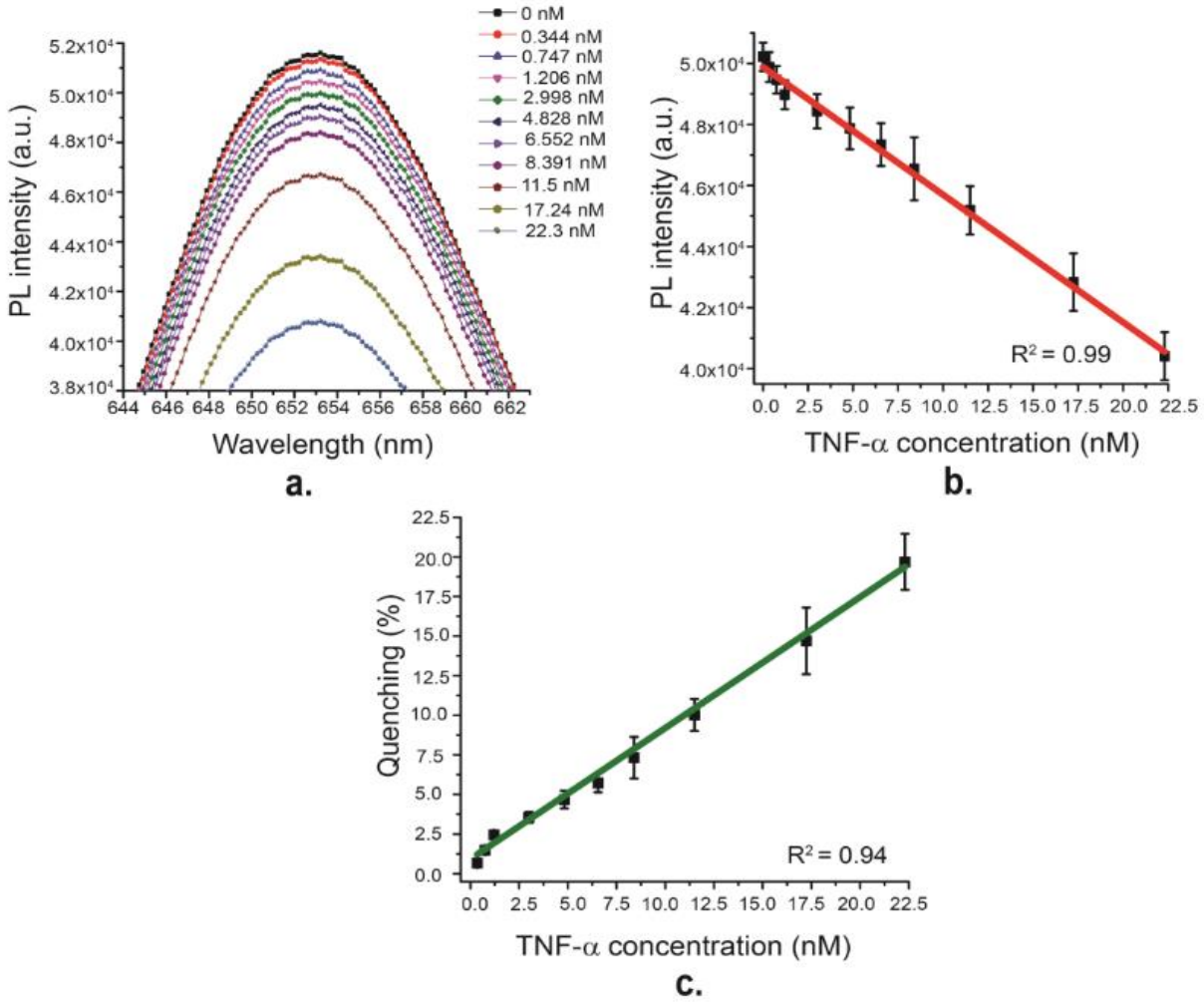

Figure 12. (a) PL intensity curves of the sensor (b) Average PL intensity of the sensor. Both (a-b) shows a decrease in photoluminescence as more TNF-α is added to the sensor. Consequently, a linear increase is observed in the (c) quenching curve of the sensor with increase in TNF-α concentration. Experiments were conducted in triplicates (n = 3).

The limit of detection of the sensor was calculated to be 1.7 ng/ml or 97.2 pM using equation (3.2), where LOD is the limit of detection of the sensor, SD_{blank} is the standard deviation exhibited by the blank sample and sensitivity is the slope of the quenching curve (shown in Figure 12 (c)).

$$LOD = {(3 \times SD_{blank})}/{sensitivity} \qquad (3.2)$$

The limit of detection of this sensor has been compared to that present in previously published literature in Table 4. According to it, this sensor has a lower limit of detection than several other sensor platforms used to detect TNF-α previously.

Table 4. Comparative analysis of the parameters of the TNF-alpha detecting DNA aptasensor with various sensors published in the literature.

Sl. No.	**Biologically Active Molecule**	**Sensor**	**Linearity Range**	**Limit of Detection**	**Reference**
1.	Aptamer	Electrochemical sensor	0-100 ng/ml	10 ng/ml	[134]
2.	Aptamer	Microfluidic sensor	0-100 ng/ml	5 ng/ml	[135]
3.	Aptamer	Electrochemical sensor	9-88 ng/ml	5.46 ng/ml	[136]
4.	Antibody based	Silicon photonic microresonator array based sensor	N/A	4.6 ng/ml	[129]
5.	Nano TNF-α	Reflectometric Interference Spectroscopy based sensor	N/A	56 ng/ml	[137]

6.	Antibody based	QCM based immunosensor	40-2000 ng/ml	25 ng/ml	[138]
7.	Antibody based (Nanoanti-TNF-α)	Potentiometric sensor	N/A	15 ng/ml	[139]
8.	**DNA aptamer based**	**Photoluminescence Spectroscopy (FRET) based optical sensor**	**0-400 ng/ml**	**1.7 ng/ml**	**This work.**

3.4.2.2. Specificity determination of sensor

Specificity of these reported sensors have been tested earlier in our previously published articles for small sized entities like metals ions [16][19][18][15]. However, the performance of these sensor topologies has not been tested extensively for biological macromolecules except glycated albumin [29]. The specificity test of the sensor complex shows almost 10 times better response towards TNF-α compared to CRP, albumin and transferrin but shows a significant amount of cross-reactivity towards thrombin protein (Figure 13). According to Orava et. al. [130], the TNF-α binding DNA aptamer has a striking similarity to the thrombin binding aptamer (TBA) in the fact that the latter also has 4 sets of GG repeats like the aptamer used in this sensor. Therefore, this cross-reactivity of thrombin towards this sensor could be potentially because of this aptamer's ability to form a G-quadruplex structure.

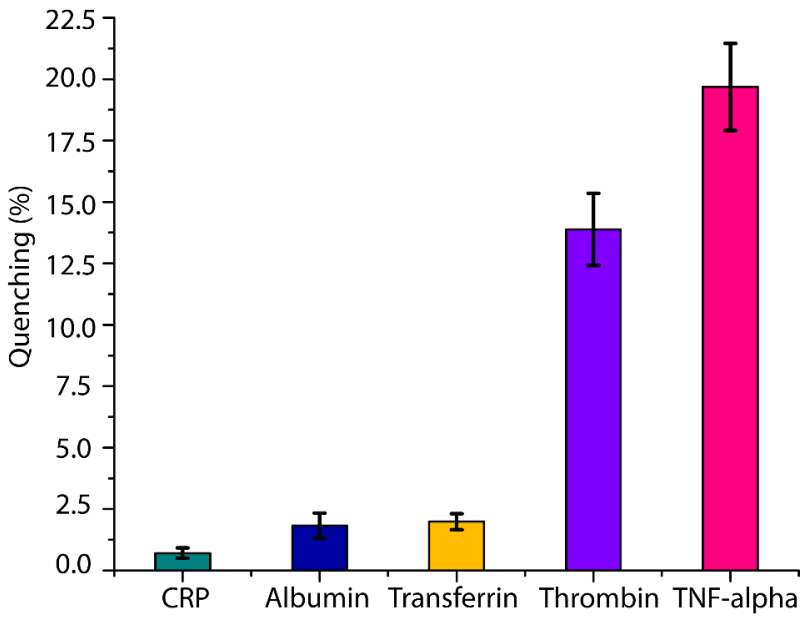

Figure 13. Quenching efficiency of sensor in the presence of TNF-alpha and control proteins. A high cross-reactivity was observed in the presence of thrombin. Experiments have been performed in triplicates (n = 3).

3.4.2.3. Sensitivity determination of sensor on clinical samples

The aptasensor was tested with human serum based samples to evaluate its practical applicability towards detecting TNF-α in biological samples. In Figure 14, the unspiked human serum exhibits quenching efficiency of 0.47±0.15%. This cross-reactivity can be attributed to the proteins, which are already present in the commercially available human serum [29]. As for the samples, where human serum was spiked with different concentrations of TNF-α, a steady increase in quenching was observed with the increase in TNF-α concentration in the serum. For instance, sample C1, which rendered a final concentration of 1 nM TNF-α in the sensor displayed an average quenching efficiency of 2.21±0.2% while sample C5, which contained around 12 nM of the target protein, exhibited a quenching efficiency of 9.76±0.37%. As can be seen in Figure 14, the quenching increased almost linearly and this behavior agreed with the calibration curve shown in Figure 12 (c). Table 5 calculates the experimental quenching efficiency by subtracting the quenching efficiency of human serum from those of the spiked

samples. The results were then compared with the calibration curve data. The quenching efficiencies of the clinical samples were found to be comparable to the calibration curve quenching efficiencies.

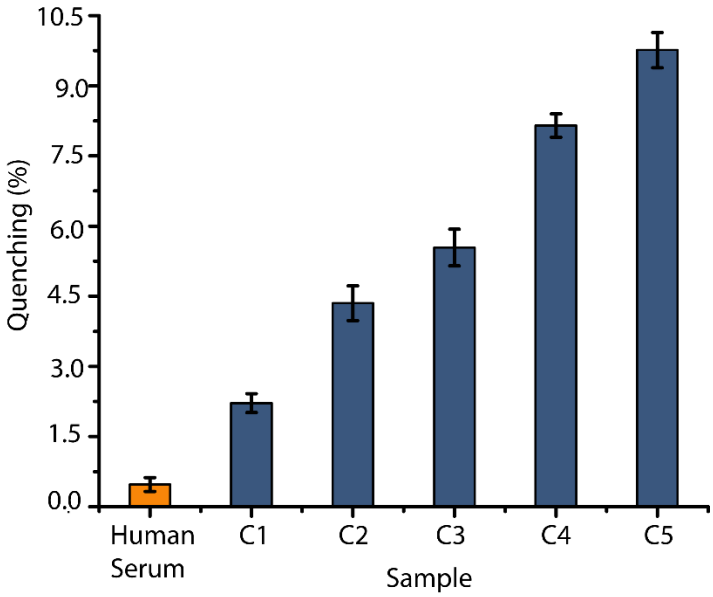

Figure 14. Response of the aptasensor in the presence of human serum based samples. Samples C1, C2, C3, C4 and C5 are human serum based samples, which rendered final TNF-α concentrations of 1 nM, 3 nM, 6 nM, 9 nM and 12 nM respectively in the sensor. It illustrated very negligible cross-reactivity with human serum while successfully detecting multiple concentrations of TNF-α spiked human serum. Experiments were conducted in triplicates (n = 3).

Table 5. Accuracy of the sensor complex in detecting TNF-α spiked human serum samples which is considered to be mimicking real life sample.

Sample	Actual prepared concentration (nM)	Quenching Efficiency (Calibration Curve) (%)	Quenching efficiency (Experimental) (%)
C1	1	1.76 ± 0.08	1.74 ± 0.35
C2	3	3.42 ± 0.17	3.88 ± 0.52
C3	6	5.91 ± 0.29	5.06 ± 0.54
C4	9	8.38 ± 0.43	7.67 ± 0.04
C5	12	10.87 ± 0.54	9.29 ± 0.53

3.5. Discussion

In this study, we have successfully developed optical nanosensors, where a TNF-α binding DNA aptamer has been employed as an active sensing element. Binding of TNF-α to the aptamer

results in a conformational change in the latter, thereby, pushing the quantum dot (donor) and the gold nanoparticle quencher (acceptor) closer to each other causing FRET. The sensor takes advantage of this phenomenon, making it the basis for the detection of TNF-α and achieves a detection limit as low as 1.7 ng/ml or 97.2 pM.

The fact that this sensor detects TNF- α in human serum based clinical samples effectively makes it a potential candidate for application in medical and biological diagnostics. Added advantages of this nanosensor include greater shelf life and stability compared to other enzyme based detection platforms, which suffer from several drawbacks such as high pH and temperature sensitivity [69] along with greater chances of denaturation in vitro [70]. Besides, the sample requirement for this sensor is as low as 4-5 μl only and it also doesn't require complex sample preparation. To the best of our knowledge, the TNF-α binding aptamer used in this study has never been incorporated in a FRET based optical sensor earlier. The proposed sensor design can also be applied towards detecting a wide variety of targets such as metal ions, proteins, cells etc. The only parameter that will vary in each sensor will be the sensing element i.e. the aptamer. This is because aptamers specific to a target can be generated via SELEX [23]. Further investigation of this nanosensor with more clinical samples can open up more avenues in inflammatory biomarker detection and monitoring.

4. Aptasensor based detection of C – Reactive Protein for infectious disease monitoring.

(This chapter is entirely copied from my conference paper with the following citation:

Ref [140] S. Ghosh, A. Metlushko, S. Chaudhry, M. Dutta, and M. Stroscio, "Detection of C-Reactive Protein using network – deployable DNA aptamer based optical nanosensor," in *IEEE-EMBS International Conference on Biomedical and Health Informatics*, Chicago, IL, USA, May 19-22, 2019.)

4.1. Overview

Aptamer based sensors have been observed to have excellent recognition capacity towards various types of target molecules such as metal ions, proteins and other biomolecules. In this study, we report an optical 'turn off' nanosensor, which consists of a deoxyribonucleic acid aptamer attached to a quantum dot on the 5' terminus and gold nanoparticle on the 3' terminus. The sensor uses the principle of fluorescence resonance energy transfer to detect C - reactive protein. With an increase in the target concentration in the sensor, the photoluminescence intensity decreases resulting in an increase in quenching efficiency. The nanosensor has a limit of detection as low as 1.77 picomolar and is observed to be highly specific to C-reactive protein. It also successfully detects the target protein in clinical samples exhibiting around 10% quenching at 10 picomolar target concentration. Future work on this sensor will involve investigation of this sensor in an *in vivo* environment so that it can be deployed for inflammatory disease management.

4.2. Background

Sepsis is a life threatening clinical syndrome that is caused in response to infection. Recent surveys have shown sepsis to be one of the leading causes of death in the United States [141]. At an early stage of sepsis, there have often been cases of misleading clinical symptoms where the

traditional markers of infection such as Body Temperature (BT) and White Blood Cell (WBC) count remain unchanged [142]. Hence, owing to the lack of any diagnostic confirmatory test, it is highly difficult to predict, diagnose and subsequently treat this condition. Recent studies have successfully used biomarker proteins to detect diseases. Human C-reactive protein (CRP) (molecular weight ≈ 25 kDa) is an active inflammatory biomarker [143], which is used to diagnose sepsis [144]. CRP has the ability to bind to phosphocholine and recognize foreign pathogens. It can also induce inflammatory cytokines and tissue factor in monocytes [143]. Studies report that plasma CRP level is a good indicator of the presence and severity of sepsis [142]. Previous studies have been performed to determine CRP levels, commonly through the use of electrochemical sandwich-type aptasensors [145], immunoassays [146], and SERS-based assays [147]. Wang et al. designed an RNA aptamer (specific to CRP)-based electrochemical aptasensor using zinc ion functionalized silica microspheres as immunoprobes to detect CRP [145]. Luo et al. employed monoclonal antibodies against distinct epitopes of CRP in a quantum dot-labeled microplate immunoassay to detect the protein [146]. Nguyen et al. reported a SERS substrate based on plasmonic mesoporous template to detect sepsis biomarkers using the principles of immunoassay [147]. Lv et al. developed a fluorescent-linked immunoabsorbent assay (FLISA) using an antibody coated microplate to capture CRP and then quantify it using a water soluble CdSe/ZnS quantum dot probe in a microplate reader [148].

The objective of this study is to report a simple optical nanosensor for the detection of CRP (Figure 15). It utilizes a deoxyribonucleic acid (DNA) aptamer as the main sensing element. The transduction method of this sensor relies on the principle of fluorescence resonance energy transfer (FRET), which is dependent on the average distance between the FRET donor - acceptor pairs. Changes in this distance cause a difference in the fluorescence intensity of the

semiconductor quantum dot (QD) nanocrystals. Our group has previously utilized this sensor design strategy to successfully detect other biomarker proteins like Glycated Albumin (GA) [29], Tumor Necrosis Factor-alpha (TNF-alpha) [89] and metal ions like lead and potassium [16] etc. These nanosensors are network deployable for subsequent parallel processing of detection signatures.

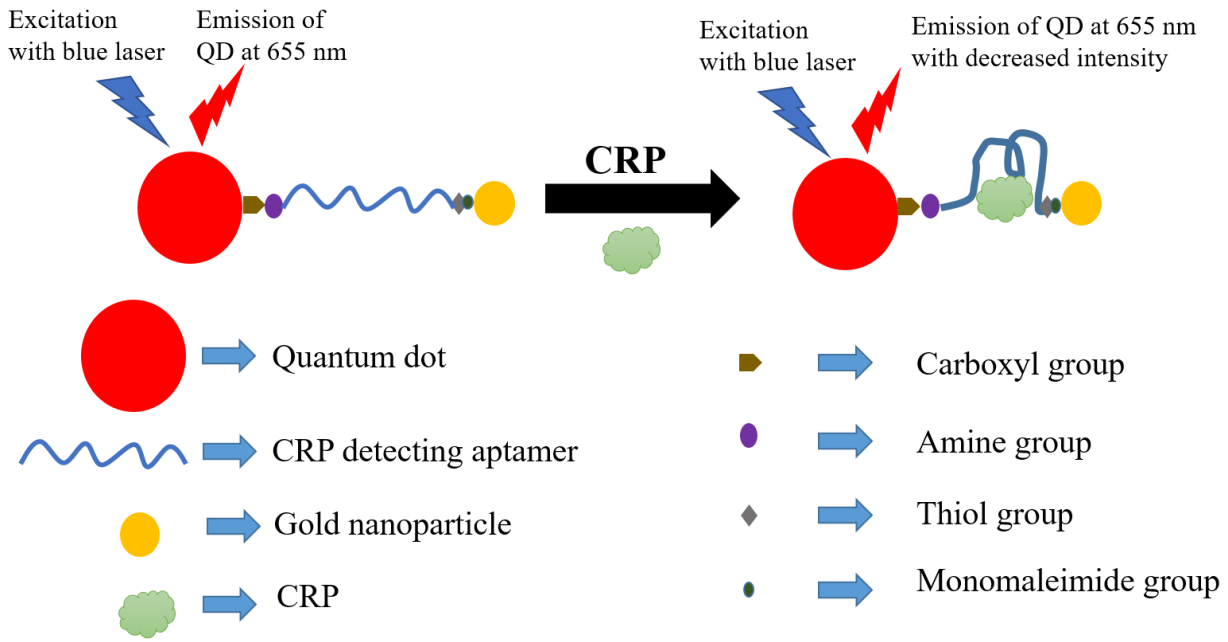

Figure 15. Design strategy used in the optical nanosensor for CRP detection. This figure shows the phenomenon of FRET, which decreases the photoluminescence intensity when the target protein binds to the DNA aptamer.

4.3. Experimental Methods

In this study, the single stranded DNA aptamer used to detect CRP consisted of 40 bases. It was purchased from Biosearch Technologies (Petaluma, CA). The 5'end of the aptamer was functionalized with an amine group while the 3' was modified with a thiol functional group (5'AminoC6/CGAAGGGGATTCGAGGGGTGATTGCGTGCTCCATTTGGTG/Thiol C6 SS 3'). The aptamer was dissolved in 414 µl of Tris Ethylenediamine Tetraethyl Acetate (EDTA) buffer to obtain 100 µM aptamer solution while also preventing cation induced degradation.

4.3.1. Materials

CRP was purchased from EMD-Millipore (Temecula, CA).1-ethyl-3-(3-dimethylaminopropyl)-carbodiimide (EDC) and tris (2-carboxyethyl) phosphine (TCEP) were obtained from Pierce Biotechnology (Rockford, IL). GA, Human Serum (HS), Thrombin, TNF-alpha and Transferrin (TFE) were purchased from Sigma Aldrich (St. Louis, MO). Carboxyl coated 20 nm CdSe/ZnS QDs e-flour ITK 655NC were obtained from Life Technologies (Carlsbad, CA). Monomaleimide functionalized 1.4 nm nanogold particles was purchased from Nanoprobes (Yaphank, NY). Nanosep molecular weight cutoff (MWCO) filters of 3k and 100k pore sizes were obtained from Pall Lifesciences (Ann Arbor, MI).

4.3.2. Synthesis of molecular beacon

A mixture of 20 μl of 100 μM CRP detecting aptamer and 9 μl of TCEP was allowed to incubate for 30 minutes at room temperature. This step facilitates the reduction of the dithiol groups in the aptamer. 100 μl of deionized water was added to one vial of gold nanoparticles (6 nmoles). This solution was further added to the aptamer-TCEP mixture in order to obtain a quencher-aptamer ratio of 3:1. After incubating the resulting solution for 2 hours at room temperature, it was centrifuged twice at 5000 rpm for 15 minutes each using a 3k MWCO filter in order to remove the excess unbound gold nanoparticles from the solution. Following each centrifugation cycle, the supernatant was washed with 50 μl of deionized water. 13 μl of carboxylated CdSe/ZnS QD (0.1 nmoles) was added to 87 μl of 10 mM borate buffer (pH 7.4) in order to synthesize a 100 μl QD solution. EDC/NHS coupling chemistry was used to bind the QDs to the DNA aptamer. 23 μl of 4 μg/μl EDC/Sulpho NHS solution was added to a mixture of 100 μl QD solution and the filtered CRP aptamer/gold nanoparticle solution. Subsequently, the final mixture was allowed to shake gently for 2 hours at room temperature. After that, the samples were centrifuged five times at 7000 rpm for 5 minutes each using 100k MWCO filter. To remove the unbound aptamers and

EDC from the sensor, the supernatant was washed with 50 µl of 50 mM borate buffer (pH 8.3) after each centrifugation cycle.

4.3.3. Secondary structure prediction of DNA aptamer

The secondary structure of the CRP detecting DNA aptamer was predicted using M-fold webserver [79][80][81]. The difference in secondary structures were compared by varying the temperature and Na^+ concentrations.

4.3.4. Optical detection of CRP

4.3.4.1. Sensitivity and specificity determination of aptasensor

The stock solutions of 50 pM, 100 pM, 500 pM, 1 nM, 50 nM, 100 nM, 500 nM and 10 µM CRP were prepared by serially diluting 3 mg/ml (120 µM) solution of the protein using 0.01XPBS. 5 µl of these CRP samples were subsequently added to 750 µl of the sensor solution. To facilitate binding between the DNA aptamer and the target protein, the cuvette was left undisturbed for an hour, following which, the photoluminescence (PL) intensities were recorded using a USB4000 Ocean Optics (Dunedin, FL, USA) spectrophotometer with a continuous 375 nm LED excitation.

Specificity of the optical nanosensor was determined using the same method as mentioned above. The control protein solutions (TFE, GA, Thrombin and TNF-alpha) were also prepared using 0.01XPBS. The concentrations of these proteins were kept at 65 nM or above in the sensor.

4.3.4.2. Sensitivity determination of aptasensor using clinical samples

The clinical samples were prepared by spiking commercially available human serum with different concentrations of the CRP protein. They were made in such a way that the final concentrations of the protein in the sensor solution were 0.5 pM, 1 pM, 5 pM and 10 pM CRP.

4.4. Results and Discussion

4.4.1. Secondary structure predication of DNA aptamer

The secondary structure (Figure 16 (a-f)) of the CRP binding DNA aptamer was obtained using the M-fold webserver software. Table 6 summarizes the Na^+ concentrations and temperature conditions, for which the secondary structures were determined, along with their corresponding Gibb's free energy (ΔG) values. Figure 16 (a-c, e) show the presence of two hairpin loops at A^4-T^{10} and C^{32}-G^{37} along with stack formation at C^1-G^{13}, G^2-C^{12}, A^3-T^{11}, and C^{31}-G^{38}. However, at higher sodium concentrations (10 mM and 100 mM), the hair pin loop at C^{32}-G^{37} and the stack formation at C^{31}-G^{38} disappear as the temperature increases to 37 ºC (Figure 16 (d, f)). In Table 6, it is observed that at room temperature (20 ºC), the Gibb's free energy values decrease with the increase in Na^+ concentrations. However, no such pattern is observed for the Gibb's free energy values at 37 ºC, which is considered as the physiological temperature.

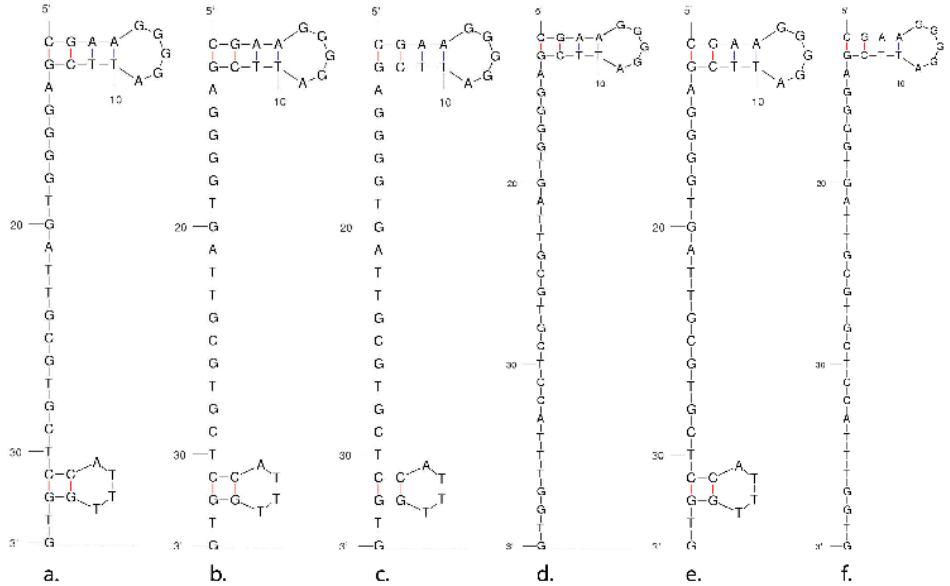

Figure 16. Secondary structures of the CRP binding DNA aptamer when the Na^+ concentrations and temperature are (a) 1.37 mM and 20 ºC, (b) 1.37 mM and 37 ºC (c) 10 mM and 20 ºC, (d) 10 mM and 37 ºC, (e) 100 mM and 20 ºC and (f) 100 mM and 37 ºC respectively.

Table 6. Gibb's free energy values of the CRP binding aptamer under different Na^+ concentrations and temperature conditions

Serial number	Parameters for Gibb's Free Energy		
	Na^+ concentration (mM)	Temperature (°C)	ΔG (kcal/mol)
1.	1.37	20	-1.85
2.	1.37	37	-1.85
3.	10	20	-3.02
4.	10	37	-0.87
5.	100	20	-4.38
6.	100	37	-1.78

4.4.2. Optical detection of CRP

4.4.2.1. Sensitivity and specificity determination of aptasensor

As can be observed in Figure 17 (a-b), the photoluminescence exhibited by the nanosensor decreases when the concentration of the target protein CRP increases from 0 pM to 65 nM. Figure 17 (b) indicates that the average PL intensity (n = 3) decreases exponentially with increase in protein concentration. Figure 18 (a) shows that sensor exhibits quenching efficiencies of 3.205 ± 0.442% at 0.3 pM and 31.85 ± 0.326% at 65 nM CRP respectively. The quenching occurs because of FRET, which can be attributed to the phenomenon of the DNA aptamer binding to CRP, hence, bringing the QD and the gold nanoparticle quencher closer (Figure 15). Aptamer-protein binding facilitates a conformational change in the DNA aptamer, which ultimately is responsible for a change of distance between the donor (QD) and the acceptor (gold nanoparticle quencher). During FRET, a dipole-dipole interaction takes place between the QD and the gold nanoparticle quencher. This results in an intersystem energy transfer from the QD to the gold nanoparticle

quencher. Hence, a decrease in PL intensity and an increase in quenching is observed with the successive addition of CRP because greater number of quantum dots get involved in FRET [19]. The quenching efficiency of the nanosensor has been calculated using equation (4.1), where Q.E. (%) is the quenching efficiency expressed in percentage, I_{blank} is the maximum photoluminescence intensity before the addition of the target analyte and I_{CRP} is the peak photoluminescence intensity after the addition of CRP.

$$Q.E(\%) = \left({}^{I_{blank} - I_{CRP}}/_{I_{blank}} \right) \times 100 \qquad (4.1)$$

Figure 18 (a) shows that the quenching behavior of the nanosensor follows the Hill chemical kinetics. According to the Hill formalism, the quenching efficiency for this sensor can also be expressed as:

$$Q.E\ (\%) = 33.274 \times \frac{x^{0.335}}{(33.407^{\,0.335} + x^{0.335})} \qquad (4.2)$$

Based on the definition of the Hill's equation, 33.407 pM refers to the concentration at which half of the receptors are occupied by the target. The Hill co-efficient of 0.335 refers to negative cooperativity with respect to substrate binding. Also, from the equation theory, the average binding constant (K_D) can be estimated as 3.239 pM.

Figure 18 (b) shows that the sensor follows a linear quenching behavior when the concentration of CRP is converted to the logarithmic scale. According to it, the quenching increases linearly between CRP concentrations of 3 pM to 65 nM. Based on this curve, the limit of detection of the sensor was calculated using equation (4.3), where LOD_{CRP} is the limit of detection of the sensor, SD_{blank} is the standard deviation exhibited by the blank sample and $Sensitivity_{CRP}$ is the slope of the quenching curve shown in Figure 18 (b).

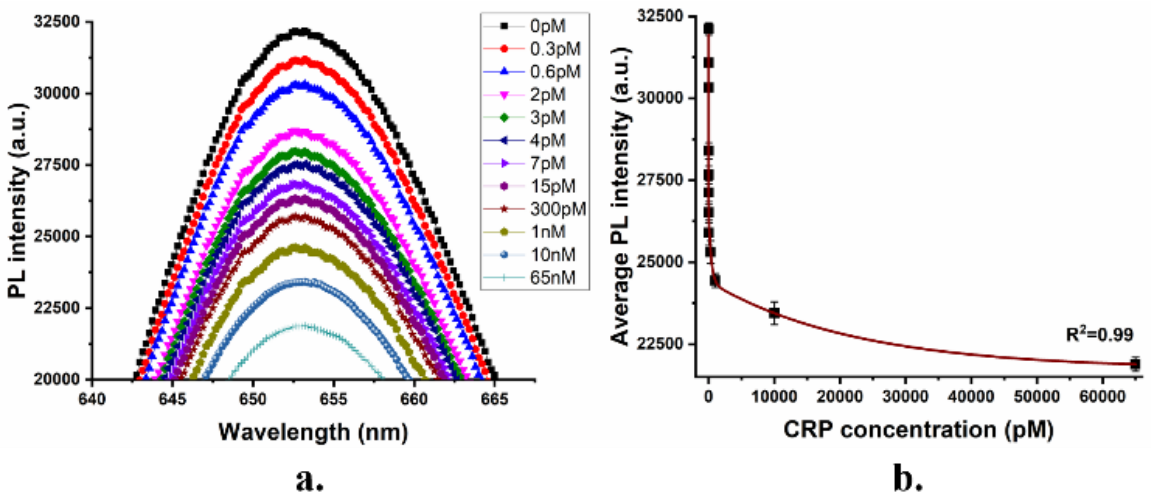

Figure 1. (a) PL intensity curves of the CRP detecting sensor (b) Average PL intensities of the sensor show a decrease in the photoluminescence with increase in concentration of CRP. Experiments have been conducted in triplicates (n = 3).

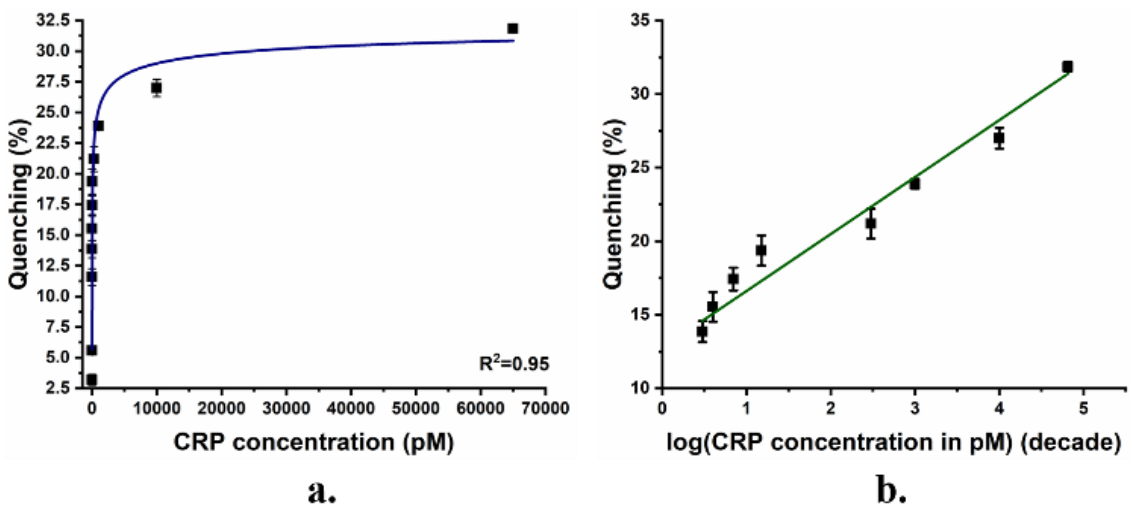

Figure 2. (a) Quenching behavior of CRP detecting sensor with respect to target protein concentration (pM) (b) Linear quenching behavior of the sensor on a logarithmic scale for CRP concentrations between 3 pM – 65 nM. Experiments have been conducted in triplicates (n = 3).

$$LOD_{CRP} = \frac{3 \times SD_{blank}}{Sensitivity_{CRP}} \qquad (4.3)$$

The limit of detection of the sensor was estimated to be 1.77 pM or 45 pg/ml. Table 7 compares the limit of detection of this sensor with previously published literature and it has been determined that the limit of detection of this sensor is lower than several other published CRP sensing platforms. According to studies, the normal concentration of CRP in healthy human

serum is lower than 10 mg/L. It increases to 10 - 40 mg/L during viral infection, 40 – 200 mg/L during bacterial infections and >200 mg/L during conditions like sepsis. Very low concentrations of CRP (<1 mg/L) has been associated with vascular risks [2] or osteoarthritis [143]. These concentration levels fall well within the detection limit of the sensor and, hence, can be used to detect CRP as a biomarker for several types of disease conditions.

Table 7. Comparative summary of the limit of detection exhibited by various CRP detecting platforms.

Serial number	**Comparitive analysis of sensing platforms**		
	Type of sensor	**Limit of detection**	**Reference**
1.	Quantum dot based optical immunosensor	0.06 μg/ml	[146]
2.	Magnetic immunoassay	1 ng/ml	[149]
3.	Electrochemical immunosensor	2.2 ng/ml	[150]
4.	Quantum dot based optical immunosensor	0.46 ng/ml	[148]
5.	Microfluidic immunoassay	1 ng/ml	[151]
6.	**Optical aptasensor**	**45 pg/ml**	**This work**

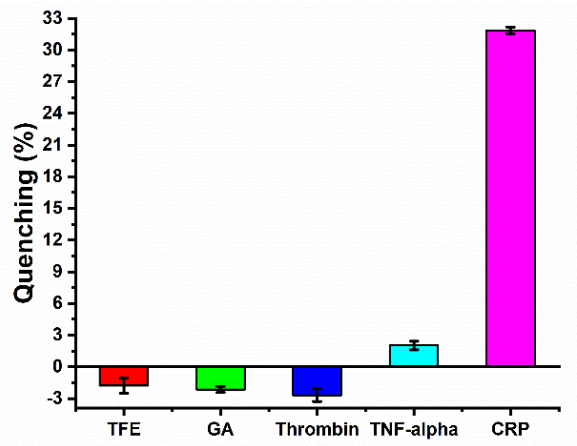

Figure 3. Response of CRP detecting nanosensor when tested with control proteins. Experiments have been conducted in triplicates (n = 3).

According to Figure 19, the sensor complex is highly selective towards CRP and exhibits almost 10 times better response towards CRP when compared to control protein TNF-alpha. There is no cross reactivity with the other control proteins TFE, GA and thrombin as they show negative quenching while CRP facilitates positive quenching.

4.4.2.2. Sensitivity determination of aptasensor using clinical samples

To evaluate the viability of the sensor in detecting CRP in septic samples, it was tested with CRP spiked human serum. The sensor exhibited some cross-reactivity (Q.E. (%) = 0.871 ± 0.33 %) towards unspiked human serum. This behavior can be attributed to the presence of proteins and other biomolecules in the commercially available human serum [29][89]. As can be observed from Figure 20, quenching increases steadily as the concentration of CRP in the sensor solution increases. For instance, at 0.5 pM CRP concentration, the sensor exhibits 3.323 ± 1.1% quenching while at 10 pM CRP concentration, it shows 9.606 ± 1.577% quenching.

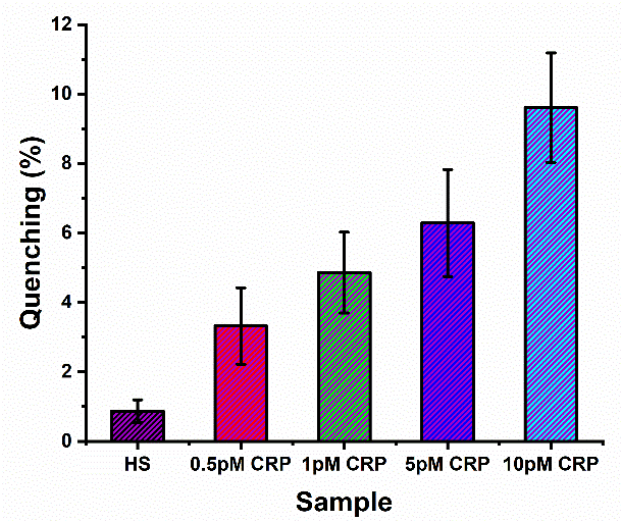

Figure 20. Response of CRP detecting nanosensor to clinical samples. Experiments have been conducted in triplicates (n = 3).

4.5. Conclusion

In this study, we have successfully detected CRP using an optical nanosensor, which employs a DNA aptamer as the primary sensing element. This sensor operates on the principle of FRET,

which is induced when the DNA aptamer changes its conformation after binding to CRP. The design of this sensor is quite simple as it can be easily synthesized by wet chemical method and does not require any specialized equipment. It can also be flexibly used for detecting several other types of molecules by just using the DNA aptamer specific to that molecule. Other advantages include low sample requirement (5 μl), greater shelf life and higher stability when compared to enzyme based sensing platforms, which suffer from several drawbacks such as high pH and temperature sensitivity along with greater chances of denaturation in vitro [89]. Further investigation of this sensor in a cellular environment can help inflammatory disease monitoring. As discussed previously, such nanoscale aptasensors may be deployed as networks for parallel processing of analyte detection.

5. Detection of calcium ions using quantum dot based optical aptasensors

5.1. Overview

This work proposes the synthesis and characterization of an optical aptasensor for the detection of calcium (Ca^{2+}) ions. This sensor design operates on the principle of Fluorescence Resonant Energy Transfer (FRET) and utilizes a quantum dot – gold nanoparticle as the donor – quencher pair. The DNA aptamer undergoes a conformational change on binding with Ca^{2+}, and this changes the distance between the quantum dot and the gold nanoparticle, conjugated on the 5' terminal and 3' terminal of the aptamer respectively. Consequently, the quantum dot emission undergoes quenching. An increase in quenching has been observed with an increase in the target ion concentration with a limit of detection up to 3.77 pM. The sensor has been characterized to have a high specificity for Ca^{2+} in comparison to other metal ions like sodium, magnesium and potassium.

5.2. Background

Calcium ions play an important role in the physiological processes like contraction, excitation, gene expression etc. [152] while also contributing significantly to diseases like HIV, Schizophrenia and Alzheimer's disease [153]. A direct correlation between increased Ca^{2+} levels and long term mortality was established after an acute ischemic stroke (Chung et. al) [154]. Feske et. al highlights the role of Ca^{2+} signaling in congenital immunodeficiency syndromes along with autoimmunity and inflammatory conditions [155]. It has been observed that in systemic lupus erythematosus (SLE), signaling through the B-Cell Receptor in B cells is abnormal and results in increased Ca^{2+} signals. Therefore, based on the significance of the metal ion in healthcare, the objective of this study is to design a sensor, which rapidly detects Ca^{2+}.

A number of sensing platforms for Ca^{2+} have been published in literature. A zinc oxide nanorod-extended gate field effect transistor (MOSFET) was designed by Asif et al. This sensor detected Ca^{2+} linearly between 1 μM and 1 mM [156]. An optical sensor reported by Ankireddy et al consisted of highly fluorescent ethylenediaminetetraaceticacid (EDTA)-CDs (ECDs) and detected Ca^{2+} in human serum with a detection limit as low as 77 pM [157]. An AlGaN/GaN transistor functionalized with poly (vinylchloride)-based (PVC) membranes were employed by Asadnia et al. as a sensing platform for Ca^{2+} [158]. Kim et al. functionalized gold nanoparticles with calsequestrin and used them to detect Ca^{2+} colorimetrically in human serum [159]. Other methods of detection include ion selective electrodes [160] microfluidic chips [161], potentiometric detection [162][163] etc. In this manuscript, we have designed an optical turn off sensor, which consists of a DNA aptamer attached to a quantum dot on one end and a gold nanoparticle on the other end. This sensor detects calcium ions based on the principle of FRET, which changes the photoluminescence intensity of the semiconductor quantum dot crystal depending on its distance with the gold nanoparticle quencher. Our group has also used this sensing strategy to detect other biologically significant metal ions such as potassium [20][16], lead [16][15] and mercury [17].

5.3. Methods

5.3.1. Materials used for synthesis and testing of molecular beacon

Calcium chloride dihydrate ($CaCl_2$. $2H_2O$), 2M Magnesium chloride ($MgCl_2$) solution and 5M Sodium chloride (NaCl) solution were obtained from Sigma Aldrich (St. Louis, MO). 4.6 M Potassium chloride (KCl) solution was purchased from Fischer Chemicals (Fairlawn, NJ). The DNA aptamer for this study was purchased from Biosearch Technologies (Petaluma, CA). Carboxyl coated CdSe/ZnS QDs e-flour ITK 655NC (diameter = 20 nm) was obtained from Life

Technologies (Carlsbad, CA) while monomaleimide functionalized nanogold particles (diameter = 1.4 nm) was purchased from Nanoprobes (Yaphank, NY). 1-ethyl-3-(3-dimethylaminopropyl) - carbodiimide (EDC) and tris (2-carboxyethyl) phosphine (TCEP) were purchased from Pierce Biotechnology (Rockford, IL). Sulpho NHS was purchased from Thermo Scientific (Rockford, IL). Nanosep molecular weight cutoff (MWCO) filters of 3k and 100k pore sizes were purchased from Pall Lifesciences (Ann Arbor, MI).

5.3.2. Aptamer structure and concentration

The DNA aptamer used in this study for detecting calcium ions consisted of 12 bases. It had been modified with an amine group on the 5' terminal and a thiol functional group on the 3' terminal (5'Amino C6/GGGGTTTTGGGG/Thiol C6 SS 3'). To obtain 100 μM aptamer stock solution, the aptamer was dissolved into 654 μl of Tris Ethylenediamine Tetraethyl Acetate (EDTA) buffer in order to prevent cation induced degradation.

5.3.3. Preparation of molecular beacon

The molecular beacon was synthesized based on the protocol reported by Ghosh et al [29][89]. Briefly, 9 μl of TCEP was mixed with 20 μl of the 100 μM calcium detecting aptamer and allowed to incubate for 30 minutes at room temperature. This facilitates the reduction of the dithiol groups in the aptamer. 100 μl of de-ionized water was added to one vial of gold nanoparticles (6 nmoles) to form a solution, which was further added to the aptamer-TCEP mixture such that the quencher-aptamer ratio is 3:1 approximately. Following the addition, the mixture was incubated for 2 hours at room temperature after which it was centrifuged (Fisher Scientific Accuspin micro (Fisher Scientific, USA)) twice at 5000 rpm for 15 minutes each using a 3k MWCO filter. Consequently, the excess unbound gold nanoparticles were removed from the

solution. 50 μl of de-ionized water was used to wash the supernatant after each centrifugation. A 100 μl DNA QD solution was prepared by mixing 13 μl of carboxylated CdSe/ZnS QDs (0.1 nmoles) with 87 μl of 10 mM borate buffer (pH 7.4). Subsequently, this solution was added to the filtered DNA aptamer/gold nanoparticle solution in the presence of 23 μl of 4 μg/μl EDC/Sulpho NHS solution. At room temperature, the sample was allowed to shake gently for 2 hours, following which, the mixture was centrifuged five times at 7000 rpm for 5 minutes each using a 100k MWCO filter in 50 mM borate buffer (pH 8.3). A washing step followed each cycle of centrifugation. Basically, 50 μl of the 50 mM borate buffer (pH 8.3) was used to wash the supernatant left on the MWCO filter. This step ensured the removal of unbound aptamers and EDC from the sensor solution.

5.3.4. Preparation of DSS peptide conjugated calcium ion detecting aptasensors

9 μl of TCEP was mixed with 20 μl of the 100 μM calcium detecting aptamer and allowed to incubate for 30 minutes at room temperature. This facilitates the reduction of the dithiol groups in the aptamer. 100 μl of de-ionized water was added to one vial of gold nanoparticles (6 nmoles) to form a solution, which was further added to the aptamer-TCEP mixture such that the quencher-aptamer ratio is 3:1 approximately. Following the addition, the mixture was incubated for 2 hours at room temperature after which it was centrifuged (Fisher Scientific Accuspin micro (Fisher Scientific, USA)) twice at 5000 rpm for 15 minutes each using a 3k MWCO filter. Consequently, the excess unbound gold nanoparticles were removed from the solution. 50 μl of de-ionized water was used to wash the supernatant after each centrifugation. A 100 μl DNA QD solution was prepared by mixing 13 μl of carboxylated CdSe/ZnS QDs (0.1 nmoles) with 87 μl of 10 mM borate buffer (pH 7.4). A ratio of 2.3 mg of the DSS peptide to 230 μl of de-ionized

water was used to prepare a 10 mg/ml DSS peptide solution. The entire DSS solution along with 100 μl QD solution was added to the filtered TNF-α aptamer/gold nanoparticle solution in the presence of 30 μl of 4 μg/μl EDC/Sulfo NHS solution. At room temperature, the sample was allowed to shake gently for 2 hours, following which, the mixture was centrifuged five times at 7000 rpm for 5 minutes each using a 100k MWCO filter in 50 mM borate buffer (pH 8.3). A washing step followed each cycle of centrifugation. Basically, 50 μl of the 50 mM borate buffer (pH 8.3) was used to wash the supernatant left on the MWCO filter. This step ensured the removal of unbound aptamers and EDC from the sensor solution.

5.3.5. Aptamer structure determination

The secondary structure of the calcium ion detecting DNA aptamer was determined using a prediction software called M-fold webserver [79][80][81]. The secondary structures were compared at various temperatures and ionic (Na^+) concentration combinations: 1.) 20 ^oC, 1.37 mM Na^+, 2.) 20 ^oC, 10 mM Na^+, 3.) 20 ^oC, 150 mM Na^+, 4.) 37 ^oC, 1.37 mM Na^+, 5.) 37 ^oC, 10 mM Na^+ and 6.) 37 ^oC, 150 mM Na^+. 20 ^oC has been considered as the room temperature and the temperature in which the optical characterization experiments were conducted while 37 ^oC is the standard physiological temperature. The rationale behind choosing the above mentioned sodium ion concentrations is that the Na^+ concentration for this aptasensor is approximately 1.37 mM while the concentration of Na^+ in a mammalian cell and blood is around 12 mM and 145 mM respectively [132].

5.3.6. Sensitivity and specificity determination of sensor

The 1 M $CaCl_2$ stock solution was prepared by mixing 1 g $CaCl_2$ and 10 ml de-ionized water. This stock solution was serially diluted to obtain solutions having concentrations of 700 p

M, 3500 pM, 7000 pM, 35 nM, 700 nM and 3500 nM, respectively. These solutions were used as working solutions for testing the optical sensitivity of the aptasensor. 5 μl of these working solutions were added to 750 μl of the sensor solution in the cuvette, which was then allowed to stand undisturbed for 5 minutes. This time period ensured the binding of the calcium ion to the DNA aptamer in the sensor. The photoluminescence intensities were subsequently recorded using a USB4000 Ocean Optics (Dunedin, FL, USA) spectrophotometer with a continuous 375 nm LED excitation.

1 mM stock solutions of the control analytes (NaCl, $MgCl_2$ and KCl) were obtained by serially diluting the respective 5 M NaCl, 2 M $MgCl_2$ and 4.6 M KCl solutions. The respective stock solutions were then serially diluted to obtain 1 μM and 100 μM working solutions. These working solutions were added to the sensor solution in such a way that the final concentration of the control analytes were 660 pM, 7 nM, 600 nM and 7 μM. The PL spectra corresponding to the controls were recorded after 5 μl of the control ion was added to 750 μl of the sensor solution and allowed to stand disturbed for 5 minutes.

5.4. Results and discussion

5.4.1. Aptamer structure determination

The secondary structures, as predicated by the M – fold webserver, was determined to be similar under all the ionic and temperature parameters used. As can be observed in Figure 21, the external loop is composed of 5 single strand bases along with 1 closing helices. Additionally, the hairpin loop had a closing pair at G^1-T^7. According to Table 8, the Gibb's free energy increases with an increase in temperature. No such observation was made for sodium ion concentration variation. The aptamer was chosen from the work reported by Miyoshi et al. [164]. They

determined that the DNA aptamer underwent a structural transition from antiparallel to parallel G- quadruplex in the presence of Ca^{2+}. This characteristic was utilized to induce FRET in the proposed sensor here.

Table 8. Gibb's free enery values of the DNA aptamer when the temperature and sodium ion concentrations are varied in the M – fold software

Parameters	
Temperature (ºC) / Na^+ concentration (mM)	**ΔG (kcal/mol)**
20 / 1.37	2.71
37 / 1.37	2.85
20 / 10	2.71
37 / 10	2.85
20 / 150	2.61
37 / 150	2.76

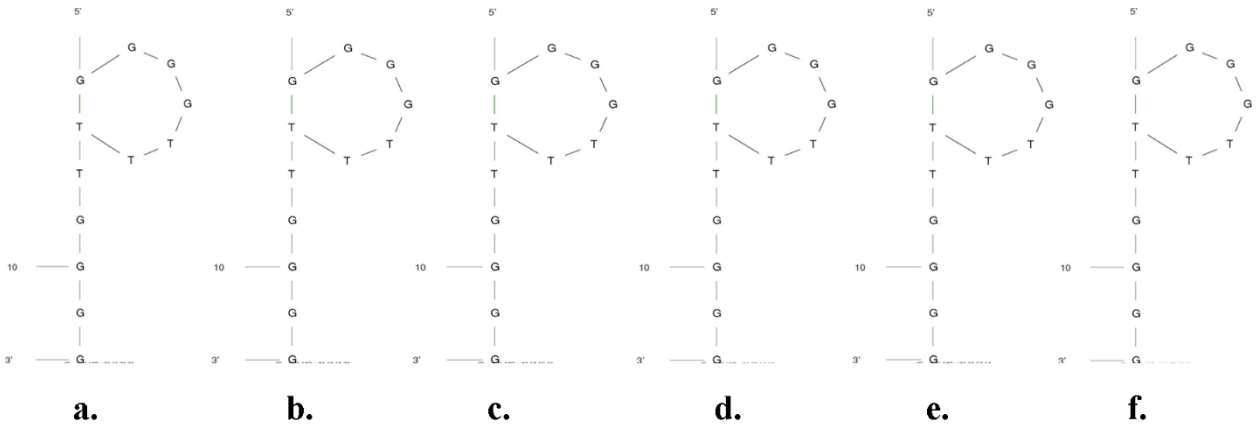

Figure 4. Secondary structure of aptamer when the temperature and Na^+ concentrations are (a) 20 ^{0}C and 1.37 mM (b) 37 ºC and 1.37 mM (c) 20 ºC and 10 mM (d) 37 ºC and 10 mM (e) 20 ºC and 150 mM (f) 37 ºC and 150 mM respectively.

5.4.2. Sensitivity and specificity determination of sensor

Figure 22 (a) shows a gradual decrease in the PL intensity with an increase in the concentration of calcium ions from 0 pM to 35 nM. A consistent repetition of this behavior is observed in Figure 22 (b) when the experiments are repeated in quintuplicates (n = 5), where the average PL intensity decreases with an increase in the target ion concentration.

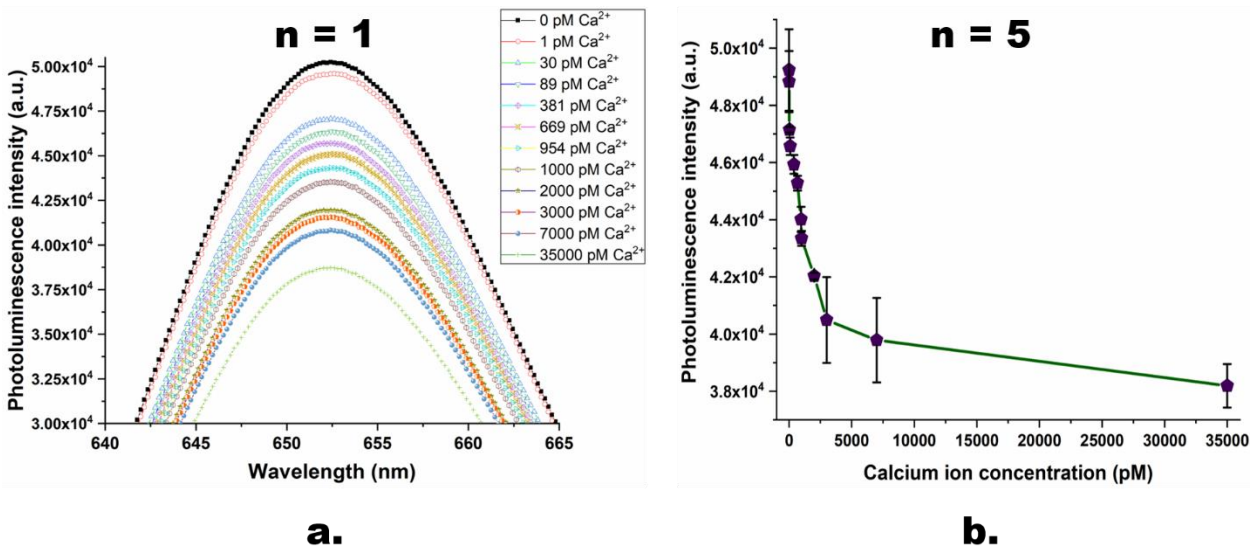

Figure 22. (a) Change of PL intensity with calcium ion concentration. (b) Average change in the PL intensity of molecular beacons with calcium ion concentration when experiments are repeated in quintuplicates (n = 5).

Figure 23 shows the quenching behavior of the sensor samples. Quenching Efficiency (%) has been calculated using equation (5.1), where I_{blank} is the peak photoluminescence intensity before the addition of target, I_{Ca} is the peak photoluminescence intensity after the addition of Ca^{2+} and Quenching Efficiency (%) is the quenching efficiency of the sensor.

$$Quenching\ Efficiency\ (\%) = {}^{I_{blank} - I_{Ca}}/_{I_{blank}} \qquad (5.1)$$

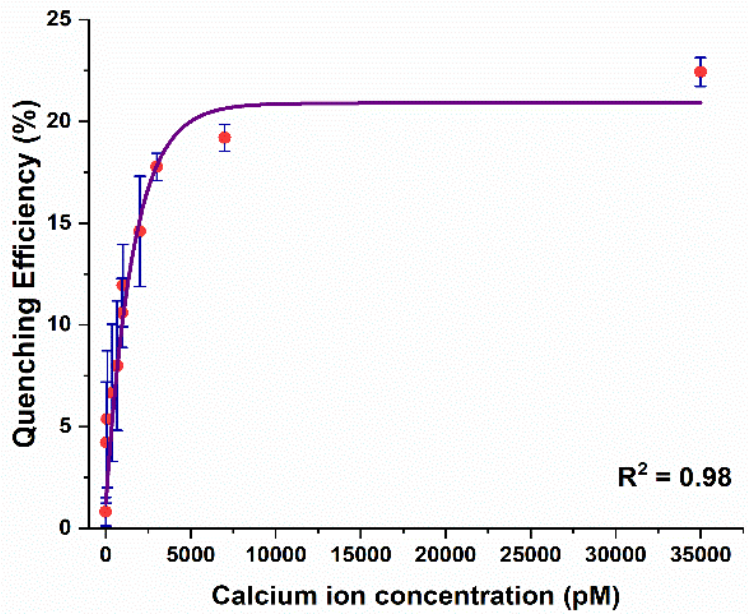

Figure 5. Quenching behavior of the aptasensor when the concentration of calcium ion is varied between 0 pM to 35 nM. Experiments have been repeated in quintuplicates (n = 5).

According to Figure 23, the sensor achieves average quenching efficiencies of 4.2 ± 2.97 % and 22.42 ± 0.71 % at 30 pM and 35 nM Ca^{2+} concentration, respectively. This behavior can be attributed to the phenomenon of FRET, where the DNA aptamer binds to the target analyte and changes its conformation, because of which, the donor (QD) and the quencher (gold nanoparticles) are driven closer to each other. Consequently, owing to a dipole – dipole interaction between the FRET pair, there is an intersystem transfer of energy from the donor to the quencher. This reduces the resulting emission from the QDs, causing a decrease in the PL intensity. As the concentration of the target ion is increased, greater number of DNA aptamers bind to them and hence, a higher number of QDs participate in FRET. In this case, the DNA aptamer has been reported to have an antiparallel G-quadruplex structure initially. Addition of Ca^{2+} induces the formation of a parallel G-quadruplex structure and finally to a G-wire structure. The parallel G-quadruplex has been found to be unstable and hence, the aptamer rapidly

transitions to the G-wire structure. The quenching behavior of the nanosensor follows the Hill chemical kinetics. In the Hill formalism, the quenching efficiency can be expressed as:

$$Quenching\ Efficiency = 23.765 \times \frac{x^{0.765}}{(906.703^{0.765} + x^{0.765})} \quad (5.2)$$

Based on the definition of the Hill's equation, 906.703 pM refers to the concentration at which half of the receptors are occupied by the target. The Hill co-efficient of 0.765 is the slope of the Hill curve and also refers to negative cooperativity with respect to substrate binding. Also, from the equation theory, the average binding constant (K_D) can be estimated as 183 pM.

$$LOD = {}^{3 \times SD_0}/_{Sensitivity_{Ca}} \quad (5.3)$$

From the results obtained in equation (5.3), where the SD_0 is the normalized standard deviation of the blank sensor sample while $Sensitivity_{Ca}$ is the slope of the quenching curve (Figure 23), the limit of detection (LOD) was calculated to be 3.77 pM or 0.55 pg/ml (assuming molecular weight of the $CaCl_2.2H_2O$ = 147 g/mol). The LOD obtained from this sensor has been compared with several other sensing platforms for Ca^{2+} in Table 9.

Table 9. Summary of several sensors for calcium detection published in literature.

Serial Number.	**Primary sensing agent**	**Sensing platform**	**LOD**	**Reference**
1.	Calmodulin (CaM)	Fiber optic sensor	5×10^{-8} M	[165]
2.	Carboxylic polyether antibiotic A23187	Fiber optic sensor	1×10^{-7} M	[166]

3.	lonophore N,N,N',N'-tetracyclohexyl-3-oxapentanediamide	Calcium selective electrode	100 pM	[160]
4.	Sensing membrane consisting of modified merocyanine photoacid polymer and a calcium ionophore in plasticized poly(vinyl chloride)	Optical sensor	5×10^{-4} M	[167]
5.	$NiCo_2O_4$ nanostructures on 3-dimensional graphene foam	Electrochemical sensor	4.45 μM	[168]
6.	α-furildioxime ionophore	Potentiometric sensor	1.25×10^{-7}M	[162]
7.	Arsenazo III (1,8-dihydroxynaphthalene-3,6-disulfonic acid-2,7-bis[(azo-2)-phenyl arsenic acid])	Microfluidic fiber optic sensor	2.68×10^{-5} M	[161]
8.	2-[(2-hydroxyphenyl)imino]-1,2- diphenylethanone (HD)	Potentiometric sensor	8.0×10^{-7} M	[163]
9.	Ethylenediaminetetraacetic	Optical sensor	77 pM	[157]

	acid (EDTA)-Carbon Dots			
10.	Hexametaphosphate-capped CdS QDs	Optical sensor	4 μM	[169]
11.	4,4′,4″,4‴-((3,6-dicyanobenzene-1,2,4,5-tetrayl)tetrakis(sulfanediyl))tetra-benzoic acid	Optical sensor	0.6 μM	[170]
12.	**DNA aptamer**	**Optical sensor**	**3.77 pM**	**This work**

The sensor was observed to have significant selectivity towards Ca^{2+} when compared to the control metal ions like Na^{+}, Mg^{2+} and K^{+}. These cations were specifically chosen because of their importance and abundance in the physiological system. Figure 24 shows the quenching behavior of the control ions in the picomolar (pM) and nanomolar (nM) concentration range. In Figure 24 (a), the quenching efficiencies have been compared between all the four ions while keeping their concentrations same (660 pM and 7 nM). Ca^{2+} was shown to have a significantly high quenching efficiency compared to the Na^{+}, Mg^{2+} and K^{+} at both 660 pM and 7 nM concentrations respectively (Figure 24(b)), indicating a high selectivity of the sensor towards calcium in the pM concentration range. A similar response was observed even when the concentration of the control ions are much higher (660 nM and 7 μM) in the sensor solution. Their quenching efficiencies were significantly lower than that of Ca^{2+} at 35 nM concentration in the sensor. This further established the specificity of the aptasensor towards Ca^{2+}.

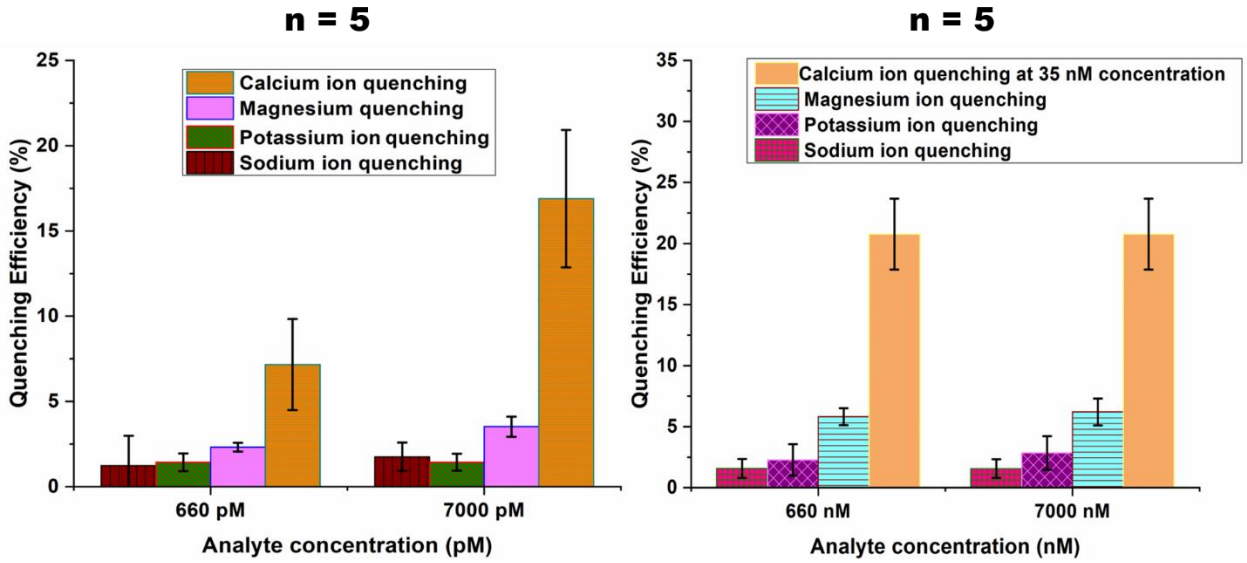

Figure 6. Response of calcium ion detecting nanosensor when tested with control ions like sodium (Na^+). Potassium (K^+) and Magnesium (Mg^{2+}). Quenching efficiencies of the target ion has been compared with that of the control ions in the pM concentration range (a) as well as in the nM range (b). Experiments have been conducted in quintuplicates (n = 5).

5.5. Conclusion

This study reports a simple DNA aptamer based optical sensor, which detects Ca^{2+} between 0 pM to 35 nM. It employs a DNA aptamer as the primary Ca^{2+} sensing element and operates on the principle of FRET. It has the ability to detect the target ion up to a lower limit of 3.77 pM. The primary advantages of this sensor lies in its ability to successfully detect Ca^{2+} at a very low concentration. Additionally, it has very low sample requirement (5 μl) and is quite flexible i.e. the same sensing strategy can used to detect other analytes by replacing the sensing element with a DNA aptamer specific to the analyte.

6. Study on the response of FRET based aptasensors in a cellular environment for the detection of biomolecules

(This chapter is partially copied from my paper submitted to Nature Scientific Reports with the following citation:

S. Ghosh, Y. Chen, J. Sebastian, A. George, M. Dutta, and M. A. Stroscio, "A study on the response of FRET based DNA aptasensors in intracellular environment," *Sci. Rep*, 2019. [Currently under review])

6.1. Overview

This chapter reports a study on the response of FRET based DNA aptasensors in the intracellular environment. Herein, we extend previous studies of aptasensors functioning in the extracellular environment to detection of antigens in the intracellular environment. An essential step in this research is the use of a novel means of achieving the endocytosis of aptasensors. Specifically, it is demonstrated that functioning aptasensors are successfully endocytosed by functionalizing the aptasensors with endocytosis-inducing DSS peptides. A summarized study on the detection of intracellular TNF-α and calcium ions along with an initial confirmatory procedure involving GA detecting aptasensors have been presented here.

6.2. Background

Cell penetrating peptides (CPP) are short peptides composed of about 5 - 30 amino acids. In recent years, CPPs have come under focus because these are capable of carrying cargo inside cells by penetrating the biological membrane [171]. Because of this ability, the CPPs are used in intracellular drug delivery since they are suitable for conjugation with various biomolecules. Additionally, they have also been observed to have low toxicity [171][172]. In this study, we have employed the DSS peptide, which belongs to the phosphophoryn protein family, to investigate the response of the quantum dot based aptasensors in an intracellular environment.

The phosphophoryns are typically rich in amino acids like aspartic acid and serine [173][174]. The DSS peptide also has some lysine group for the purpose of conjugation with the carboxylated quantum dots of the aptasensors. In this chapter is reported the synthesis strategy of the DSS conjugated aptasensors. The DSS conjugated GA detecting molecular beacons have been tested to determine the amount of DSS peptide to be used for any future synthesis process. The other DSS conjugated molecular beacons reported here have been used to determine the functionality of the sensor in an intracellular environment.

6.3. Methods

An overall synthesis strategy of the DSS peptide conjugated with the aptasensors has been represented in Figure 25. Specific reagent amounts and DNA sequences for each case have reported in the protocols given below.

6.3.1. Preparation of DSS conjugated GA detecting molecular beacons

The GA binding DNA aptamer used in this study was purchased from Biosearch Technologies (Petaluma, CA). It consists of 23 bases and has been modified on both ends with an amine group on the 5' and a thiol group on the 3' (5'Amino C6/TGCGGTTGTAGTACTCGTGGCCG/Thiol C6 SS 3'). The aptamer was dissolved into Tris Ethylenediamine Tetraethyl Acetate (EDTA) buffer to obtain 100 μM aptamer solution. This step was conducted in order to prevent cation induced degradation of DNA bases. 9 μl of TCEP was added to 20 μl of the 100 μM GA aptamer and the mixture was allowed to incubate for 30 minutes at room temperature. This step facilitated the reduction of the dithiol groups in the aptamer. 100 μl of gold nanoparticle solution was synthesized by adding the same volume of de-ionized water to one vial of gold nanoparticles. This was further added to the aptamer-TCEP mixture in order to achieve a 3:1 ratio between the

quencher and the aptamer. The resulting solution was then incubated for 2 hours at room temperature. Subsequently, it was centrifuged twice at 5000 rpm for 15 minutes each using a 3k MWCO filter in order to remove the excess unbound gold nanoparticles from the solution. After each centrifugation, 50 μl of de-ionized water was used to wash the supernatant. The centrifuge used for all centrifugation steps was the Fisher Scientific Accuspin micro (Fisher Scientific, USA). A 100 μl QD solution was synthesized by mixing 87 μl of 10 mM borate buffer (pH 7.4) and 13 μl of carboxylated CdSe/ZnS QD. Four different amounts of DSS peptide was added during four different synthesis experiments of the peptide conjugated sensor. The concentrations of the peptide are summarized Table 3. EDC/NHS coupling chemistry was used to bind the QDs to the DNA aptamer as well as to bind the DSS peptide to the QD. 100 μl of the QD solution and 230 μl of DSS peptide solution (with the corresponding concentration mentioned in Table 3) was added to the filtered GA aptamer/gold nanoparticle solution in the presence of 30 μl of 4 μg/μl EDC/Sulfo NHS solution. The resulting solution was then allowed to shake for 2 hours at room temperature. Subsequently, the samples were centrifuged five times at 7000 rpm for 5 minutes each using a 100k MWCO filter in 50 mM borate buffer (pH 8.3). The supernatant was washed with 50 μl of the 50 mM borate buffer (pH 8.3) after each centrifugation. This step allowed the unbound aptamers and excess EDC to get eliminated from the sensor solution.

Table 10. Amount and concentration of the DSS peptide added to the GA molecular beacons.

DSS peptide amount (mg)	**Volume of water added (μl)**	**Concentration of DSS peptide added to the molecular beacon (mg/ml)**
0.46	230	2
0.92	230	4
1.15	230	5
2.3	230	10

6.3.2. Preparation of DSS conjugated TNF-α detecting molecular beacons

The TNF-α binding DNA aptamer used in this study was purchased from Biosearch Technologies (Petaluma, CA). It consists of 25 bases and has been modified on both ends with an amine group on the 5' and a thiol group on the 3' (5'AminoC6/TGGTGGATGGCGCAGTCGGCGACAA/Thiol C6 SS 3'). To obtain a 100 μM aptamer solution, the aptamer was dissolved into 887 μl of EDTA buffer. 9 μl of TCEP was added to 20 μl of the 100 μM TNF-α aptamer and the mixture was allowed to incubate for 30 minutes at room temperature. 100 μl of gold nanoparticle solution was synthesized by adding the same volume of de-ionized water to one vial of gold nanoparticles. This was further added to the aptamer-TCEP mixture in order to achieve a 3:1 ratio between the quencher and the DNA aptamer. The resulting solution was then incubated for 2 hours at room temperature. Subsequently, it was centrifuged twice at 5000 rpm for 15 minutes each using a 3k MWCO filter in order to remove the excess unbound gold nanoparticles from the solution. After each centrifugation, 50 μl of de-ionized water was used to wash the supernatant. The centrifuge used

for all centrifugation steps was the Fisher Scientific Accuspin micro (Fisher Scientific, USA). A 100 μl QD solution was synthesized by mixing 87 μl of 10 mM borate buffer (pH 7.4) and 13 μl of carboxylated CdSe/ZnS QD. 2.3 mg of the DSS peptide was added to 230 μl of de-ionized water in order to make a 10 mg/ml peptide solution. EDC/NHS coupling chemistry was used to bind the QDs to the DNA aptamer as well as to bind the DSS peptide to the QD. 100 μl of the QD solution and 230 μl of the DSS peptide was added to the filtered TNF-α aptamer/gold nanoparticle solution in the presence of 30 μl of 4 μg/μl EDC/Sulpho NHS solution. The resulting solution was then allowed to shake for 2 hours at room temperature. Subsequently, the samples were centrifuged five times at 7000 rpm for 5 minutes each using a 100k MWCO filter in 50 mM borate buffer (pH 8.3). The supernatant was washed with 50 μl of the 50 mM borate buffer (pH 8.3) after each centrifugation. This step allowed the unbound aptamers and excess EDC to get eliminated from the sensor solution.

6.3.3. Preparation of DSS conjugated Ca^{2+} detecting molecular beacons

The calcium detecting DNA aptamer was purchased from Biosearch Technologies (Petaluma, CA). It consists of 12 bases and has been modified on both ends with an amine group on the 5' and a thiol group on the 3' (5'AminoC6/ GGGGTTTTGGGG /Thiol C6 SS 3'). To obtain a 100 μM aptamer solution, the aptamer was dissolved into 654 μl of EDTA buffer. 9 μl of TCEP was added to 20 μl of the 100 μM calcium detecting aptamer. The mixture was allowed to incubate for 30 minutes at room temperature so that the dithiol groups in the aptamer get reduced. One vial of gold nanoparticles (6 nmoles) was added to 100 ml of de-ionized water to form a solution, which was further added to the aptamer-TCEP mixture (quencher: aptamer = 3:1 approximately). This mixture was then incubated for 2 hours at room temperature after which it was centrifuged

(Fisher Scientific Accuspin micro (Fisher Scientific, USA)) twice at 5000 rpm for 15 minutes each using a 3k MWCO filter. The supernatant after each centrifugation was washed with 50 µl of de-ionized water. 13 µl of carboxylated CdSe/ZnS QDs (0.1 nmoles) was mixed with 87 µl of 10 mM borate buffer (pH 7.4) to form a 100 µl QD solution. A 10 mg/ml DSS peptide solution was prepared by adding 2.3 mg of the DSS peptide to 230 µl of de-ionized water. 30 µl of 4 µg/µl EDC/Sulfo NHS solution was added to a mixture of the 100 µl of the QD solution, 230 µl of the DSS peptide and the filtered calcium aptamer/gold nanoparticle solution in order to facilitate binding. Subsequently, this mixture was allowed to shake for 2 hours at room temperature following which the samples were centrifuged five times at 7000 rpm for 5 minutes each using a 100k MWCO filter in 50 mM borate buffer (pH 8.3). The supernatant obtained after each centrifugation cycle was washed with 50 µl of the 50 mM borate buffer (pH 8.3).

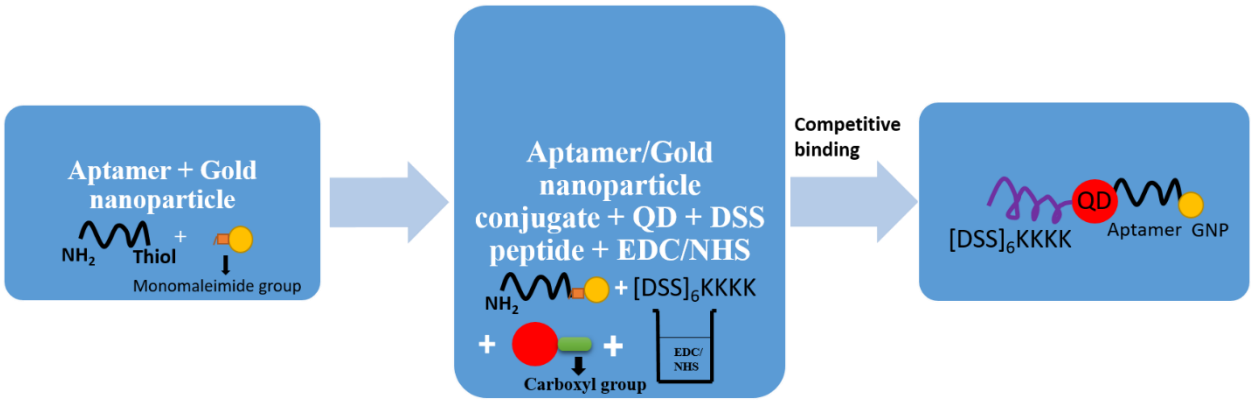

Figure 25. Design and synthesis strategy of DSS conjugated molecular beacon nanoconstruct.

6.3.4. Characterization of DSS conjugated molecular beacons

To test the DSS conjugated GA detecting molecular beacons, mouse pre-osteocyte cells (MC3T3 E1) were cultured in α-MEM with 10 % FBS and 1 % Antibiotic-Antimycotic (100X, Life technologies) at 37 °C in a humidified incubator with 5% CO_2. Approximately 250,000 cells

were seeded on a ϕ 25 mm cover glass in one of the wells of a 6 well culture plate. On the following day, the aptasensors were added to interact with the cells.

The DSS conjugated TNF-α detecting molecular beacons were characterized using mouse monocyte/macrophage cells (RAW264.7), which were cultured in DMEM with 10 % FBS and 1 % Antibiotic-Antimycotic at 37 °C in a in a humidified incubator with 5% CO_2. Approximately, 100,000 cells were seeded on a ϕ 12 mm cover glass in a well of 24 well culture plate. The cells were stimulated / differentiated by lipopolysaccharides (100 ng/ml, Sigma) for 16 hours to induce bacterial infection. Subsequently, the aptasensors were added to interact with the cells. Once the sensors were added, the reaction was paused briefly followed by rinsing twice with PBS. The cells were then fixed with 10% formalin (PBS neutralized) at 37 °C for 1 hr. The cover glass were mounted on a glass slide with mounting agent with DAPI (VectorLab) after washing with PBS thrice.

The DSS conjugated calcium ion detecting molecular beacons were tested using mouse pre-osteocyte cells (MC3T3 E1 - ATCC, Manassas, VA), which were cultured in α-MEM (Corning Inc. Corning, NY) with 10 % FBS (Thermo Fisher Scientific, Waltham, MA) and 1 % Antibiotic-Antimycotic (100X, Life Technologies) at 37 °C in a humidified incubator with 5% CO_2. Around 300,000 cells were seeded on a ϕ 25 mm cover glass in one of the wells of a 6 well culture plate. The following day the aptasensors (0.1 mg/ml) were added. After 1 hour, the cells were washed with pre warmed PBS without calcium and magnesium three times to remove un-incorporated/free molecular beacons. Following Thapsigargin (TG - final concentration at 1 μM) ((MilliporeSigma, Burlington MA) in PBS without calcium and magnesium were added to trigger the calcium release from endoplasmic reticulum store. At the indicated time point, formaldehyde solution (37%) (Thermo Fisher Scientific, Waltham, MA) was added at 1/10 of

TG solution volume (20 μL to 200 μL) to stop the reaction and fix cells for 1 hour at room temperature. After washing with PBS for 3 times, the cover glass were mounted on a glass slide with mounting agent with DAPI (VectorLab, Burlingame, CA).

In all the cases the fluorescence images were obtained using a Zeiss LSM 710 Confocal Microscope in Research Resources Center of University of Illinois at Chicago or with a Zeiss Observer D1 Microscope.

6.4. Results and discussion

6.4.1. Characterization of DSS conjugated molecular beacons

The interaction between the DSS peptide conjugated GA detecting molecular beacons and the cells were tested to determine whether there was a successful conjugation between the peptide and the sensors. Ravindran et al. previously showed that the DSS peptide facilitates cellular uptake. To reduce peptide wastage, three different concentrations of the peptide was initially tested to determine the optimal concentration at which future experiments would be conducted. The working concentrations of the DSS peptide used during the cell culture process are shown in Table 11. As shown in Figure 26 (a - h), the quantum dots in the molecular beacon was observed to be surrounding the nucleus for all the four working concentrations of the peptide (10 μg/ml, 20 μg/ml, 25 μg/ml and 50 μg/ml). However, based on the concentration of the quantum dots around the cell nucleus in Figure 26 (a-h), it was determined that the best concentration of the DSS peptide for future endocytosis experiments was 50 μg/ml. Hence, the DSS stock concentration of 10 mg/ml was used in future synthesis protocols of the DSS peptide conjugated aptamer sensor.

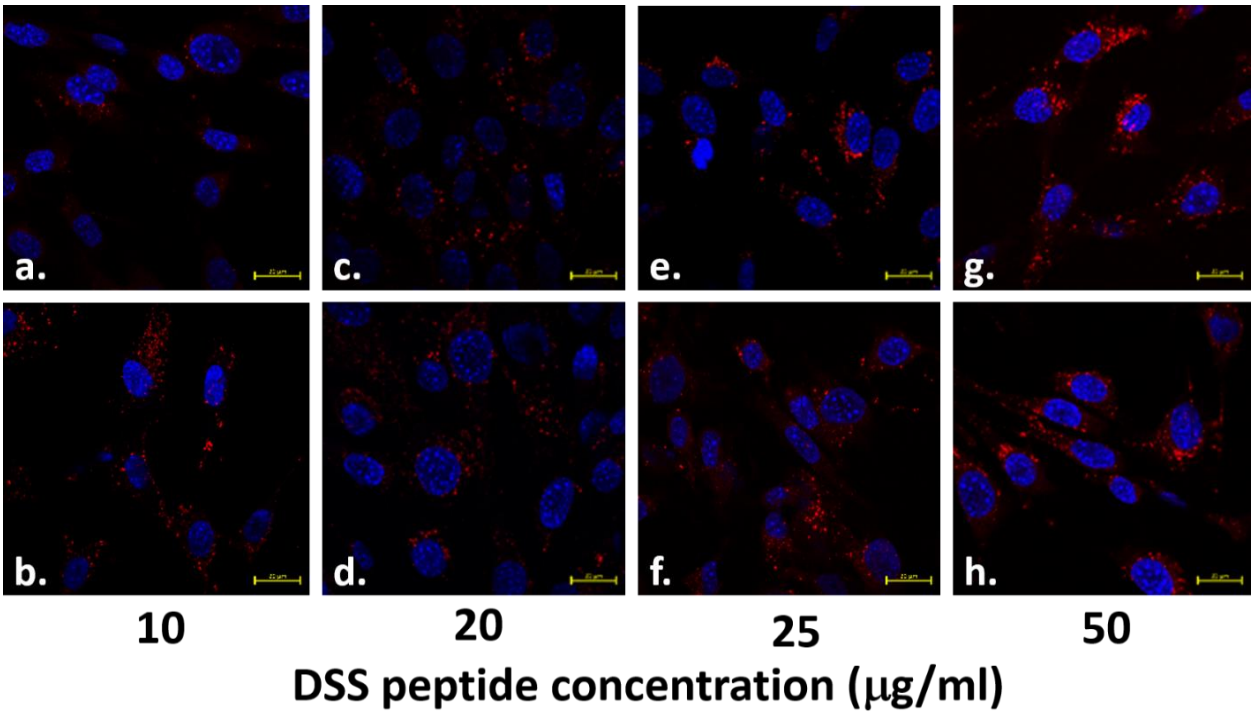

Figure 26. Entrance of the DSS conjugated molecular beacons inside the MC3T3 cells. The cell nucleus has been shown in blue while the quantum dots are shown in red. The concentration of the 655 nm quantum dots (red) around the cell nucleus (blue) is compared in the presence of (a-b) 10 μg/ml, (c-d) 20 μg/ml, (e-f) 25 μg/ml, and (g-h) 50 μg/ml concentration of the DSS peptide, used during the synthesis process.

Table 11. Final concentrations of DSS peptide used during cell culture experiments. Stock concentration stands for the concentration of DSS peptide added during the synthesis of the molecular beacons (Section 6.3.1, Table 10). Working concentration of peptide stands for the diluted concentration of the DSS peptide used during the cell culture testing (Section 6.3.4 for GA detecting molecular beacons). The working concentration expressed in mg/ml (third column) has been converted to μg/ml (fourth column).

Stock Concentration (mg/ml)	**Dilution factor**	**Working concentration of peptide (mg/ml)**	**Working concentration of peptide (μg/ml)**
2	200	0.0100	10
4	200	0.0200	20
5	200	0.0250	25
10	200	0.0500	50

Figure 27 (a-c) shows macrophage cells (RAW 264.7) in the presence of the DSS peptide conjugated TNF-α detecting aptasensors. In Figure 27 (d-f), the macrophage cells were treated with bacterial lipopolysaccharide to induce infection, which resulted in an intracellular production of the pro-inflammatory cytokine TNF-α. As can be observed in Figure 27 (d-f), there was a decrease in the fluorescence intensity emitted by the quantum dots when compared to the emission observed on Figure 27 (a-c). This phenomenon indicates the occurrence of FRET.

To detect whether the sensors were specifically detecting TNF-α, the interaction between MC3T3 cells and the DSS conjugated aptasensors were studied. The rationale behind this is that these cells don't produce TNF-α. As can be seen in Figure 28 (a-b), there is no change in the quantum dot fluorescence emission. This showed that despite having a high cross reactivity with thrombin in the calibration data [89], no such interference was observed in the data shown below. The sensor displays successful quenching and hence FRET in the presence of TNF-α.

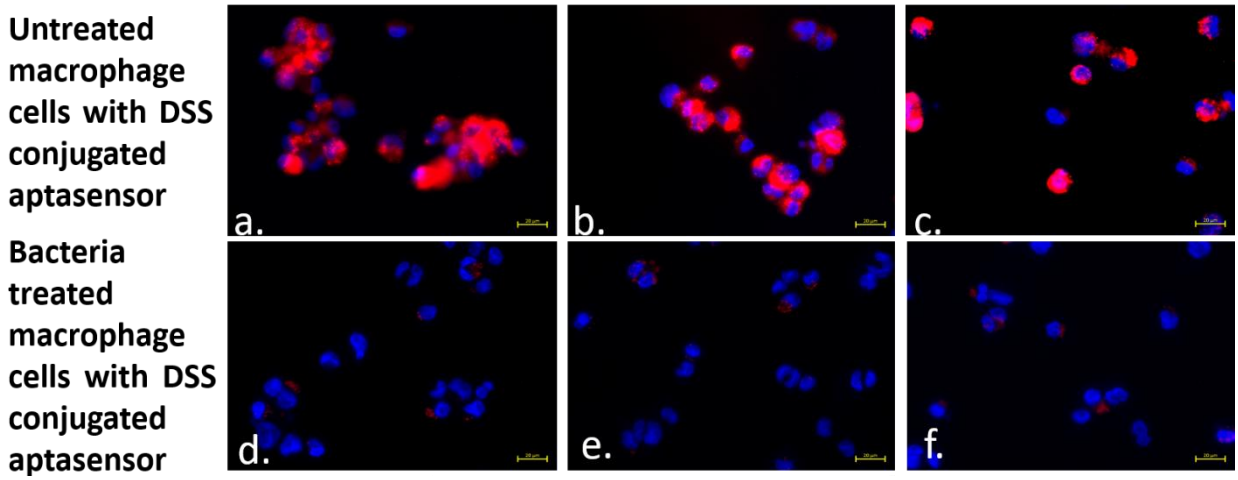

Figure 27. The phenomenon of FRET has been illustrated here. A decrease in fluorescence intensity is observed when the sensor interacts with the bacterial lipopolysaccharide treated macrophage cells in (d-f) compared to the non-infected macrophage cells in (a-c).

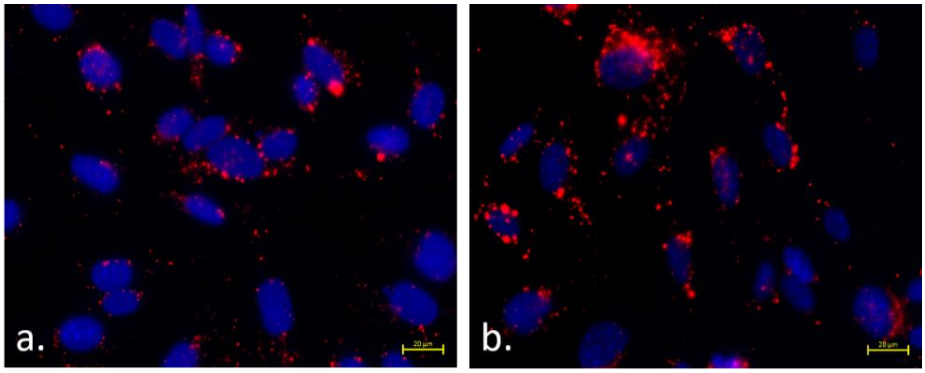

Figure 28. Response of DSS conjugated TNF-α detecting aptasensors to MC3T3 cells, which don't produce the cytokine. No quenching was observed in both a, b.

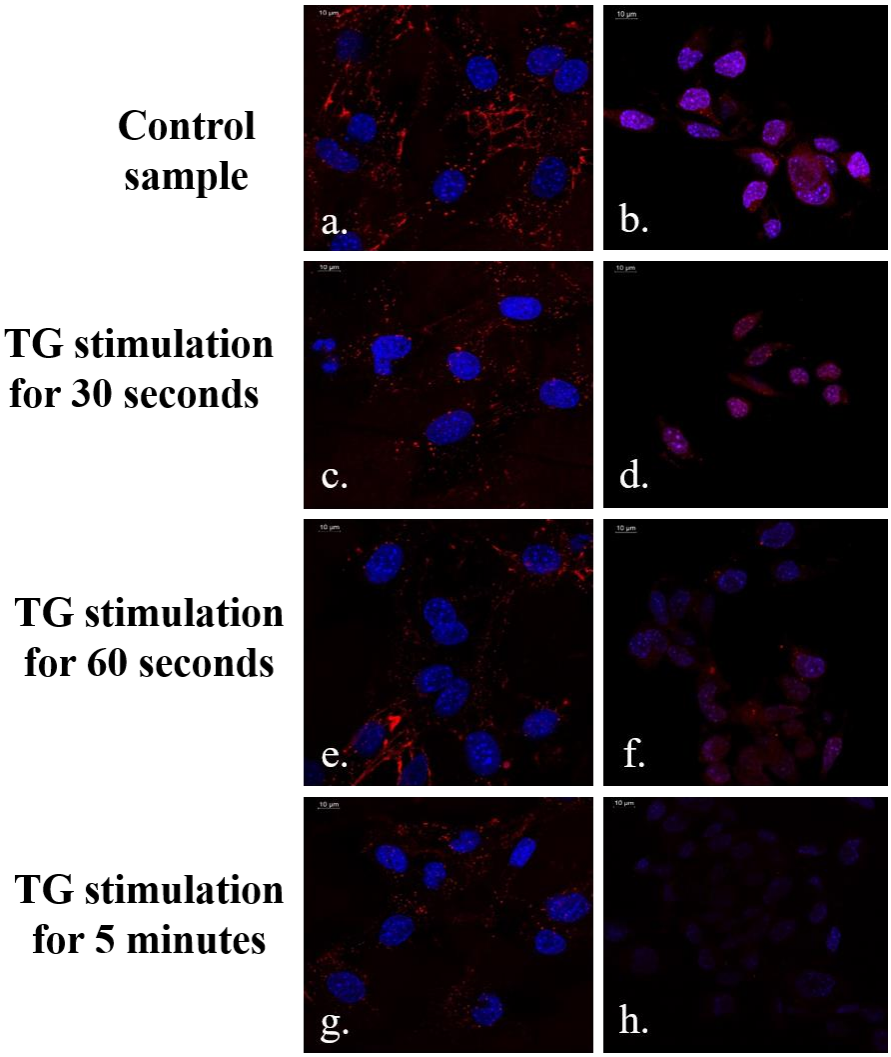

Figure 29. Interaction between the DSS conjugated calcium ion detecting molecular beacons and MC3T3 cells in the presence of no TG stimulation (a-b) 30 seconds of TG stimulation (c-d) 60 seconds of TG stimulation (e-f) and 5 minutes of TG stimulation (g-h). Successful quenching phenomenon has indicated with progression of time and TG stimulation.

The DSS conjugated calcium detecting aptasensors were tested in MC3T3 cells, which stimulated using TG at various time points. TG stimulation allows the intracellular production of calcium ions. A higher intensity QD emission from the MC3T3 cells was observed in Figure 29 (a, b) in the absence of TG stimulation, indicated as control sample. With the progress in time, TG stimulation increases intracellular Ca^{2+} levels (Figure 29 (c-h)). Therefore, greater number of aptasensors binds to the higher concentration of Ca^{2+}, causing greater reduction in the fluorescence emission. This phenomenon confirmed the occurrence of FRET in the presence of the target metal ion.

6.5. Conclusion

The aptasensors reported in this study consists of a DSS peptide and molecular beacon specific for the detection of biomarkers like GA and TNF-α as well as physiologically relevant metal ions like calcium. The DSS peptide is a cell penetrating peptide capable of dragging a cargo inside the cell towards the nucleus. It is conjugated to the aptasensors using the principle of competitive binding. Successful conjugation of the peptide to the sensors has been confirmed using GA detecting molecular beacons. All the aptasensors reported here employ a single stranded oligonucleotide as the primary sensing element and operates on the principle of FRET. This peptide-molecular beacon nanoconstruct can successfully detect TNF-α inside the macrophage cells and calcium ions in MC3T3 cells when the appropriate DNA aptamer is used. Besides, it also enjoys the flexibility of being able to detect other biomarker proteins by just replacing the sensing element (DNA aptamer).

7. Graphene oxide based aptasensor for the detection of C - Reactive Protein.

7.1. Overview

In this study, we report the design and characterization of a graphene oxide – aptasensor complex, which successfully detects CRP. The molecular beacon consisting of a donor – quencher pair along with a DNA aptamer has been bound to a graphene oxide substrate so that it opens up a way to theranostic constructs. As described here, the sensing complex can selectively detect CRP between 0 pM to 1000 pM with a limit of detection estimated to be in the range of 0.5 pM to 1 .6 pM. It also demonstrates quenching in the presence of human serum based samples spiked with various concentrations of CRP.

7.2. Background

The successful design of theranostic constructs has attracted a lot of attention in the field of bioengineering. This is because such agents can simultaneously detect diseases and can deliver drugs at targeted pathologies [175]. Since, its inception, various forms graphene have been widely used in biomedical diagnostics. Some of its advantages include a flat two dimensional nanostructure, high conductivity, ease of functionalization and biocompatibility etc [176][177].

In this study, a molecular beacon, comprised of a quantum dot, gold nanoparticle and a DNA aptamer, has been anchored to a graphene oxide substrate. The beacon operates on the principle of FRET and utilizes the quantum dot – gold nanoparticle as the donor – quencher pair, which are bound to one another via the DNA aptamer (Figure 30). The substrate is conjugated to the beacon via a linker aptamer. The entire complex has been used to detect CRP in both PBS and human serum.

7.3. Methods

7.3.1. Synthesis of sensor complex

The CRP specific DNA aptamer used in this study consists of 40 bases. It was purchased from Biosearch Technologies (Petaluma, CA). The 5'end of the aptamer was functionalized with an amine group while the 3' was modified with a thiol functional group (5'AminoC6/CGAAGGGGATTCGAGGGGTGATTGCGTGCTCCATTTGGTG/Thiol C6 SS 3'). The aptamer was dissolved in 414 μl of Tris Ethylenediamine Tetraethyl Acetate (EDTA) buffer to obtain 100 μM aptamer solution while also preventing cation induced degradation.

100 μl of gold nanoparticle solution was synthesized by adding the same volume of de-ionized water to one vial of gold nanoparticles. This was further added to the aptamer-TCEP mixture in order to achieve a 3:1 ratio between the quencher and the DNA aptamer. The resulting solution was then incubated for 2 hours at room temperature. Subsequently, it was centrifuged twice at 5000 rpm for 15 minutes each using a 3k MWCO filter in order to remove the excess unbound gold nanoparticles from the solution. After each centrifugation, 50 μl of de-ionized water was used to wash the supernatant. The centrifuge used for all centrifugation steps was the Fisher Scientific Accuspin micro (Fisher Scientific, USA).

A 100 μM solution of the 10 nm ssDNA linker (5'd Pyrene-dU-$(AG)_{17}$ A-Amino C7 3') was prepared in ethylene-diamine-tetraacetic acid (EDTA) buffer. 9 μl of the 100 μM linker solution was added to the DNA aptamer/gold nanoparticle mixture in order to facilitate competitive binding in a 7:3 aptamer to linker ratio.

A 100 μl QD solution was synthesized by mixing 87 μl of 10 mM borate buffer (pH 7.4) and 13 μl of carboxylated CdSe/ZnS QD. 100 μl of the QD solution was added to the CRP aptamer/gold nanoparticle/ssDNA linker solution in the presence of 23 μl of 4 μg/μl EDC/Sulfo NHS solution.

The resulting solution was then allowed to shake for 2 hours at room temperature. Subsequently, the samples were centrifuged five times at 7000 rpm for 5 minutes each using a 100k MWCO filter in 50 mM borate buffer (pH 8.3). The supernatant was washed with 50 µl of the 50 mM borate buffer (pH 8.3) after each centrifugation. This step allowed the unbound aptamers and excess EDC to get eliminated from the sensor solution.

1 ml of 500mg/l single layer graphene oxide was added to the filtered molecular beacon solution and incubated overnight. The solutions were subsequently divided into 4 aliquots having equal volumes. These aliquots were then diluted with nuclease free water to reach the final volume of 1 ml. The resulting solutions were then centrifuged until the all unbound molecular beacons were eliminated from the sensor-substrate complex.

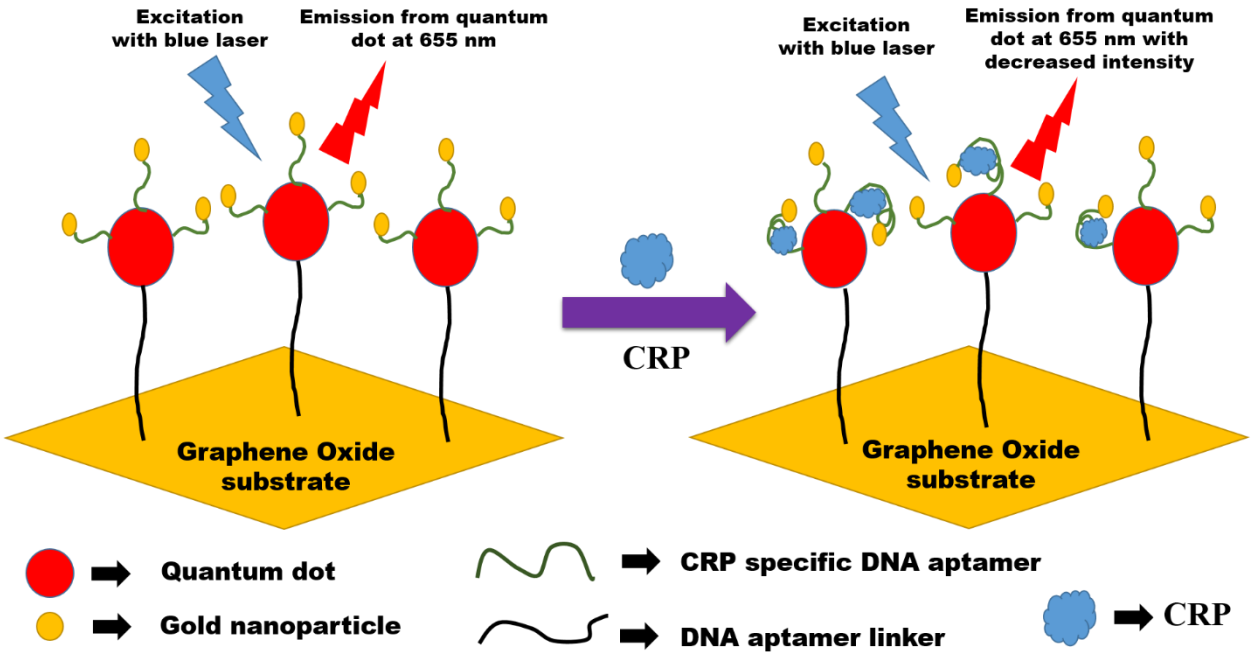

Figure 8. Design and sensing strategy of FRET based molecular beacon anchored to a graphene oxide substrate for CRP sensing.

7.3.2. Optical characterization of sensor complex

CRP stock solutions having 50 pM, 100 pM, 500 pM, 1 nM and 50 nM concentrations were prepared by serially diluting 3 mg/ml (120 μM) solution of the protein in 0.01XPBS. 5 μl of these CRP samples were then added to 750 μl of the sensor/substrate complex. To facilitate binding between the DNA aptamer and the target protein, the cuvette was left undisturbed for an hour, following which, the photoluminescence intensities were recorded using a USB4000 Ocean Optics (Dunedin, FL, USA) spectrophotometer with a continuous 375 nm LED excitation.

To test the selectivity of the sensor / substrate complex towards CRP, 5 μl of the control protein solutions were added to 750 μl sensor solution and allowed to stand undisturbed for an hour to facilitate binding. The control proteins chosen were albumin, TNF-α, TFE, Thrombin and IgG and all of them were kept at a concentration of 1000 pM in the sensor solution respectively.

The clinical samples were prepared by spiking human serum with various concentrations of CRP. The human was mixed with the protein in such a way that the final concentration of CRP in the sensor solution remained 1 pM, 5 pM and 10 pM. The photoluminescence intensities were recorded one hour after adding 5 μl of the spiked serum to 750 μl sensor solution.

7.4. Results and discussion

As shown in Figure 31 (a), the PL intensity decreased with the gradual increase in the concentration of CRP (0 pM – 1000 pM concentration range) in the sensor complex. A similar behavior was observed over multiple samples (Figure 31 (b)). This phenomenon was attributed to the successful binding of the DNA aptamer to the target protein CRP, thereby, causing a change in the distance between the quantum dot – gold nanoparticle pair. This resulted in quenching, shown in Figure 32 (a). The quenching efficiency represented in Figure 32 (a-b) has been calculated using the same equation (4.1) of chapter 4.

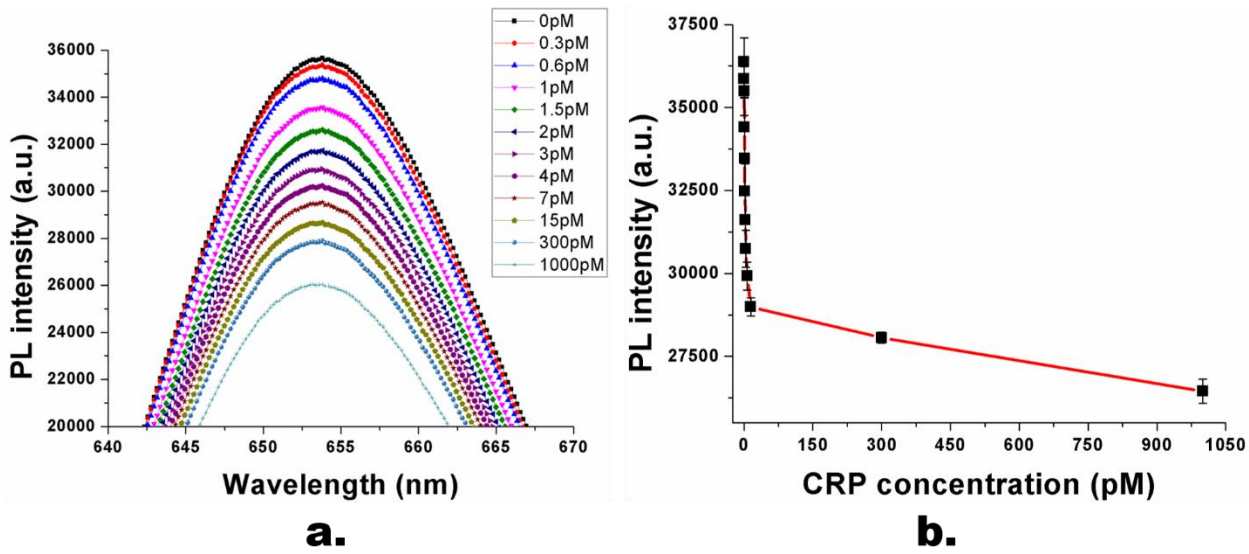

Figure 9. Decrease in photoluminescence intensity with an increase in CRP concentration in the sensor (a). Average photoluminescence intensity decrease over multiple samples with an increase in CRP concentration (b). Experiments were conducted in triplicates (n = 3).

The quenching curve shown in Figure 32 (a) obeys the Hill equation, shown in equation (7.1):

$$Quenching\ Effieciency = \frac{25.052 \times x^{1.346}}{2.872^{1.346} + x^{1.346}} \qquad (7.1)$$

Based on the definition of the Hill's equation, 2.872 pM refers to the concentration at which half of the receptors are occupied by the target. The Hill co-efficient of 1.346 is the slope of the Hill curve and also refers to positive cooperativity with respect to substrate binding. As per Figure 32 (a), the slope of the Hill curve is 1.346 pM. However, Figure 32 (b) shows the linear region of the quenching curve between 0 pM – 4 pM CRP concentration. This curve has a slope of about 3.9157 pM. Therefore, considering both these parameters, it is estimated that the limit of detection falls within a range of 0.5 pM to 1.6 pM using equation (4.3) in chapter 4.

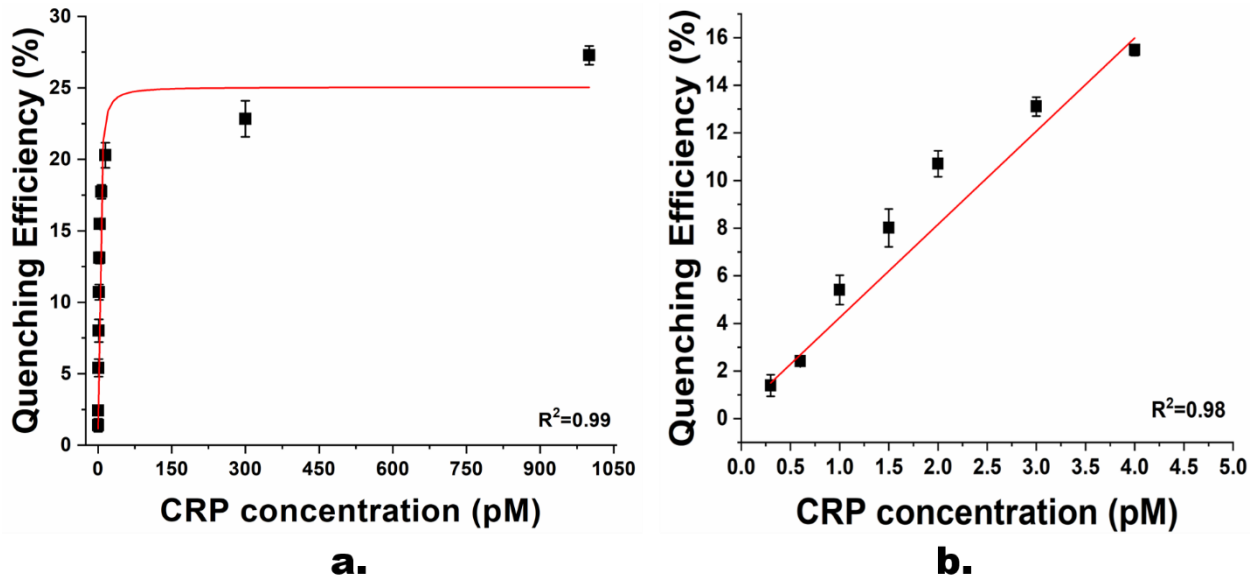

Figure 10. Quenching behavior of the aptasensor/graphene substrate complex (a). Linear quenching region of the sensor complex (b). Experiments were conducted in triplicates (n = 3).

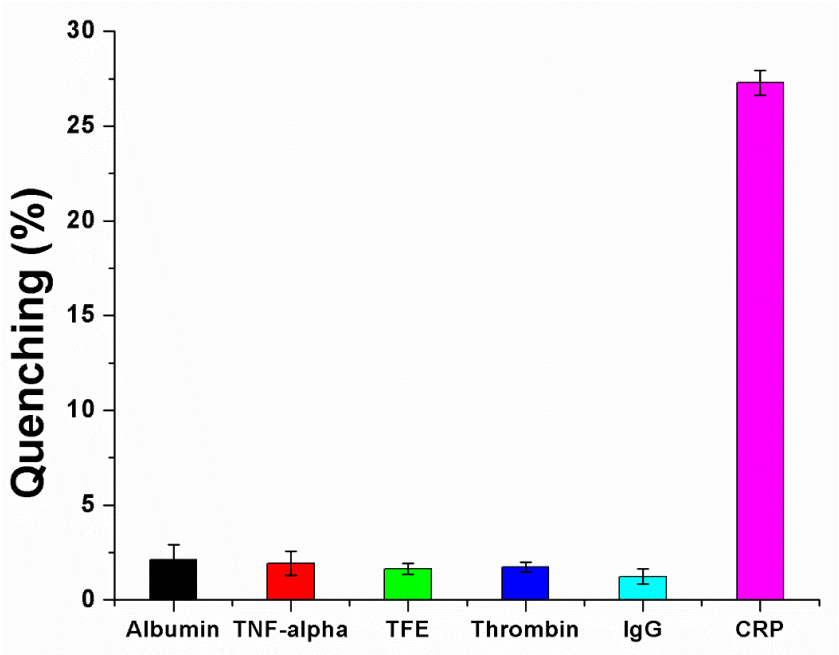

Figure 33. Response of aptasensor/GO substrate complex to various control proteins. Experiments were conducted in triplicates (n = 3).

The sensor complex was tested with various other proteins besides CRP to investigate its specificity towards the target protein. It was observed to have significant selectivity towards CRP compared to the control proteins. As shown in Figure 33, the quenching demonstrated by the

sensor complex towards 1 nM CRP is much greater when compared to the quenching calculated for the other proteins, which were also kept at 1 nM concentration.

The sensor complex was also tested with human serum based samples. These samples were prepared by spiking the serum with various concentrations of CRP. As can be observed in Figure 34, there was a slight cross reactivity with unspiked human serum. This could be attributed to the presence of several proteins including CRP and other small molecules in the serum. However, there was also a gradual increase in quenching with the increase in CRP concentration. Table 12 summarizes the actual quenching efficiencies in the presence of the spiked human serum samples. These values were obtained by subtracting the quenching efficiency of the sensor complex for unspiked human serum from that of the spiked human serum samples.

Table 12. Experimental quenching efficiencies displayed by the aptasensor complex in response to human serum based samples

Sample	**Quenching Efficiency (%) (Experimental)**	**Approx. Quenching Efficiency (%) (Calibration)**
1 pM CRP	3.149 ± 1.245	5.404 ± 0.616
5 pM CRP	6.771 ± 2.294	15.481 ± 0.232
10 pM CRP	10.447 ± 3.395	17.735 ± 0.485

It was observed that the experimental values shown in Table 12 (column 2) was different from the quenching efficiencies calculated for the calibration curve (Figure 32) (shown in column 3 of Table 12). This phenomenon could be attributed to a possible interaction between the graphene oxide substrate with the several types of molecules present in the human serum.

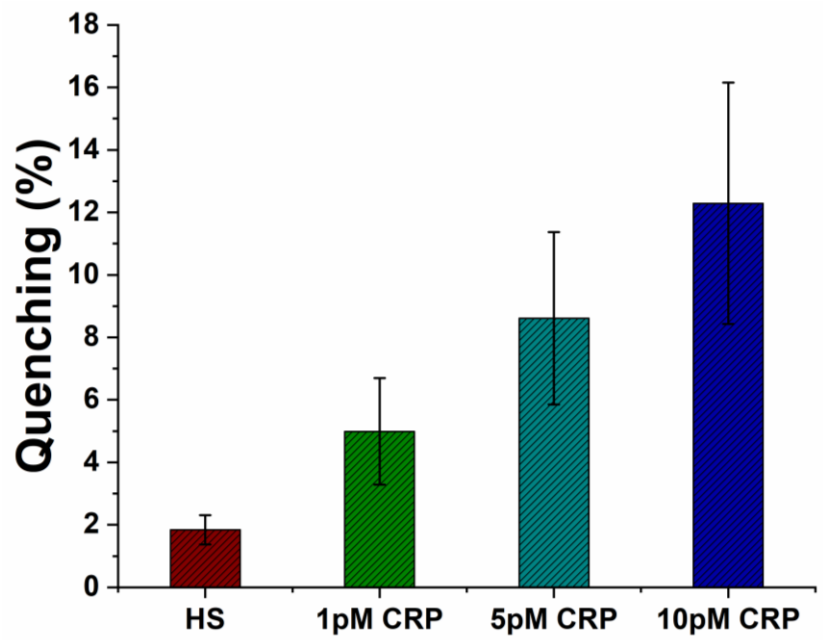

Figure 11. Response of aptasensor/GO substrate complex towards human serum based samples. Experiments were conducted in triplicates (n = 3).

7.5. Conclusion

This work reports a preliminary study on the design and response of a graphene oxide / molecular beacon sensing complex for the detection of CRP. The complex is observed to successfully detect the protein in the concentration region of 0 – 1 nM and has a limit of detection in the range of 0.5 pM to 1.6 pM. The sensor does display some drawbacks, which includes a narrow detection range and disparity between the quenching responses for the human serum based samples and the PBS based calibration samples. However, this work opens up a new avenue in theranostics because the graphene substrate can be conjugated with drugs and used for the delivery of therapeutic agents while utilizing the molecular beacon for diagnostics. Therefore further studies should be done to study the interaction between human serum and graphene oxide.

8. Spectral characterization of biomolecules by using Raman spectroscopy / SERS.

(This chapter is partially copied from my papers submitted to Nature Scientific Reports with the following citation: S. Ghosh, Y. Chen, J. Sebastian, A. George, M. Dutta, and M. A. Stroscio, "A study on the response of FRET based DNA aptasensors in intracellular environment," Sci. Rep, 2019. [Currently under review])

8.1. Raman / SERS spectra of biomarker proteins

8.1.1. Overview

This study employs Raman spectroscopy to analyze the secondary structure and composition of several biomolecules like proteins, enzymes, human serum etc. In this study, the Raman spectra of biomarker proteins like CRP, TNF-α, IL-6 and PCT relevant for the detection of sepsis as well as GA, which as discussed in previous chapters is a biomarker for another inflammatory condition diabetes mellitus. Raman spectra for GA, CRP, IL-6 and PCT have been studied while the SERS spectrum of TNF-α has been analyzed.

8.1.2. Background

Cytokines overproduced from systemic inflammation include pro-inflammatory TNF-α, interleukin-6 (IL-6) and Procalcitonin (PCT), which contribute to the development of infectious diseases like sepsis [178]. New research suggests that the host that may be signaling changes induced by sepsis is TNF-α, which has an amino acid sequence identical to cachectin [179]. PCT serves as an important indicator of neonatal sepsis [180]. Another biomarker protein which plays a significant role as an indicator of sepsis is CRP.

Diabetes mellitus has also been considered as an inflammatory disease. As discussed in the earlier chapters, the most common method of detecting this disease is regular glucose measurements. Recent studies, however, have shed light on two other biomarkers glycated hemoglobin and glycated albumin. While glycated hemoglobin may not be applicable for

diabetic patients with hemolytic disorders, GA has been found to be a relevant indicator for all types of patients.

Therefore, the objective of this study is to obtain the Raman / SERS spectra of the above mentioned biomarker proteins so that it can be used by clinicians and researchers for further investigation of such inflammatory conditions.

8.1.3. Methods

8.1.3.1. SERS substrate

The SERS substrate is a silver nanorod (AgNR) based multiwell array. This is fabricated using the oblique angle deposition technique at the University of Georgia, Athens [181][182]. The substrate consists of glass microscope slide coated with a titanium adhesion layer on which the silver (Ag) nanorods are grown. Polydimethylsiloxane (PDMS) is deposited on the surface to obtain the 4x10 well arrays. To prevent contamination the substrate was kept sealed and in a nitrogen atmosphere until use. Previously published studies show that this substrate has a SERS enhancement factor of more than 10^8.

8.1.3.2. Experimental procedure

The stock solution of TNF-α had a concentration of 10μg/ml. Raman measurements of GA, CRP, IL-6 and PCT were performed with Renishaw inVia Reflex Raman spectrometer using 633 nm HeNe laser excitation and 17.5 mW laser power.

SERS studies of TNF-α were carried out on the silver nanorod (AgNR) based SERS substrate. 5 μl of the sample to be tested is deposited on one of the wells. It is allowed to stand overnight so that it gets adsorbed on the surface of the well.

8.1.4. Results and discussion

8.1.4.1. Analysis of the Raman spectra of Glycated Albumin

The Raman spectrum of GA has been shown in Figure 35 (a). The peaks were assigned their corresponding characteristics using previously published literature and have been summarized in Table 13. The spectrum shows the presence of GA has been reported to have 67% alpha(α)-helix , which is clearly indicated in the Raman spectra shown in Figure 35 (a). Albumin is primarily α - helical in structure. However, literature suggests that glycation leads to a partial conversion of this α - helix structure to a β-sheet. This is confirmed by the Raman spectrum shown in Figure 35 (b). It shows peaks at 1221 cm^{-1}, 1242 cm^{-1} and 1313 cm^{-1}, all of which are indicate β - sheet structure in proteins. Additionally, the peak at 900 cm^{-1} confirm the presence of glucose / ribose, which is another indicator of glycation.

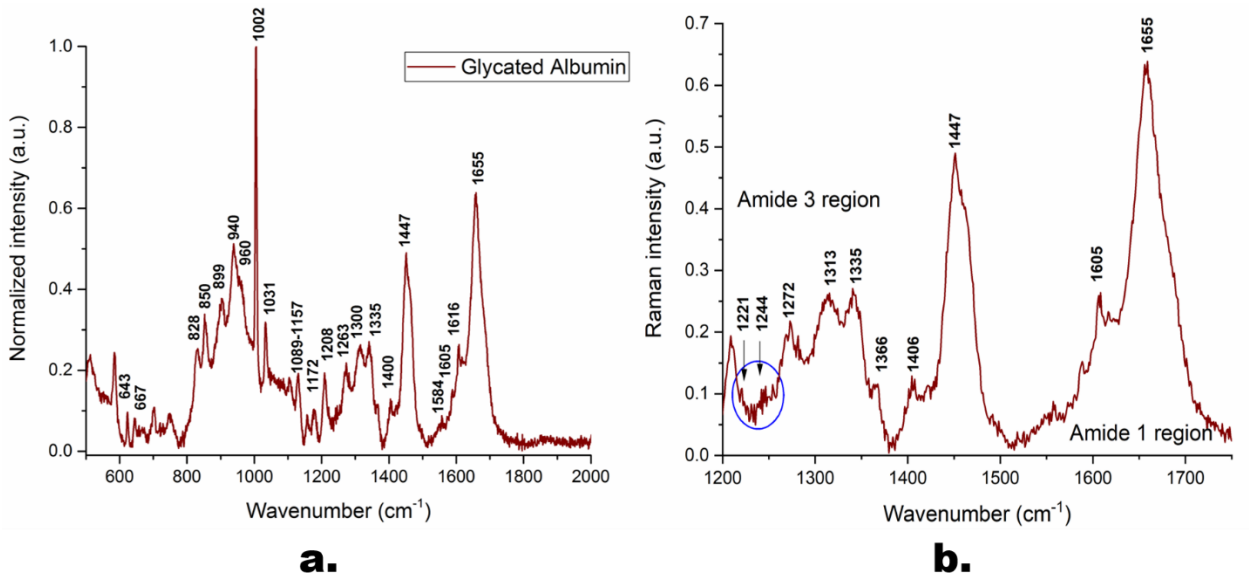

Figure 35. (a) Raman spectrum of Glycated Albumin. (b) Amide regions in the Raman spectrum of the protein. Frequencies in wavenumbers of major peaks have been indicated here.

Table 13. Wavenumber and the possible characteristics of major Raman peaks of Glycated Albumin [183]

Wavelength (cm^{-1})	**Possible characteristics**
622	C-C twisting mode in phenylalanine
647	Tyrosine

700	C-S stretching in methionine
724	C-S stretching in proteins
746	Symmetric breathing of tryptophan
828	Ring breathing mode in tyrosine
850, 1605, 1616	C=C stretching in tyrosine
900	Glucose / Ribose
938	C-C stretching in protein backbone
1005, 1032, 1103, 1208, 1584, 1605	Phenylalanine
1130	C-N stretching in proteins
1157	C-C / C-N stretching in proteins
1172	C-H deformation, Tyrosine
1263, 1335, 1400	Amide 3 region
1318	Amide 3 region (α-helix structure)
1447	CH_2 deformation in proteins
1557	Amide 2, Tryptophan, Tyrosine
1655	Amide 1 region (α-helix structure)

8.1.4.2. Analysis of the Raman spectra of CRP

Figure 36 (a) shows the Raman spectrum of CRP and Table 14 shows the modes assigned to each peak shown in the figure. Additionally Figure 36 (b) focuses on the amide regions of the Raman spectra so that greater information about the secondary structure of the protein can be obtained. CRP is a pentameric protein [184] with 187 amino acids in a single polypeptide chain. It has been found that there are 18 moles of serine followed by 17 moles of valine and 12 moles

each of leucine in 1 mole of CRP [185]. The peak at 3062 cm^{-1} can be attributed to the stretching vibrations of hydroxyl and ammonium groups in serine [186]. Previous studies report that CRP has 50% beta-sheet, 12% α - helix, 24% beta(β)-turn, and 14% unordered structure [187]. The broad peak between 1230-1277 cm^{-1} indicates the presence of the amide 3 band and also confirming the presence of β-sheet (1242 cm^{-1}), unordered structure (1260 cm^{-1}) and α-helix structure (1267 cm^{-1} and 1277 cm^{-1}) [183]. The amide 1 region at 1671 cm^{-1} indicate the presence of an antiparallel β-sheet structure.

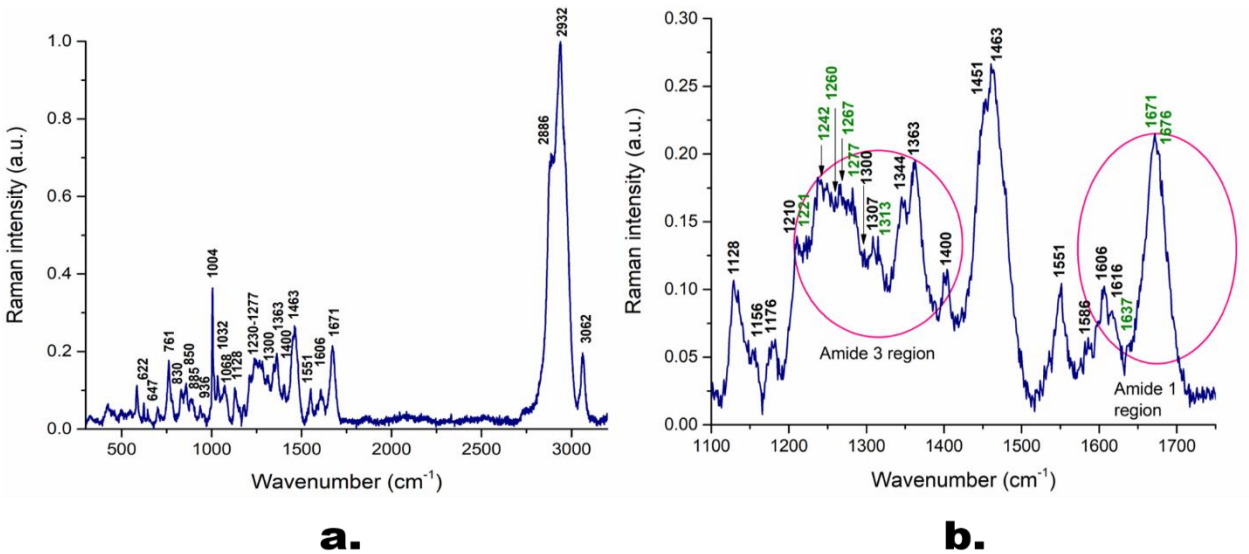

Figure 36. (a) Raman spectrum of C - Reactive Protein. (b) Amide 1 and 3 regions in the Raman spectrum of the protein. Frequencies in wavenumbers of major peaks have been indicated here.

Table 14. Wavenumber and the possible characteristics of major Raman peaks of CRP [183]

Wavenumber (cm^{-1})	**Possible characteristics**
622	C-C twisting mode in Phenylalanine
647	Tyrosine
700	C-S stretching: Methionine
761	C-C stretching mode in amino acid backbone, Tryptophan

830, 850	C_2=C_3 stretching: Tyrosine
885	Tryptophan
936	C-C stretching: protein backbone (α-helix backbone, valine, proline)
1004, 1032	Phenylalanine
1068	Proline
1128	C-N stretching in proteins
1178	Tyrosine
1230-1277	Amide 3 region
1300	Amide 3, C-N stretching
1332	C_a-H deformation, tryptophan
1363	C-H deformation in valine
1400	Amide 3 region
1463	C-H deformation
1551	Amide 2 region, indole ring vibration in tryptophan
1606	Phenylalanine
1671	Amide 1 region
2886	C-H stretching in valine, leucine, lysine
2932	C-H stretching in methionine
3062	Serine

8.1.4.3. Analysis of the Raman spectra of Interleukin-6

IL-6 is composed of about 185 -212 amino acids, out of which leucine has the highest occurrence. As can be observed in Figure 37 and Table 15, the Raman spectrum of IL-6 has prominent peaks at 1083 cm^{-1}, 1337 cm^{-1} and 1395 cm^{-1}, all of which can be attributed to the presence of leucine. Previous studies report that IL-6 has both α-helix and β–sheet structure with a greater α-helix content. This is clearly indicated in the medium sized peak at 981 cm^{-1}, which is attributed to the presence of some β–sheet structure. A stronger peak at 1281 cm^{-1} is indicative of the protein being primarily α-helical in structure.

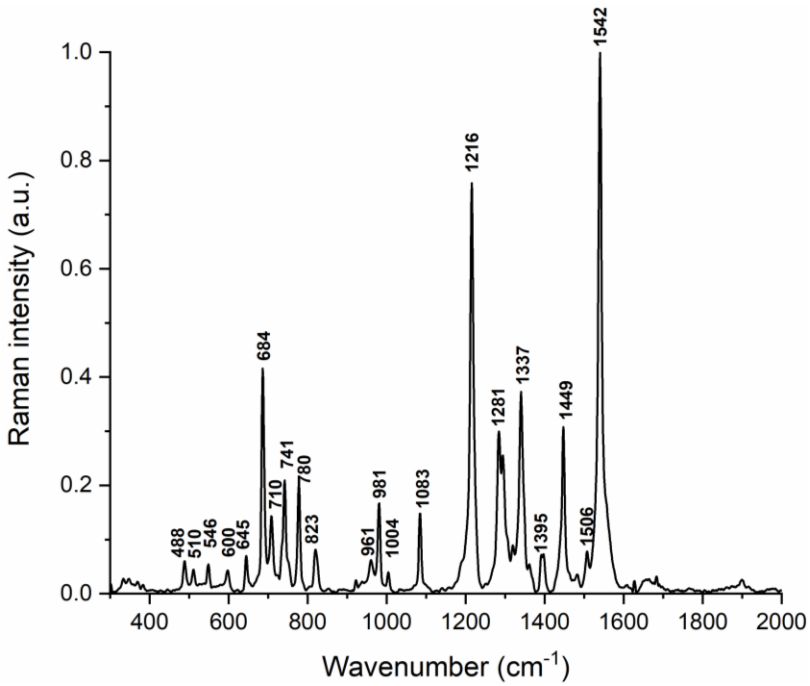

Figure 12. Raman spectrum of Interleukin-6. Frequencies in wavenumbers of major peaks have been indicated here.

Table 15. Wavenumber and the possible characteristics of major Raman peaks of IL-6 [183][188][189][190][191][192][193].

Wavenumber (cm^{-1})	**Possible characteristics**
488	NH_3^+ ion torsion in threonine
510, 546	S-S vibration in cysteine

600	COO^- wagging in glycine
645	C-C twisting in phenylalanine
684	C-S stretching in cysteine
710	CO_2^- wagging in isoleucine
741	Lysine
780	Glutamic acid
823	Tyrosine
961	Tryptophan
981	C-C stretching of β-sheet proteins
1004	Ring deformation in phenylalanine
1083	C-N stretching in leucine
1216	C-N stretching in amino acids
1281	Amide 3 (alpha helix)
1337	Amide 3, CH_2 deformation in leucine
1395	Symmetric CH_2 deformation in leucine
1449	C-H vibration in amino acids
1506	N=H bending
1542	Amide 2

8.1.4.4. Analysis of the Raman spectra of Procalcitonin

Figure 38 (a) represents the Raman spectrum of the biomarker protein Procalcitonin while Table 16 shows the assignments of the peaks derived from the Raman spectrum. The protein, which is the peptide precursor of calcitonin, has a molecular weight of about 13-14 kDa and is composed

of 116 amino acids approximately [180]. As per the Raman spectrum, strong peaks contributed by amino acids like leucine and glycine are observed at 532 cm^{-1} and 591 cm^{-1} respectively. The peak at 482 cm^{-1} couldn't be identified. Figure 38 (b) focuses on the Amide 3 and Amide 1 regions of the protein. Peaks at 1221 cm^{-1} and 1245 cm^{-1} indicate the presence of β-sheet structure while peaks at 1302 cm^{-1}, 1318 cm^{-1}, 1321 cm^{-1} and 1645 cm^{-1} show the predominant presence of the α-helical structure.

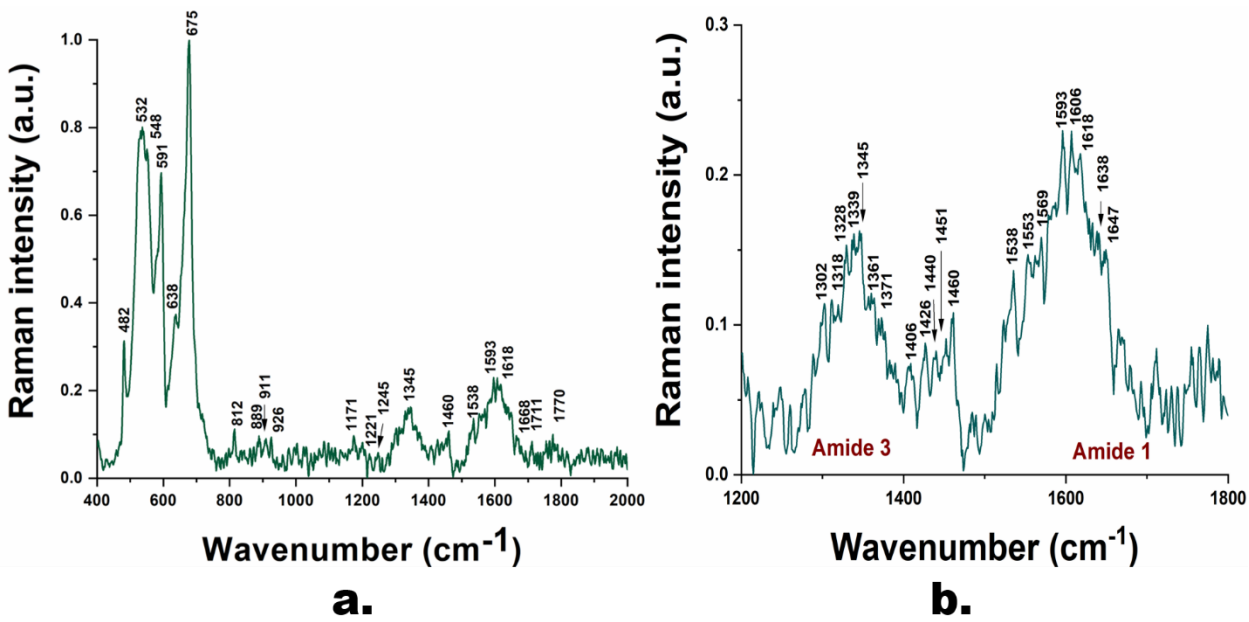

Figure 13. (a) Raman spectrum of Procalcitonin. (b) Amide regions in the Raman spectrum of the protein. Frequencies in wavenumbers of major peaks have been indicated here.

Table 16. Wavenumber and the possible characteristics of major Raman peaks in Procalcitonin [183][188].

Wavenumber (cm^{-1})	**Possible characteristics**
532	CO_2 rocking in leucine
548	CO_2 rocking in valine
591	Glycine
638	C-S stretching in proline

675	Possibly C-S stretching in cysteine
812	Serine
889	Arginine
911	Glutamic acid
926	C-C stretching in alanine
1171	Proline
1221, 1245	Amide 3 (β-sheet structure)
1302, 1318, 1321	α-helix structure in proteins
1345	C-H deformation in leucine
1460	C_β asymmetric rocking in alanine
1538	Amide carbonyl group vibrations
1593	C=C stretching in aromatic amino acids like phenylalanine and tyrosine
1618	Amide 1, C=C stretching in amino acids
1638	Amide 1 (α-helix structure and β-sheet structure)
1645	Amide 1 (α-helix structure)
1668, 1711, 1770	C=O stretching in amino acids like glutamic acid and aspartic acid

8.1.4.5. Analysis of SERS spectra of TNF-α

TNF-α is a cell signaling protein, which has a molecular weight of about 17-22 kDa and is comprised of 145-185 amino acids. Literature suggests that TNF-α is primarily β-sheet in structure [194], which has been clearly indicated by the prominent Raman peaks at 980 cm^{-1},

1222 cm^{-1} and 1243 cm^{-1} in Figure 39. Table 17 summarizes the characteristics assigned to the major peaks marked in the Raman spectrum of the protein.

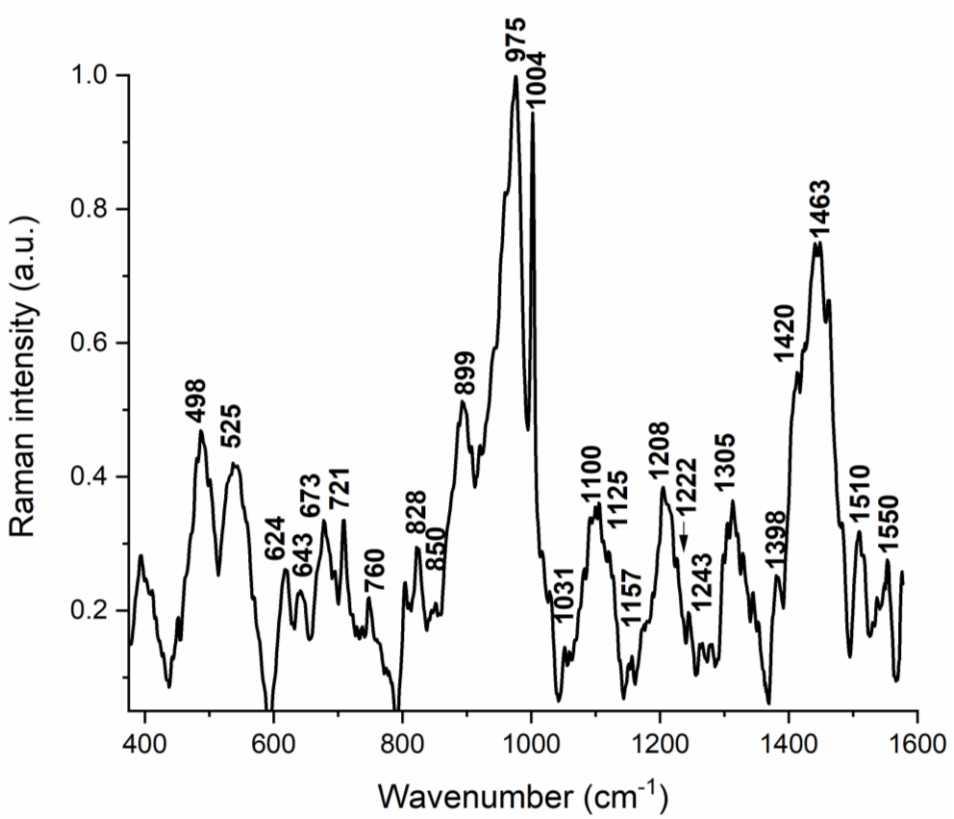

Figure 39. SERS spectrum of TNF-α. Frequencies in wavenumbers of major peaks have been indicated here.

Table 17. Wavenumber and the possible characteristics of major SERS peaks in TNF-α [183][188][195].

Wavenumber (cm^{-1})	**Possible characteristics**
498, 525	S-S vibration in cysteine
624	C-C torsion in phenylalanine
643	Tyrosine
673	C-S stretching in cysteine
721	C-S vibration in tryptophan
828, 850	Tyrosine

899	C-C vibration
943	CCN vibration, C-C vibration
980	β-sheet structure in proteins
1004	Phenylalanine
1100, 1125,1157	C-N vibration
1208	Tyrosine + Phenylalanine, Amide 3 region
1222, 1243	Amide 3 (β-sheet structure)
1305	Amide 3 region, lysine
1398	C=O symmetric stretching , CH_2 deformation in amino acids
1412	C band rocking in lysine
1463	Amide 2, asymmetric bending of CH_3 in leucine
1510	NH_3 symmetric bending in glycine
1550	Amide 2 region

8.2. Raman / SERS of other biomolecules

8.2.1. Background

DSS peptide is a cell penetrating peptide, which is composed of aspartic acid and serine [174]. As mentioned in one of the earlier chapters, it has the ability to drag cargo inside the cell towards the nucleus. It has been employed by our research group to study the response of our aptasensors in intracellular diagnostics.

Furin is a calcium dependent serine protease [196]. It is responsible for proteolytically activating several proprotein substrates and pathogenic agents [197] and also plays a crucial role in cancer metastasis [198] and embryogenesis [197]. Several studies show that furin, a proprotein

convertase (PC), can process various proproteins like the HIV-1 glycoprotein gp160 [199], the insulin receptor [200], the BMP-4 [201][202] etc. Furin has also been demonstrated to be useful biomarkers for cardiovascular risk stratification assessment in type II diabetes mellitus patients [203], autoimmune diseases [204]r as well as in neurodegenerative disorders such as Alzheimer's disease [205] etc. Hence, an analysis of the Raman spectra of furin can be useful in identifying its presence.

PepO is a neutral endopeptidase, which has a molecular weight of 70 kDa approximately. It plays a critical role in bacterial infections. It has been found to be a plasminogen and fibronectin binding protein [206]. Because of its role in host cell invasion during bacterial infections, its structure and composition can contribution to a better understanding of the process. Hence, studying the Raman spectra of PepO can be useful for the clinicians and researchers.

Human serum is an important component of blood and it doesn't contain any red blood cells, white blood cells and clotting factors. It is rich in proteins and therefore it is extensively used in infectious disease detection. Recent studies also prove its potential application in cancer diagnosis [207]. Therefore, a Raman / SERS signature of the healthy serum can be useful in differentiating between diseased serum and the healthy counterpart.

8.2.2. Methods

Raman measurements of DSS peptide, furin, and human serum were performed with Renishaw inVia Reflex Raman spectrometer using 633 nm HeNe laser excitation and 17.5 mW laser power. SERS studies of human serum and PepO were carried out on the silver nanorod (AgNR) based SERS substrate. 5 μl of the sample to be tested is deposited on one of the wells. It is allowed to stand overnight so that it gets adsorbed on the surface of the well.

8.2.3. Results and discussion

8.2.3.1. Analysis of Raman spectra of DSS peptide

The Raman spectrum and the possible peak assignments of the DSS peptide from 300 cm^{-1} to 3100 cm^{-1} have been shown in Figure 40 and Table 18, respectively. Three peaks (410 cm^{-1}, 433 cm^{-1} and 600 cm^{-1}) remained unidentified and hence doesn't have any possible characteristics. The peak at 1232 cm^{-1} corresponds to the Amide 3 region of the peptide while the peak at 1564 cm^{-1} falls in the Amide 2 region of the peptide. Additionally, the peak at 1564 cm^{-1} might also be contributed by COO^- stretching in aspartic acid. The peak at 1671 cm^{-1}, which corresponds to the Amide 1 region of the peptide, also indicates the presence of antiparallel beta sheet structure. Previous studies have shown that the beta sheet structure is important for cellular uptake. Therefore, the structural information from the Raman spectrum provides insight into the cell penetrating characteristic of the peptide.

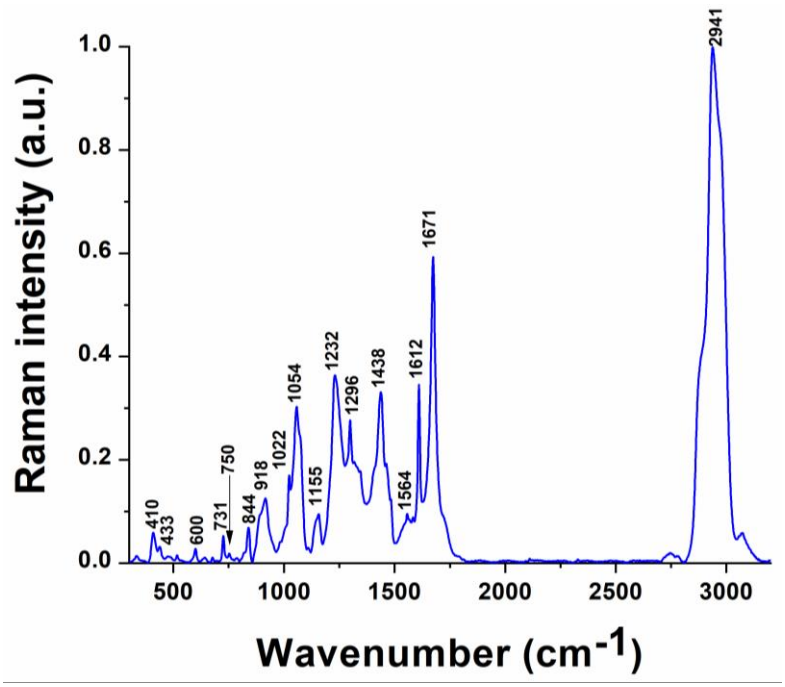

Figure 40. Raman spectrum of DSS peptide. Frequencies in wavenumbers of major characteristic peaks have been indicated here.

Table 18. Wavenumber and the possible characteristics of major peaks indicated in the Raman spectra of DSS peptide [208][209][188][186][210][183][211][212]

Wavenumber (cm^{-1})	**Characteristics**
731	COO^- bending in aspartic acid
838	C-C and C-N stretching in aspartic acid
918	C_α-C_β stretching in serine
1022	Possible β - sheet structure assignment
1054	C_α–C stretching / CH_2 rocking (out of plane) in serine
1155	CH_2 twisting in serine
1232	Amide 3 region (C-N stretching and N-H bending)
1296	C-H bending in serine
1564	Amide 2 region/ COO^- stretching in aspartic acid/lysine
1614	NtH_3^+ asymmetric bending in lysine
1671	Amide 1 region (antiparallel beta sheet structure)
2941	C-H stretching in lysine

8.2.3.2. Analysis of Raman spectra of furin

Figure 41 (a) represents the Raman spectrum of furin from 300 cm^{-1} to 3200 cm^{-1}. Table 19 summarizes the Raman peak assignments for the spectra obtained for furin. The doublet 1232 cm^{-1} and 1239 cm^{-1} shown in Figure 41(b) can be attributed to the amide 3 region of proteins, which demonstrate β - turn or β - sheet like secondary structure [213]. On the other hand, the peak at 1265 cm^{-1}, which also likely falls in the amide 3 region of proteins, indicate that furin also exhibits an alpha helical structure [183]. Previous studies conducted by Henrich et. al. show

that the three dimensional structure of mouse furin contains both helices and β - strands [214]. Weak peaks at around 806 cm^{-1} and 984 cm^{-1} have previously been observed in the amino acids tryptophan and methionine, respectively, but they could not be assigned to any specific functional group [188]. The W7 tryptophan doublet has been usually observed at 1340 cm^{-1} and 1360 cm^{-1} [215][216]. However, in this case, the doublet has been shifted to 1352 cm^{-1} and 1360 cm^{-1}. This band arises due to Fermi resonance between an N_1=C_8 stretching like in-plane vibrations and a combination of out-of-plane vibrations [217]. Strong Raman peaks were observed in the region 2900 cm^{-1} to 3000 cm^{-1}. These peaks correspond to the C-H stretching region, which could possibly arise from the amino acid serine (2908 cm^{-1}) and also from Lysine/ Isoleucine/ Cysteine (2943 cm^{-1}) [212].

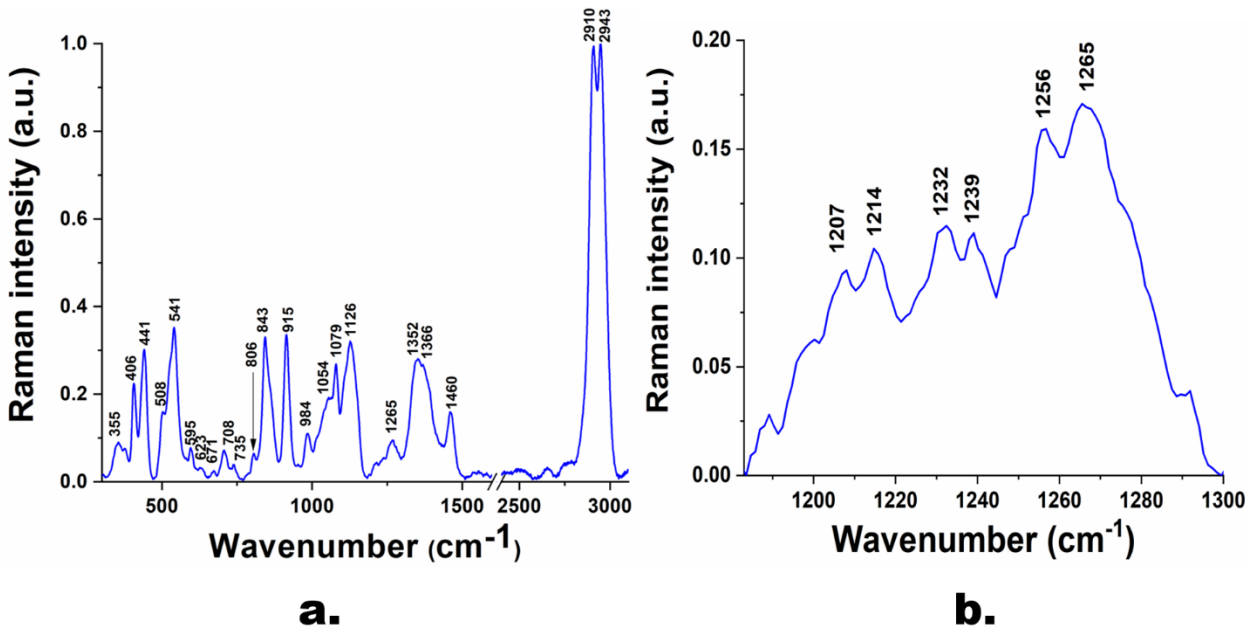

Figure 41. Raman spectrum of furin in the (a) 300 cm^{-1} to 3000 cm^{-1} range and (b) 1100 cm^{-1} to 1300 cm^{-1} range, respectively.

Table 19. Wavenumber and the possible characteristics of the peaks indicated in the Raman spectrum of furin [213][183][188][212][218][219][220][221][222][223][224][225][226]

Wavenumber (cm^{-1})	**Possible peak assignments**
355	C-C-N bending in glycine
406	N-C-C deformation in alanine
441	N-C-S stretching in amino acids
508	C-OH torsion of methoxy group
541	S-S stretching in amino acid cysteine
595	C=O out of plane bending in glutamic acid
623, 671	Ring deformation + C-C stretching mode in histidine
703	CO_2 wagging in threonine
735	C-S stretching (thiocyanate peak with 441cm^{-1})
843	Skeletal stretching vibration in proline
915	N_t-C_α in histidine
1054	C-O & C-N stretching in proteins
1079	C-C vibrations in lysine
1126	C-N stretching vibrations in proteins
1207	NH_2 twisting mode in lysine
1214	C-N stretching ; C-O stretching & C-C_6H_5 stretching in tyrosine
1232, 1239	Amide 3 (β - turn/ β - sheet structure)
1256	Amide 3; Twisting of CH_2 in glutamic acid
1265	Amide 3 (α - helix structure)
1352, 1360	Tryptophan W7 doublet

1462	C-H deformation in serine
2908	C-H stretching in serine
2943	C-H stretching (Lysine, Isoleucine, Cysteine)

8.2.3.3. Analysis of Raman spectra of PepO

Figure 42 represents the Raman spectrum of PepO with the major peaks marked while Table 20 reports the possible assignments corresponding to the peaks. As can be observed, there are two peaks (1266 cm^{-1} and 1316 cm^{-1}), both of which indicate the presence of α-helix structure [183]. Additionally, presence of amino acids such as histidine, tyrosine, leucine etc. have been observed at 675 cm^{-1}, 821 cm^{-1} and 849 cm^{-1} respectively.

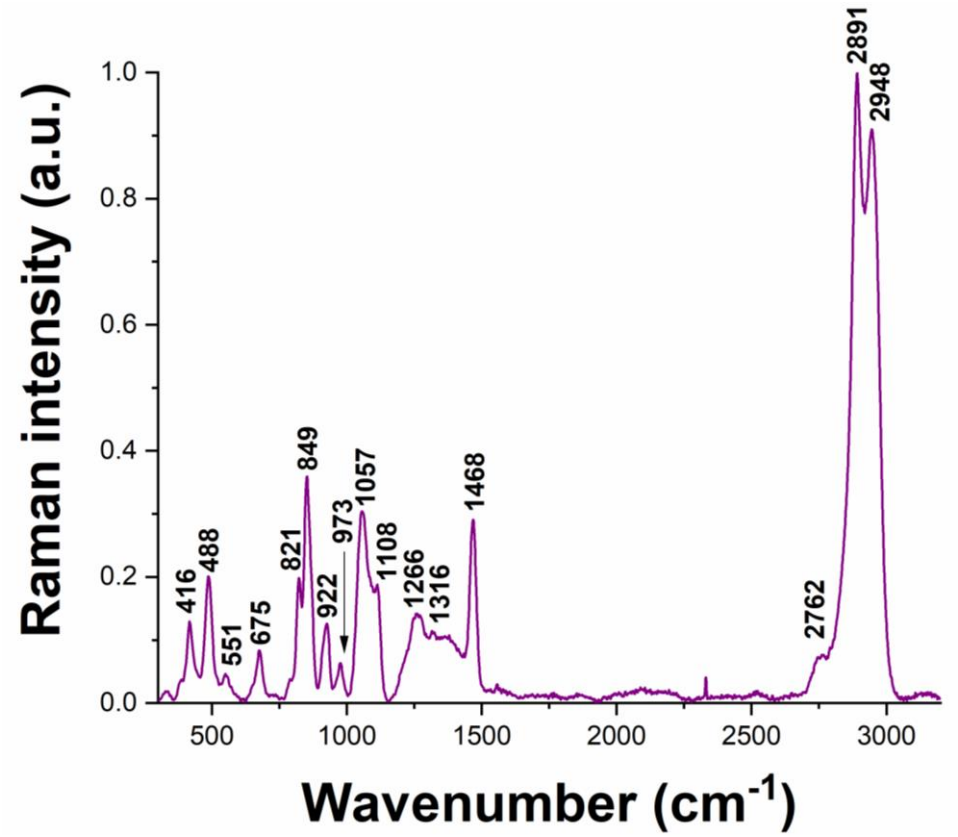

Figure 42. Raman spectrum of PepO. Frequencies in wavenumbers of major peaks have been marked.

Table 20. Wavenumber and the possible characteristics of the Raman spectra of PepO [183][188].

Wavenumber (cm^{-1})	**Possible peak assignments**
416, 488	These two medium peaks could be due to glycerol, which could be residues from their isolation process or Threonine
675	C-C stretching mode in histidine
821	Out of plane ring breathing mode in tyrosine
849	Single bond stretching vibrations in amino acids; CH_3 rocking in leucine
922	C-C stretch of proline ring
973	CH_3 rocking and CCH bending in proteins
1057	C-O and C-N stretching in proteins
1108	Phenylalanine
1266, 1316	Amide 3 (alpha helix structure)
1468	C=N stretching
2891	CH_2 symmetric stretch in proteins
2948	C-H stretching in Isoleucine

8.2.3.4. Analysis of SERS vs. Raman spectrum of human serum

Figure 43 provides a comparison between the Raman and the SERS spectrum of human serum while Table 21 compares the Raman and the SERS peak assignments. Based on the observation in Figure 43, it is quite clear that the SERS spectrum provides more distinctive peaks for complex samples like human serum. Also, as can be seen in Table 21, there have been

considerable shifts between the Raman and the SERS peaks. Since human serum is rich in proteins, presence of several amino acids have been noted at 496 cm^{-1}, 514 cm^{-1}, 524 cm^{-1}, 574 cm^{-1}, 624 cm^{-1}, 856 cm^{-1} etc. Additionally, presence of DNA / RNA molecules have been observed at 785 cm^{-1}, 811 cm^{-1} etc.

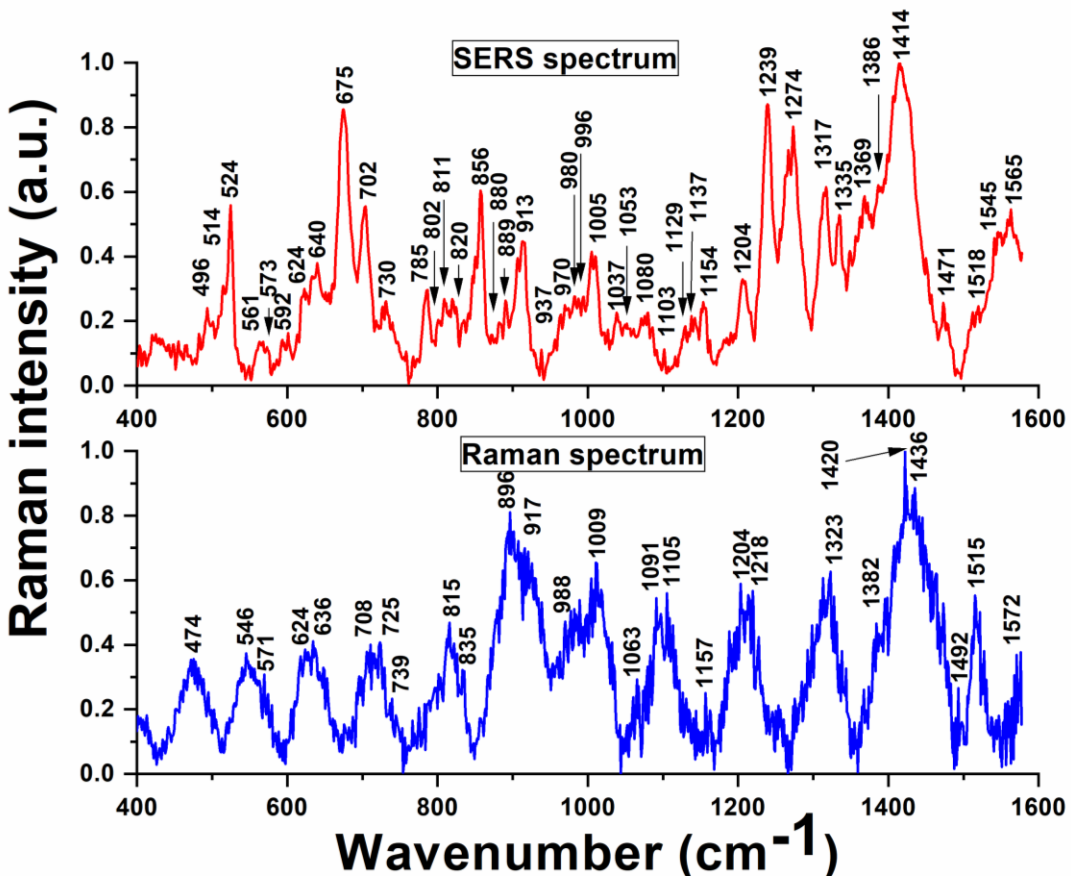

Figure 14. SERS vs. Raman spectrum of human serum. Wavenumbers of major peaks have been marked.

Table 21. Raman vs. SERS peaks in wavenumbers and the possible characteristics of human serum [183][188].

SERS peak (cm^{-1})	**Raman peak (cm^{-1})**	**Possible peak assignments**
496, 514	474	S-S vibration: Cysteine

524	-	S-S vibration: Cysteine, S-S disulfide stretching in proteins
561	546	C-H bending out of plane
573	571	Tryptophan, guanine
590	-	Glycerol
624	624	C-C twisting mode in Phenylalanine
640	636	C-S stretching and C-C twisting in tyrosine
675	708	C-S stretching in cysteine
702	725	C-S stretching: Methionine
732	739	Phosphatidylserine
785	-	Ring breathing modes of DNA/RNA
802	-	Ring breathing mode in uracil
811	-	O-P-O stretching mode: RNA
820	-	C-C stretching: proline and hydroxyproline
828	-	Tyrosine
856	-	Amino acid side chain vibrations: proline and hydroxyproline
880	-	Ring deformation mode, Tryptophan
889	896	Methylene (CH_2) rocking
913	917	Glucose
936	-	C-C stretching: protein backbone (α-helix backbone, valine, proline)
970	-	Phosphate monoester groups in phosphorylated

		proteins
980	988	C-C stretching in β-sheet proteins, =CH bending in lipids
996	-	Glycogen
1005, 1037	1009	Phenylalanine
1053	1063	C-O stretching, C-N stretching in proteins
1080	1091	Phospholipids, Phosphate vibrations in nucleic acids
1103, 1129, 1137, 1154	1105,1157	C-N stretching
1204	1204	Amide 3 region, Vibrations of CH_2 wagging from glycine backbone and side chains of proline
1239, 1274	1218	Amide 3 region
1317	1323	Ring breathing modes of DNA/RNA, C-H deformation in proteins
1335	-	CH_3CH_2 deformation in DNA, Tryptophan
1369	1382	Guanine, lipids, tryptophan
1386	-	CH_3 band
1414	1420	C=C stretching
1471	1492	C=N stretching
1518	1515	C=C stretching in carotenoids
1545	-	C_6-H deformation mode
1565	1572	COO^- stretching

8.2.4. Conclusion

The Raman / SERS spectra of several biomarkers relevant for the detection of sepsis have been studied in this work and their major vibrational modes were identified. Signature spectra of other complex biomolecules such as furin, PepO, DSS and human serum were also presented here. These spectral findings will benefit clinicians and researchers with disease diagnostics and investigation.

9. Conclusion and Future Work

The work reported here presents the findings on two broad categories of research: Optical aptasensors and Raman spectroscopy. The optical aptasensors were found to successfully detect biomarker proteins like GA, TNF-α and CRP as well as metal ions like Ca^{2+}. These aptasensors were also determined to be functional in an intracellular environment in the presence of a cell penetrating peptide called DSS. Therefore, such aptasensors can be potentially incorporated in point of care setups for clinical applications. Future work to study the selectivity of these sensors in different cellular environments can provide more insight into their specificity towards the target analyte.

The graphene oxide based aptasensor was designed to detect CRP. This study opens up an avenue in the field of theranostics because GO can be easily functionalized with therapeutic agents. However, in this reported study, the sensor is able to detect CRP within a small range of concentration. Observations also indicated a difference in the quenching efficiencies for the PBS based samples and the human serum based samples. Hence, future work should involve studying the interaction of GO with human serum and its contents. Also, studies might be conducted to modify the design of the sensor in order to achieve a wider detection concentration range.

The Raman / SERS studies focuses on studying on the composition and secondary structure of various biomolecules. The SERS substrate proved to be a useful tool for studying complex biomolecules such as human serum. Therefore, it can be used in future works for investigating more such molecules. The previously unknown spectrum of furin and PepO, respectively, can be potentially used in understanding pathogenic infection based diseases.

Additionally, the SERS spectrum of human serum can be used as a reference spectra to compare with diseased serums.

Cited Literature

[1] R. Kumar, D. Chaudhari, and R. Kumar, "Biomarkers of sepsis : Recent advancements," *Apollo Med.*, vol. 12, no. 4, pp. 239–242, 2015.

[2] W. Ansar and S. Ghosh, "C-reactive protein and the biology of disease," *Immunol. Res.*, vol. 56, no. 1, pp. 131–142, 2013.

[3] E. O. Chukwuocha, M. C. Onyeaju, and T. S. T. Harry, "Theoretical Studies on the Effect of Confinement on Quantum Dots Using the Brus Equation," *World J. Condens. Matter Phys.*, vol. 2, no. 2, pp. 96–100, 2012.

[4] X. Meshik, "Quantum Dot- and Aptamer-Based Nanostructures for Biological Applications," PhD Thesis, University of Illinois at Chicago, Chicago, USA 2016.

[5] B. O. Dabbousi, J. Rodriguez-Viejo, F. V. Mikulec, J. R. Heine, H. Mattoussi, R. Ober, K. F. Jensen, and M. G. Bawendi, "(CdSe) ZnS core− shell quantum dots: synthesis and characterization of a size series of highly luminescent nanocrystallites," *J. Phys. Chem. B*, vol. 101, no. 46, pp. 9463–9475, 1997.

[6] M. A. Stroscio, M. Dutta, K. Narwani, P. Shi, D. Ramadurai, B. Kohanpour, and S. Rufo, "Integrating and tagging biological structures with nanoscale semiconductor quantum dot structures," in *Biological Nanostructures and Applications of Nanostructures in Biology*, Springer, 2004, pp. 1–36.

[7] K. Kong, C. Kendall, N. Stone, and I. Notingher, "Raman spectroscopy for medical diagnostics—From in-vitro biofluid assays to in-vivo cancer detection," *Adv. Drug Deliv. Rev.*, vol. 89, pp. 121–134, 2015.

[8] K. J. I. Ember, M. A. Hoeve, S. L. McAughtrie, M. S. Bergholt, B. J. Dwyer, M. M. Stevens, K. Faulds, S. J. Forbes, and C. J. Campbell, , "Raman spectroscopy and regenerative medicine: a review," *npj Regen. Med.*, vol. 2, no. 1, pp. 1-10, 2017.

Cited Literature (continued)

[9] M. Nyberg, K. Ramser, and O. A. Lindahl, "Cancer detection probe combining Raman and resonance sensor technology-experimental study on temperature dependence and effects of molding," in *World Congress on Medical Physics and Biomedical Engineering,* Munich, Germany, Sept. 7-12, 2009, pp. 331–334.

[10] G. S. Bumbrah and R. M. Sharma, "Raman spectroscopy–Basic principle, instrumentation and selected applications for the characterization of drugs of abuse," *Egypt. J. Forensic Sci.*, vol. 6, no. 3, pp. 209–215, 2016.

[11] S. Siddhanta and C. Narayana, "Surface enhanced Raman spectroscopy of proteins: implications for drug designing," *Nanomater. Nanotechnol.*, vol. 2, pp. 1, 2012.

[12] S. L. McCall, P. M. Platzman, and P. A. Wolff, "Surface enhanced Raman scattering," *Phys. Lett. A,* vol. 77, no. 5, pp. 381–383, 1980.

[13] E. J. Zeman and G. C. Schatz, "An accurate electromagnetic theory study of surface enhancement factors for silver, gold, copper, lithium, sodium, aluminum, gallium, indium, zinc, and cadmium," *J. Phys. Chem.*, vol. 91, no. 3, pp. 634–643, 1987.

[14] C. Feng, S. Dai, and L. Wang, "Optical aptasensors for quantitative detection of small biomolecules: A review," *Biosens. Bioelectron.*, vol. 59, pp. 64–74, 2014.

[15] K. L. Brenneman, S. Poduri, M. A. Stroscio, and M. Dutta, "Optical detection of lead (II) ions using DNA-based nanosensor," *IEEE Sens. J.*, vol. 13, no. 5, pp. 1783–1786, 2013.

[16] X. Meshik, K. Xu, M. Dutta, and M. A. Stroscio, "Optical detection of lead and potassium ions using a quantum-dot-based aptamer nanosensor," *IEEE Trans. Nanobioscience*, vol. 13, no. 2, pp. 161–164, 2014.

[17] K. L. Brenneman, B. Sen, M. A. Stroscio, and M. Dutta, "Aptamer-based optical bionano sensor for mercury (II) ions," in *2010 IEEE Nanotechnology Materials and Devices Conference,* Monterey, CA, USA, Oct 12-15, 2010, pp. 221–224.

Cited Literature (continued)

[18] A. Darbandi, D. Datta, K. Patel, G. Lin, M. A. Stroscio, and M. Dutta, "Molecular beacon anchored onto a graphene oxide substrate," *Nanotechnology*, vol. 28, no. 37, p. 375501, 2017.

[19] D. Datta, K. Sarkar, S. Mukherjee, X. Meshik, M. A. Stroscio, and M. Dutta, "Graphene oxide and DNA aptamer based sub-nanomolar potassium detecting optical nanosensor," *Nanotechnology*, vol. 28, no. 32, p. 325502, 2017.

[20] T.-C. Wu, S. Biswas, M. Dutta, and M. A. Stroscio, "Quantum-dot-based aptamer beacon for the detection of potassium ions," *IEEE Trans. Nanotechnol.*, vol. 10, no. 5, pp. 991–995, 2011.

[21] Y. Xiao, A. A. Lubin, A. J. Heeger, and K. W. Plaxco, "Label-free electronic detection of thrombin in blood serum by using an aptamer-based sensor," *Angew. Chemie Int. Ed.*, vol. 44, no. 34, pp. 5456–5459, 2005.

[22] J. Zhao, Y. Zhang, H. Li, Y. Wen, X. Fan, F. Lin, L. Tan, and S. Yao, "Ultrasensitive electrochemical aptasensor for thrombin based on the amplification of aptamer–AuNPs–HRP conjugates," *Biosens. Bioelectron.*, vol. 26, no. 5, pp. 2297–2303, 2011.

[23] S. Farid, X. Meshik, M. Choi, S. Mukherjee, Y. Lan, D. Parikh, S. Poduri, U. Baterdene, C. E. Huang, and Y. Y. Wang, P. Burke, M. Dutta, and M. A. Stroscio, "Detection of Interferon gamma using graphene and aptamer based FET-like electrochemical biosensor," *Biosens. Bioelectron.*, vol. 71, pp. 294–299, 2015.

[24] S. Mukherjee, X. Meshik, M. Choi, S. Farid, D. Datta, Y. Lan, S. Poduri, K. Sarkar, U. Baterdene, C. E. Huang, Y. Y. Wang, P. Burke, M. Dutta, and M. A. Stroscio, "A graphene and aptamer based liquid gated FET-like electrochemical biosensor to detect adenosine triphosphate," *IEEE Trans. Nanobioscience*, vol. 14, no. 8, pp. 967–972, 2015.

[25] D. Datta, X. Meshik, S. Mukherjee, K. Sarkar, M. Choi, M. Mazouchi, S. Farid, Y. Y. Wang, P. Burke, M. Dutta, and M. A. Stroscio, "Submillimolar Detection of Adenosine Monophosphate Using Graphene-Based Electrochemical Aptasensor," vol. 16, no. 2, pp. 196–202, 2017.

Cited Literature (continued)

[26] Y. Wang, Z. Li, D. Hu, C.-T. Lin, J. Li, and Y. Lin, "Aptamer/graphene oxide nanocomplex for in situ molecular probing in living cells," *J. Am. Chem. Soc.*, vol. 132, no. 27, pp. 9274–9276, 2010.

[27] Z. Liu, J. T. Robinson, X. Sun, and H. Dai, "PEGylated nanographene oxide for delivery of water-insoluble cancer drugs," *J. Am. Chem. Soc.*, vol. 130, no. 33, pp. 10876–10877, 2008.

[28] U. Ladiwala, A. Bankapur, B. Thakur, C. Santhosh, and D. Mathur, "Raman spectroscopic detection of rapid, reversible, early-stage inflammatory cytokine-induced apoptosis of adult hippocampal progenitors/stem cells," *arXiv Prepr. arXiv1401.7497*, 2014.

[29] S. Ghosh, D. Datta, M. Cheema, M. Dutta, and M. A. Stroscio, "Aptasensor based optical detection of glycated albumin for diabetes mellitus diagnosis," *Nanotechnology*, vol. 28, no. 43, pp. 435505, 2017.

[30] W. H. Organization, "Global report on diabetes," 2016. [Online]. Available: https://apps.who.int/iris/bitstream/handle/10665/204871/9789241565257_eng.pdf;jsessionid=F62EED676663E6E97157985D08C0EAA6?sequence=1

[31] "About Diabetes," *International Diabetes Federation*, 2015. [Online]. Available: http://www.idf.org/about-diabetes.

[32] "Hyperglycemia (High Blood Glucose)," *American Diabetes Association*. [Online]. Available: http://www.diabetes.org/living-with-diabetes/treatment-and-care/blood-glucose-control/hyperglycemia.html.

[33] H. F. Bunn, K. H. Gabbay, and P. M. Gallop, "The glycosylation of hemoglobin: relevance to diabetes mellitus," *Science (80-.).*, vol. 200, no. 4337, pp. 21–27, 1978.

[34] T. Kouzuma, T. Usami, M. Yamakoshi, M. Takahashi, and S. Imamura, "An enzymatic method for the measurement of glycated albumin in biological samples," *Clin. Chim. Acta*, vol. 324, no. 1, pp. 61–71, 2002.

Cited Literature (continued)

[35] P. Reed, D. Bhatnagar, H. Dhar, and P. H. Winocour, "Precise measurement of glycated serum albumin by column affinity chromatography and immunoturbidimetry," *Clin. Chim. acta*, vol. 161, no. 2, pp. 191–199, 1986.

[36] M. Inaba, S. Okuno, Y. Kumeda, S. Yamada, Y. Imanishi, T. Tabata, M. Okamura, S. Okada, T. Yamakawa, and E. Ishimura, "Glycated albumin is a better glycemic indicator than glycated hemoglobin values in hemodialysis patients with diabetes: effect of anemia and erythropoietin injection," *J. Am. Soc. Nephrol.*, vol. 18, no. 3, pp. 896–903, 2007.

[37] M. Koga, "Glycated albumin; clinical usefulness," *Clin. Chim. Acta*, vol. 433, pp. 96–104, 2014.

[38] J. Anguizola, R. Matsuda, O. S. Barnaby, K. S. Hoy, C. Wa, E. DeBolt, M. Koke, and D. S. Hage, "Review: Glycation of human serum albumin," *Clin. Chim. Acta*, vol. 425, pp. 64–76, 2013.

[39] N. Furusyo and J. Hayashi, "Glycated albumin and diabetes mellitus," *Biochim. Biophys. Acta (BBA)-General Subj.*, vol. 1830, no. 12, pp. 5509–5514, 2013.

[40] M. Koga and S. Kasayama, "Clinical impact of glycated albumin as another glycemic control marker," *Endocr. J.*, vol. 57, no. 9, pp. 751–762, 2010.

[41] M. P. Cohen, "Intervention strategies to prevent pathogenetic effects of glycated albumin," *Arch. Biochem. Biophys.*, vol. 419, no. 1, pp. 25–30, 2003.

[42] L. C. Maillard, "Action des acidesamines sur les sucres: formation des melanoidines par voie methodique," *CR Acad. Sci.(Paris)*, vol. 154, pp. 66–68, 1912.

[43] H. E. Nursten, *The Maillard reaction: chemistry, biochemistry, and implications*. Royal Society of Chemistry, Cambridge, 2005.

Cited Literature (continued)

[44] A. Lapolla, D. Fedele, R. Reitano, L. Bonfante, M. Guizzo, R. Seraglia, M. Tubaro, P. Traldi, "Mass spectrometric study of in vivo production of advanced glycation end-products/peptides," *J. mass Spectrom.*, vol. 40, no. 7, pp. 969–972, 2005.

[45] A. Lapolla, D. Fedele, R. Seraglia, and P. Traldi, "The role of mass spectrometry in the study of non-enzymatic protein glycation in diabetes: An update," *Mass Spectrom. Rev.*, vol. 25, no. 5, pp. 775–797, 2006.

[46] Q. Zhang, J. M. Ames, R. D. Smith, J. W. Baynes, and T. O. Metz, "A perspective on the Maillard reaction and the analysis of protein glycation by mass spectrometry: probing the pathogenesis of chronic disease," *J. Proteome Res.*, vol. 8, no. 2, pp. 754–769, 2008.

[47] A. I. Ledesma-Osuna, G. Ramos-Clamont, and L. Vázquez-Moreno, "Characterization of bovine serum albumin glycated with glucose, galactose and lactose," *Acta Biochim Pol*, vol. 55, no. 3, pp. 491–497, 2008.

[48] P. Rondeau and E. Bourdon, "The glycation of albumin: structural and functional impacts," *Biochimie*, vol. 93, no. 4, pp. 645–658, 2011.

[49] T. Kouzuma, Y. Uemastu, T. Usami, and S. Imamura, "Study of glycated amino acid elimination reaction for an improved enzymatic glycated albumin measurement method," *Clin. Chim. Acta*, vol. 346, no. 2, pp. 135–143, 2004.

[50] T. J. Lyons, "Glycation and oxidation: a role in the pathogenesis of atherosclerosis," *Am. J. Cardiol.*, vol. 71, no. 6, pp. B26–B31, 1993.

[51] S. Chesne, P. Rondeau, S. Armenta, and E. Bourdon, "Effects of oxidative modifications induced by the glycation of bovine serum albumin on its structure and on cultured adipose cells," *Biochimie*, vol. 88, no. 10, pp. 1467–1477, 2006.

[52] N. Ranjan Singh, P. Rondeau, L. Hoareau, and E. Bourdon, "Identification of preferential protein targets for carbonylation in human mature adipocytes treated with native or glycated albumin," *Free Radic. Res.*, vol. 41, no. 10, pp. 1078–1088, 2007.

Cited Literature (continued)

[53] D. Datta, X. Meshik, S. Mukherjee, K. Sarkar, M. S. Choi, M. Mazouchi, S. Farid, Y. Y. Wang, P. J. Burke, M. Dutta, and M. A. Stroscio, "Sub-millimolar Detection of Adenosine Monophosphate using Graphene-based Electrochemical Aptasensor," *IEEE Trans. Nanotechnol.*, vol. 16, no. 2, pp. 196-202, 2017.

[54] B. Wu, R. Jiang, Q. Wang, J. Huang, X. Yang, K. Wang, W. Li, N. Chen, and Q. Li, "Detection of C-reactive protein using nanoparticle-enhanced surface plasmon resonance using an aptamer-antibody sandwich assay," *Chem. Commun.*, vol. 52, no. 17, pp. 3568–3571, 2016.

[55] C.-H. Leung, D. S.-H. Chan, H.-Z. He, Z. Cheng, H. Yang, and D.-L. Ma, "Luminescent detection of DNA-binding proteins," *Nucleic Acids Res.*, vol. 40, no. 3, pp. 941–955, 2012.

[56] T. Heyduk and E. Heyduk, "Molecular beacons for detecting DNA binding proteins," *Nat. Biotechnol.*, vol. 20, no. 2, pp. 171–176, 2002.

[57] J. J. Li, X. Fang, S. M. Schuster, and W. Tan, "Molecular beacons: a novel approach to detect protein–DNA interactions," *Angew. Chemie*, vol. 112, no. 6, pp. 1091–1094, 2000.

[58] Q. Wang, L. Chen, Y. Long, H. Tian, and J. Wu, "Molecular beacons of xeno-nucleic acid for detecting nucleic acid," *Theranostics*, vol. 3, no. 6, pp. 395–408, 2013.

[59] S. A. E. Marras, S. Tyagi, and F. R. Kramer, "Real-time assays with molecular beacons and other fluorescent nucleic acid hybridization probes," *Clin. Chim. Acta*, vol. 363, no. 1, pp. 48–60, 2006.

[60] K. L. Brenneman, "DNA-based Nanoconstructs for the Detection of Ions and Biomolecules with Related Raman/SERS Signature Studies", PhD Thesis, University of Illinois at Chicago, Chicago, USA, 2013.

Cited Literature (continued)

[61] R. Paroni, F. Ceriotti, R. Galanello, G. B. Leoni, A. Panico, E. Scurati, R. Paleari, L. Chemello, V. Quaino, and L. Scaldaferri, "Performance characteristics and clinical utility of an enzymatic method for the measurement of glycated albumin in plasma," *Clin. Biochem.*, vol. 40, no. 18, pp. 1398–1405, 2007.

[62] M. Yamaguchi, S. Kambe, T. Eto, M. Yamakoshi, T. Kouzuma, and N. Suzuki, "Point of care testing system via enzymatic method for the rapid, efficient assay of glycated albumin," *Biosens. Bioelectron.*, vol. 21, no. 3, pp. 426–432, 2005.

[63] M. Hatada, W. Tsugawa, E. Kamio, N. Loew, D. C. Klonoff, and K. Sode, "Development of a screen-printed carbon electrode based disposable enzyme sensor strip for the measurement of glycated albumin," *Biosens. Bioelectron.*, vol. 88, pp. 167–173, 2017.

[64] A. C. Silver, E. Lamb, W. R. Cattell, and A. B. S. J. Dawnay, "Investigation and validation of the affinity chromatography method for measuring glycated albumin in serum and urine," *Clin. Chim. acta*, vol. 202, no. 1–2, pp. 11–22, 1991.

[65] K. Yasukawa, F. Abe, N. Shida, Y. Koizumi, T. Uchida, K. Noguchi, and K. Shima, "High-performance affinity chromatography system for the rapid, efficient assay of glycated albumin," *J. Chromatogr. A*, vol. 597, no. 1–2, pp. 271–275, 1992.

[66] M. Rendell, K. Rasbold, J. Nierenberg, R. Krohn, G. Hermanson, D. Klenk, P. K. Smith "Comparison and contrast of affinity chromatographic determinations of plasma glycated albumin and total glycated plasma protein," *Clin. Biochem.*, vol. 19, no. 4, pp. 216–220, 1986.

[67] Y. Yamamoto, Y. Tahara, T. Cha, Y. Noma, M. Fukuda, E. Yamato, H. Yoneda, F. Hashimoto, C. Ohboshi, and M. Hirota, "Radioimmunoassay of glycated serum protein using monoclonal antibody to glucitollysine and coomassie-brilliant-blue-coated polystyrene beads.," *Diabetes Res.*, vol. 11, no. 1, pp. 45–49, 1989.

[68] K. Ikeda, Y. Sakamoto, Y. Kawasaki, T. Miyake, K. Tanaka, T. Urata, Y. Katayama, S. Ueda, and S. Horiuchi, "Determination of glycated albumin by enzyme-linked boronate immunoassay (ELBIA)," *Clin. Chem.*, vol. 44, no. 2, pp. 256–263, 1998.

Cited Literature (continued)

[69] R. Wilson and A. P. F. Turner, "Glucose oxidase: an ideal enzyme," *Biosens. Bioelectron.*, vol. 7, no. 3, pp. 165–185, 1992.

[70] A. L. Lehninger, *Biochemistry*. New York: Worth Publishers, 1977.

[71] Y. Fan, X. Tan, X. Liu, X. Ou, S. Chen, and S. Wei, "A novel non-enzymatic electrochemiluminescence sensor for the detection of glucose based on the competitive reaction between glucose and phenoxy dextran for concanavalin A binding sites," *Electrochim. Acta*, vol. 180, pp. 471–478, 2015.

[72] R. Pandey, N. C. Dingari, N. Spegazzini, R. R. Dasari, G. L. Horowitz, and I. Barman, "Emerging trends in optical sensing of glycemic markers for diabetes monitoring," *TrAC Trends Anal. Chem.*, vol. 64, pp. 100–108, 2015.

[73] N. C. Dingari, G. L. Horowitz, J. W. Kang, R. R. Dasari, and I. Barman, "Raman spectroscopy provides a powerful diagnostic tool for accurate determination of albumin glycation," *PLoS One*, vol. 7, no. 2, p. e32406, 2012.

[74] M. Kameya, W. Tsugawa, M. Yamada-Tajima, M. Hatada, K. Suzuki, A. Sakaguchi-Mikami, S. Ferri, D. C. Klonoff, and K. Sode, "Electrochemical sensing system employing fructosamine 6-kinase enables glycated albumin measurement requiring no proteolytic digestion," *Biotechnol. J.*, vol. 11, no. 6, pp. 797–804, 2016.

[75] M. Kameya, A. Sakaguchi-Mikami, S. Ferri, W. Tsugawa, and K. Sode, "Advancing the development of glycated protein biosensing technology: next-generation sensing molecules," *J. Diabetes Sci. Technol.*, vol. 9, no. 2, pp. 183–191, 2015.

[76] Y. Inoue, M. Inoue, M. Saito, H. Yoshikawa, and E. Tamiya, "Sensitive detection of glycated albumin in human serum albumin using electrochemiluminescence," *Anal. Chem.*, vol. 89, no. 11, pp. 5909–5915, 2017.

[77] E. Fujii, K. Shimizu, Y. K. Kurokawa, A. Endo, S. I. Sasaki, K. Kurihara, D. Citterio, H. Yamazaki, and K. Suzuki, "Determination of glycosylated albumin using surface plasmon resonance sensor," *Bunseki Kagaku*, vol. 52, no. 5, pp. 311–317, 2003.

Cited Literature (continued)

[78] C. Apiwat, P. Luksirikul, P. Kankla, P. Pongprayoon, K. Treerattrakoon, K. Paiboonsukwong, S. Fucharoen, T. Dharakul, and D. Japrung, "Graphene based aptasensor for glycated albumin in diabetes mellitus diagnosis and monitoring," *Biosens. Bioelectron.*, vol. 82, pp. 140–145, 2016.

[79] M. Zuker, "Mfold web server for nucleic acid folding and hybridization prediction," *Nucleic Acids Res.*, vol. 31, no. 13, pp. 3406–3415, 2003.

[80] J. SantaLucia, "A unified view of polymer, dumbbell, and oligonucleotide DNA nearest-neighbor thermodynamics," *Proc. Natl. Acad. Sci.*, vol. 95, no. 4, pp. 1460–1465, 1998.

[81] N. Peyret, "Prediction of nucleic acid hybridization: parameters and algorithms", PhD Thesis, Wayne State University, Detroit, USA, 2000.

[82] A. Arasteh, S. Farahi, M. Habibi-Rezaei, and A. A. Moosavi-Movahedi, "Glycated albumin: an overview of the in vitro models of an in vivo potential disease marker," *J. Diabetes Metab. Disord.*, vol. 13, no. 1, p. 49, 2014.

[83] N. M. Luscombe, R. A. Laskowski, and J. M. Thornton, "Amino acid–base interactions: a three-dimensional analysis of protein–DNA interactions at an atomic level," *Nucleic Acids Res.*, vol. 29, no. 13, pp. 2860–2874, 2001.

[84] R. Testa, E. Guerra, A. R. Bonfigli, N. Di Gaetano, G. Santini, and F. Ceriotti, "Analytical performances of an enzymatic assay for the measurement of glycated albumin," *J. Appl. Lab. Med.*, vol. 1, no. 2, pp. 162-171, 2016.

[85] S. Bunyarataphan, L. Maruset, K. Paiboonsukwong, S. Fucharoen, T. Dharakul, and D. Japrung, "Glycated albumin detection using electrochemical aptasensor for screening and monitoring of diabetes mellitus," in *Meeting Abstracts*, 2017, no. 42, p. 1956.

[86] T. Kohzuma, T. Yamamoto, Y. Uematsu, Z. K. Shihabi, and B. I. Freedman, "Basic performance of an enzymatic method for glycated albumin and reference range determination," *J. Diabetes Sci. Technol.*, vol. 5, no. 6, pp. 1455–1462, 2011.

Cited Literature (continued)

[87] K. Kobayashi, K. Yoshimoto, K. Hirauchi, and K. Uchida, "Determination of glycated proteins in biological samples based on colorimetry of 2-keto-glucose released with hydrazine," *Biol. Pharm. Bull.*, vol. 17, no. 3, pp. 365–369, 1994.

[88] PRD.7.ZQ5.10000007101, "Product Specification." [Online]. Available: http://www.sigmaaldrich.com/Graphics/COfAInfo/SigmaSAPQM/SPEC/H4/H4522/H4522-BULK_____SIGMA____.pdf.

[89] S. Ghosh, D. Datta, S. Chaudhry, M. Dutta, and M. A. Stroscio, "Rapid detection of Tumor Necrosis Factor-alpha using quantum dot based optical aptasensor," *IEEE Trans. Nanobioscience*, vol. 17, no. 4, pp. 417–423, 2018.

[90] J. D. Fisher, M. V Dileo, and W. J. Federspiel, "Investigating Cytokine Binding Using a Previously Reported TNF-Specific Aptamer," vol. 2012, no. September, pp. 135–138, 2012.

[91] M. B. Olszewski, A. J. Groot, J. Dastych, and E. F. Knol, "TNF trafficking to human mast cell granules: mature chain-dependent endocytosis," *J. Immunol.*, vol. 178, no. 9, pp. 5701–5709, 2007.

[92] Y. Liu, T. Kwa, and A. Revzin, "Simultaneous detection of cell-secreted TNF-α and IFN-γ using micropatterned aptamer-modified electrodes," *Biomaterials*, vol. 33, no. 30, pp. 7347–7355, 2012.

[93] T. Horiuchi, H. Mitoma, S. Harashima, and H. Tsukamoto, "Review Transmembrane TNF- a : structure , function and interaction with anti-TNF agents," no. March, pp. 1215–1228, 2010.

[94] G. Z. Feuerstein, T. Liu, and F. C. Barone, "Cytokines, inflammation, and brain injury: role of tumor necrosis factor-alpha.," *Cerebrovasc. Brain Metab. Rev.*, vol. 6, no. 4, pp. 341–360, 1994.

[95] R. T. Perry, J. S. Collins, H. Wiener, R. Acton, and R. C. P. Go, "The role of TNF and its receptors in Alzheimer's disease," *Neurobiol. Aging*, vol. 22, no. 6, pp. 873–883, 2001.

Cited Literature (continued)

[96] G. S. Hotamisligil, "The role of TNFα and TNF receptors in obesity and insulin resistance," *J. Intern. Med.*, vol. 245, no. 6, pp. 621–625, 1999.

[97] J. R. Bradley, "TNF-mediated inflammatory disease," *J. Pathol. A J. Pathol. Soc. Gt. Britain Irel.*, vol. 214, no. 2, pp. 149–160, 2008.

[98] Y. Yoshida, I. Waga, and K. Horii, "Quantitative and sensitive protein detection strategies based on aptamers," *PROTEOMICS–Clinical Appl.*, vol. 6, no. 11–12, pp. 574–580, 2012.

[99] J. Liu and Y. Lu, "Fast colorimetric sensing of adenosine and cocaine based on a general sensor design involving aptamers and nanoparticles," *Angew. Chemie Int. Ed.*, vol. 45, no. 1, pp. 90–94, 2006.

[100] Y. Qi and B. Li, "A Sensitive, Label-Free, Aptamer-Based Biosensor Using a Gold Nanoparticle-Initiated Chemiluminescence System," *Chem. Eur. J.*, vol. 17, no. 5, pp. 1642–1648, 2011.

[101] J. K. Herr, J. E. Smith, C. D. Medley, D. Shangguan, and W. Tan, "Aptamer-conjugated nanoparticles for selective collection and detection of cancer cells," *Anal. Chem.*, vol. 78, no. 9, pp. 2918–2924, 2006.

[102] L. Feng, Y. Chen, J. Ren, and X. Qu, "A graphene functionalized electrochemical aptasensor for selective label-free detection of cancer cells," *Biomaterials*, vol. 32, no. 11, pp. 2930–2937, 2011.

[103] Y. Luan, A. Lu, J. Chen, H. Fu, and L. Xu, "A label-free aptamer-based fluorescent assay for cadmium detection," *Appl. Sci.*, vol. 6, no. 12, p. 432, 2016.

[104] H. Huang and J.-J. Zhu, "DNA aptamer-based QDs electrochemiluminescence biosensor for the detection of thrombin," *Biosens. Bioelectron.*, vol. 25, no. 4, pp. 927–930, 2009.

Cited Literature (continued)

[105] S. Centi, L. Bonel Sanmartin, S. Tombelli, I. Palchetti, and M. Mascini, "Detection of C Reactive Protein (CRP) in Serum by an Electrochemical Aptamer-Based Sandwich Assay," *Electroanal. An Int. J. Devoted to Fundam. Pract. Asp. Electroanal.*, vol. 21, no. 11, pp. 1309–1315, 2009.

[106] J. Pultar, U. Sauer, P. Domnanich, and C. Preininger, "Aptamer–antibody on-chip sandwich immunoassay for detection of CRP in spiked serum," *Biosens. Bioelectron.*, vol. 24, no. 5, pp. 1456–1461, 2009.

[107] W. R. Algar, A. J. Tavares, and U. J. Krull, "Beyond labels: a review of the application of quantum dots as integrated components of assays, bioprobes, and biosensors utilizing optical transduction," *Anal. Chim. Acta*, vol. 673, no. 1, pp. 1–25, 2010.

[108] A. P. Alivisatos, "Semiconductor clusters, nanocrystals, and quantum dots," *Science (80-.).*, vol. 271, no. 5251, pp. 933–937, 1996.

[109] I. L. Medintz and H. Mattoussi, "Quantum dot-based resonance energy transfer and its growing application in biology," *Phys. Chem. Chem. Phys.*, vol. 11, no. 1, pp. 17–45, 2009.

[110] X. Michalet, F. F. Pinaud, L. A. Bentolila, J. M. Tsay, S. Doose, J. J. Li, G. Sundaresan, A. M. Wu, S. S. Gambhir, and S. Weiss, "Quantum dots for live cells, in vivo imaging, and diagnostics," *Science*, vol. 307, no. 5709, pp. 538–544, 2005.

[111] L. X. Hung, P. N. Thang, H. V. Nong, N. H. Yen, V. Đ. Chinh, L. V. Vu, N. T. T. Hien, W. D. de Marcillac, P. N. Hong, N. T. Loan, C. Schwob, A. Maître, N. Q. Liem, P. Bénalloul, L. Coolen, and P. T. Nga, "Synthesis, structural and optical characterization of CdTeSe/ZnSe and CdTeSe/ZnTe core/shell ternary quantum dots for potential application in solar cells," *J. Electron. Mater.*, vol. 45, no. 8, pp. 4425–4431, 2016.

[112] V. I. Klimov, A. A. Mikhailovsky, Su Xu, A. Malko, J. A. Hollingsworth, C. A. Leatherdale, H.-J. Eisler, and M. G. Bawendi, "Optical gain and stimulated emission in nanocrystal quantum dots," *Science*, vol. 290, no. 5490, pp. 314–317, 2000.

Cited Literature (continued)

[113] X. Meshik, S. Farid, M. Choi, Y. Lan, S. Mukherjee, D. Datta, M. Dutta, and M. A. Stroscio, "Biomedical applications of quantum dots, nucleic acid− based aptamers, and nanostructures in biosensors," *Crit. Rev. Biomed. Eng.*, vol. 43, no. 4, 2015.

[114] T. L. Jennings, M. P. Singh, and G. F. Strouse, "Fluorescent lifetime quenching near d= 1.5 nm gold nanoparticles: probing NSET validity," *J. Am. Chem. Soc.*, vol. 128, no. 16, pp. 5462–5467, 2006.

[115] R. Huang, Z. Xi, Y. Deng, and N. He, "Fluorescence based Aptasensors for the determination of hepatitis B virus e antigen," *Sci. Rep.*, vol. 6, p. 31103, 2016.

[116] S. K. Arya and P. Estrela, "Electrochemical immunosensor for tumor necrosis factor-alpha detection in undiluted serum," *Methods*, vol. 116, pp. 125–131, 2017.

[117] P. Kongsuphol, H. H. Ng, J. P. Pursey, S. K. Arya, C. C. Wong, E. Stulz, and M. K. Park, "EIS-based biosensor for ultra-sensitive detection of TNF-α from non-diluted human serum," *Biosens. Bioelectron.*, vol. 61, pp. 274–279, 2014.

[118] J. Wang, G. Liu, M. H. Engelhard, and Y. Lin, "Sensitive immunoassay of a biomarker tumor necrosis factor-α based on poly (guanine)-functionalized silica nanoparticle label," *Anal. Chem.*, vol. 78, no. 19, pp. 6974–6979, 2006.

[119] T. Li, Z. Si, L. Hu, H. Qi, and M. Yang, "Prussian Blue-functionalized ceria nanoparticles as label for ultrasensitive detection of tumor necrosis factor-α," *Sensors Actuators B Chem.*, vol. 171, pp. 1060–1065, 2012.

[120] S. Weng *et al.*, "Label-free electrochemical immunosensor based on K3 [Fe (CN) 6] as signal for facile and sensitive determination of tumor necrosis factor-alpha," *Sensors Actuators B Chem.*, vol. 184, pp. 1–7, 2013.

[121] Y. Hou, T. Li, H. Huang, H. Quan, X. Miao, and M. Yang, "Electrochemical immunosensor for the detection of tumor necrosis factor α based on hydrogel prepared from ferrocene modified amino acid," *Sensors Actuators B Chem.*, vol. 182, pp. 605–609, 2013.

Cited Literature (continued)

[122] M. Mazloum-Ardakani, L. Hosseinzadeh, and A. Khoshroo, "Label-free electrochemical immunosensor for detection of tumor necrosis factor α based on fullerene-functionalized carbon nanotubes/ionic liquid," *J. Electroanal. Chem.*, vol. 757, pp. 58–64, 2015.

[123] Z. Yin, Y. Liu, L.-P. Jiang, and J.-J. Zhu, "Electrochemical immunosensor of tumor necrosis factor α based on alkaline phosphatase functionalized nanospheres," *Biosens. Bioelectron.*, vol. 26, no. 5, pp. 1890–1894, 2011.

[124] T. S. Pui, P. Kongsuphol, S. K. Arya, and T. Bansal, "Detection of tumor necrosis factor (TNF-α) in cell culture medium with label free electrochemical impedance spectroscopy," *Sensors Actuators B Chem.*, vol. 181, pp. 494–500, 2013.

[125] U. Eletxigerra, J. Martinez-Perdiguero, S. Merino, R. Villalonga, J. M. Pingarrón, and S. Campuzano, "Amperometric magnetoimmunoassay for the direct detection of tumor necrosis factor alpha biomarker in human serum," *Anal. Chim. Acta*, vol. 838, pp. 37–44, 2014.

[126] S. Dai, C. Feng, W. Li, W. Jiang, and L. Wang, "Quantitative detection of tumor necrosis factor-α by single molecule counting based on a hybridization chain reaction," *Biosens. Bioelectron.*, vol. 60, pp. 180–184, 2014.

[127] M. Singh, A. Alabanza, L. E. Gonzalez, W. Wang, W. B. Reeves, and J. Hahm, "Ultratrace level determination and quantitative analysis of kidney injury biomarkers in patient samples attained by zinc oxide nanorods," *Nanoscale*, vol. 8, no. 8, pp. 4613–4622, 2016.

[128] Y.-C. Huang *et al.*, "Quantification of tumor necrosis factor-α and matrix metalloproteinases-3 in synovial fluid by a fiber-optic particle plasmon resonance sensor," *Analyst*, vol. 138, no. 16, pp. 4599–4606, 2013.

[129] M. S. Luchansky and R. C. Bailey, "Rapid, multiparameter profiling of cellular secretion using silicon photonic microring resonator arrays," *J. Am. Chem. Soc.*, vol. 133, no. 50, pp. 20500–20506, 2011.

Cited Literature (continued)

[130] E. W. Orava, N. Jarvik, Y. L. Shek, S. S. Sidhu, and J. Gariépy, "A short DNA aptamer that recognizes TNFα and blocks its activity in vitro," *ACS Chem. Biol.*, vol. 8, no. 1, pp. 170–178, 2012.

[131] T. Mori, A. Oguro, T. Ohtsu, and Y. Nakamura, "RNA aptamers selected against the receptor activator of NF-κB acquire general affinity to proteins of the tumor necrosis factor receptor family," *Nucleic Acids Res.*, vol. 32, no. 20, pp. 6120–6128, 2004.

[132] H. Lodish, A. Berk, S. L. Zipursky, P. Matsudaira, D. Baltimore, and J. Darnell, "Intracellular ion environment and membrane electric potential," in *Molecular Cell Biology. 4th edition*, WH Freeman, 2000.

[133] D. Rhodes and H. J. Lipps, "G-quadruplexes and their regulatory roles in biology," *Nucleic Acids Res.*, vol. 43, no. 18, pp. 8627–8637, 2015.

[134] Y. Liu, Q. Zhou, and A. Revzin, "An aptasensor for electrochemical detection of tumor necrosis factor in human blood," *Analyst*, vol. 138, no. 15, pp. 4321–4326, 2013.

[135] T. Kwa, Q. Zhou, Y. Gao, A. Rahimian, L. Kwon, Y. Liu, and A. Revzin, "Reconfigurable microfluidics with integrated aptasensors for monitoring intercellular communication," *Lab Chip*, vol. 14, no. 10, pp. 1695–1704, 2014.

[136] Y. Liu, Y. Liu, Z. Matharu, A. Rahimian, and A. Revzin, "Biosensors and Bioelectronics Detecting multiple cell-secreted cytokines from the same aptamer-functionalized electrode," *Biosens. Bioelectron.*, vol. 64, pp. 43–50, 2015.

[137] R. Say, S. E. Diltemiz, S. Çelik, and A. Ersöz, "Nanolabel for TNF-α determination," *Appl. Surf. Sci.*, vol. 275, pp. 233–238, 2013.

[138] Y. K. Bahk, H. H. Kim, D.-S. Park, S.-C. Chang, and J. S. Go, "A new concept for efficient sensitivity amplification of a QCM based immunosensor for TNF-α by using modified magnetic particles under applied magnetic field," *Bull. Korean Chem. Soc.*, vol. 32, no. 12, pp. 4215–4220, 2011.

Cited Literature (continued)

[139] R. Say, E. B. Özkütük, Ö. B. Ünlüer, D. Uğurağ, and A. Ersöz, "Nano anti-tumor necrosis factor-alpha based potentiometric sensor for tumor necrosis factor-alpha detection," *Sensors Actuators B Chem.*, vol. 209, pp. 864–869, 2015.

[140] S. Ghosh, A. Metlushko, S. Chaudhry, M. Dutta, and M. Stroscio, "Detection of C-Reactive Protein using network – deployable DNA aptamer based optical nanosensor," in *IEEE-EMBS International Conference on Biomedical and Health Informatics*, Chicago, IL, USA, May 19-22, 2019.

[141] F. B. Mayr, S. Yende, and D. C. Angus, "Epidemiology of severe sepsis," *Virulence*, vol. 5, no. 1, pp. 4–11, 2014.

[142] P. Povoa, E. Almeida, P. Moreira, A. Fernandes, R. Mealha, A. Aragão, and H. Sabino "C-reactive protein as an indicator of sepsis," *Intensive Care Med.*, vol. 24, no. 10, pp. 1052–1056, 1998.

[143] C. Gabay and I. Kushner, "Acute-phase proteins and other systemic responses to inflammation," *N. Engl. J. Med.*, vol. 340, no. 6, pp. 448–454, 1999.

[144] J. C. Marshall and K. Reinhart, "Biomarkers of sepsis," *Crit. Care Med.*, vol. 37, no. 7, pp. 2290–2298, 2009.

[145] J. Wang, J. Guo, J. Zhang, W. Zhang, and Y. Zhang, "RNA aptamer-based electrochemical aptasensor for C-reactive protein detection using functionalized silica microspheres as immunoprobes," *Biosens. Bioelectron.*, vol. 95, pp. 100–105, 2017.

[146] Y. Luo, B. Zhang, M. Chen, T. Jiang, D. Zhou, J. Huang, and W. Fu, "Sensitive and rapid quantification of C-reactive protein using quantum dot-labeled microplate immunoassay," *J. Transl. Med.*, vol. 10, no. 24, 2012.

[147] A. H. Nguyen, Y. Shin, and S. J. Sim, "Development of SERS substrate using phage-based magnetic template for triplex assay in sepsis diagnosis," *Biosens. Bioelectron.*, vol. 85, pp. 522–528, 2016.

Cited Literature (continued)

[148] Y. Lv, R. Wu, K. Feng, J. Li, Q. Mao, H. Yuan, H. Shen, X. Chai, and L. S. Li., "Highly sensitive and accurate detection of C-reactive protein by CdSe/ZnS quantum dot-based fluorescence-linked immunosorbent assay," *J. Nanobiotechnology*, vol. 15, no. 35, p. 35, 2017.

[149] S. F. Yang, B. Z. Gao, H. Y. Tsai, and C. B. Fuh, "Detection of c-reactive protein based on a magnetic immunoassay by using functional magnetic and fluorescent nanoparticles in microplates," *Analyst*, vol. 139, no. 21, pp. 5576–5581, 2014.

[150] W. M. Fakanya and I. E. Tothill, "Detection of the inflammation biomarker C-reactive protein in serum samples: towards an optimal biosensor formula," *Biosensors*, vol. 4, no. 4, pp. 340–357, 2014.

[151] Y. Zhao, G. Czilwik, V. Klein, K. Mitsakakis, R. Zengerle, and N. Paust, "C-reactive protein and interleukin 6 microfluidic immunoassays with on-chip pre-stored reagents and centrifugo-pneumatic liquid control," *Lab Chip*, vol. 17, no. 9, pp. 1666–1677, 2017.

[152] J. T. Russell, "Imaging calcium signals in vivo : a powerful tool in physiology and pharmacology," *Br. J. Pharmacol.*, vol. 163, pp. 1605–1625, 2011.

[153] U. Wojda, E. Salinska, and J. Kuznicki, "Critical Review Calcium Ions in Neuronal Degeneration," *IUBMB life*, vol. 60, no.9, pp. 575–590, 2008.

[154] J. Chung, W. Ryu, J. Kim, and B. Yoon, "Elevated Calcium after Acute Ischemic Stroke : Association with a Poor Short-Term Outcome and Long-Term Mortality," *J Stroke*, vol. 17, no. 1, pp. 54–59, 2015.

[155] S. Feske, "Calcium signalling in lymphocyte activation and disease," *Nat Rev Immunol.*, vol. 7, no. 9, pp. 690-702, 2007.

[156] M. H. Asif, O. Nur, M. Willander, and B. Danielsson, "Biosensors and Bioelectronics Selective calcium ion detection with functionalized ZnO nanorods-extended gate MOSFET," *Biosens. Bioelectron.*, vol. 24, no. 11, pp. 3379–3382, 2009.

Cited Literature (continued)

[157] S. R. Ankireddy and J. Kim, "Sensors and Actuators B : Chemical Highly selective and sensitive detection of calcium (II) ions in human serum using novel fluorescent carbon dots," *Sensors Actuators B. Chem.*, vol. 255, pp. 3425–3433, 2018.

[158] M. Asadnia, M. Myers, G. A.Umana-Membreno, T. M.Sanders, U. K. Mishra, B. D. Nener, M. V. Baker, and G. Parish, "Analytica Chimica Acta Ca 2 þ detection utilising AlGaN / GaN transistors with ion-selective polymer membranes," *Anal. Chim. Acta*, vol. 987, pp. 105–110, 2017.

[159] S. Kim, J. W. Park, D. Kim, D. Kim, I. H. Lee, and S. Jon, "Bioinspired Colorimetric Detection of Calcium (II) Ions in Serum Using," *Angew Chem Int Ed Engl*., vol. 48, no. 23, pp. 4138–4141, 2009.

[160] U. Schefer, D. Ammann, E. Pretsch, U. Oesch, and W. Simon, "Neutral Carrier Based Ca2 + -Selective Electrode with Detection Limit in the Sub-Nanomolar Range," *Anal. Chem.*, vol. 58, no. 11, pp. 2282–2285, 1986.

[161] P. Caglar, S. A. Tuncel, N. Malcik, J. P. Landers, and J. P. Ferrance, "A microchip sensor for calcium determination," *Anal. Bioanal. Chem.*, vol. 386, no. 5, pp. 1303–1312, 2006.

[162] A. K. Singh and S. Mehtab, "Calcium (II) -selective potentiometric sensor based on ␣ -furildioxime as neutral carrier," *Sensors Actuators B. Chem*, vol. 123, pp. 429–436, 2007.

[163] M. R. Ganjali, H. A. Zamani, P. Norouzi, M. Adib, and M. Accedy, "Novel Calcium Sensor Based on [2- (2-Hydroxyphenyl) imino] -1 , 2-diphenylethanone," *Acta Chim. Slovpp.*, vol. 62, pp. 309–316, 2005.

[164] D. Miyoshi, A. Nakao, and N. Sugimoto, "Structural transition from antiparallel to parallel G-quadruplex of d (G 4 T 4 G 4) induced by Ca 2 +," *Nucleic Acids Res.*, vol. 31, no. 4, pp. 1156-1163, 2003.

[165] T. L. Blair, S. Yang, T. Smith-palmer, and L. G. Bachas, "Fiber Optic Sensor for Ca2 + Based on an Induced Change in the Conformation of the Protein Calmodulin," *Anal. Chem.*, vol. 66, no. 2, pp. 300–302, 1994.

Cited Literature (continued)

[166] K. Suzuki, K. Tohda, Y. Tanda, H. Ohzora, S. Nishihama, and H. Inoue, "Fiber-Optic Magnesium and Calcium Ion Sensor Based," *Anal. Chem.*, vol. 384, no. 27, pp. 382–384, 1989.

[167] V. K. Johns, P. K. Patel, S. Hassett, P. Calvo-marzal, Y. Qin, and K. Y. Chumbimuni-torres, "Visible Light Activated Ion Sensing Using a Photoacid Polymer for Calcium Detection," *Anal. Chem.*, vol. 86, no. 13, pp. 6184-6187, 2014.

[168] M. Wu, S. Meng, Q. Wang, W. Si, W. Huang, and X. Dong, "Nickel − Cobalt Oxide Decorated Three-Dimensional Graphene as an Enzyme Mimic for Glucose and Calcium Detection," *ACS Appl. Mater. Interfaces*, vol. 7, no. 38, pp. 21089-21094, 2015.

[169] S. Liu, H. Wang, Z. Cheng, and H. Liu, "Hexametaphosphate-capped quantum dots as fluorescent probes for detection of calcium ion and fluoride," *Sensors Actuators B. Chem.*, vol. 232, pp. 306–312, 2016.

[170] G. Chen, Z. Zhou, and H. Feng, "An aggregation-induced phosphorescence probe for calcium ion-specific detection and live-cell imaging in Arabidopsis thaliana," *Chem. Commun.*, vol. 55, pp. 4841–4844, 2019.

[171] H. Derakhshankhah and S. Jafari, "Cell penetrating peptides: A concise review with emphasis on biomedical applications," *Biomed. Pharmacother.*, vol. 108, pp. 1090–1096, 2018.

[172] G. Guidotti, L. Brambilla, and D. Rossi, "Cell-penetrating peptides: from basic research to clinics," *Trends Pharmacol. Sci.*, vol. 38, no. 4, pp. 406–424, 2017.

[173] A. George, L. Bannon, B. Sabsay, J. W. Dillon, J. Malone, A. Veis, N. A. Jenkins, D. J. Gilbert, and N. G. Copeland, "The carboxyl-terminal domain of phosphophoryn contains unique extended triplet amino acid repeat sequences forming ordered carboxyl-phosphate interaction ridges that may be essential in the biomineralization process," *J. Biol. Chem.*, vol. 271, no. 51, pp. 32869–32873, 1996.

Cited Literature (continued)

[174] S. Ravindran, P. T. Snee, A. Ramachandran, and A. George, "Acidic domain in dentin phosphophoryn facilitates cellular uptake implications in targeted protein delivery," *J. Biol. Chem.*, vol. 288, no. 22, pp. 16098–16109, 2013.

[175] V. M. Vijayan and J. Muthu, "Polymeric nanocarriers for cancer theranostics," *Polym. Adv. Technol.*, vol. 28, no. 12, pp. 1572–1582, 2017.

[176] S. Roy and A. Jaiswal, "Graphene-based nanomaterials for theranostic applications," *Reports Adv. Phys. Sci.*, vol. 1, no. 04, p. 1750011, 2017.

[177] L. Wang, A. Wu, and G. Wei, "Graphene-based aptasensors: from molecule–interface interactions to sensor design and biomedical diagnostics," *Analyst*, vol. 143, no. 7, pp. 1526–1543, 2018.

[178] J. A. Kellum, L. Kong, M. P. Fink, L. A. Weissfeld, D. M. Yealy, M. R. Pinsky, J. Fine, A. Krichevsky, R. L. Delude, and D. C. Angus, "Understanding the inflammatory cytokine response in pneumonia and sepsis: results of the Genetic and Inflammatory Markers of Sepsis (GenIMS) Study," *Arch. Intern. Med.*, vol. 167, no. 15, pp. 1655–1663, 2007.

[179] B. Beutler and A. Cerami, "Cachectin: more than a tumor necrosis factor," *N. Engl. J. Med.*, vol. 316, no. 7, pp. 379–385, 1987.

[180] M. Adib, Z. Bakhshiani, F. Navaei, F. S. Fosoul, S. Fouladi, and H. Kazemzadeh, "Procalcitonin: a reliable marker for the diagnosis of neonatal sepsis," *Iran. J. Basic Med. Sci.*, vol. 15, no. 2, p. 777, 2012.

[181] S. B. Chaney, S. Shanmukh, R. A. Dluhy, and Y.-P. Zhao, "Aligned silver nanorod arrays produce high sensitivity surface-enhanced Raman spectroscopy substrates," *Appl. Phys. Lett.*, vol. 87, no. 3, p. 31908, 2005.

[182] J. L. Abell, J. D. Driskell, R. A. Dluhy, R. A. Tripp, and Y.-P. Zhao, "Fabrication and characterization of a multiwell array SERS chip with biological applications," *Biosens. Bioelectron.*, vol. 24, no. 12, pp. 3663–3670, 2009.

Cited Literature (continued)

[183] Z. Movasaghi, S. Rehman, and I. U. Rehman, "Raman spectroscopy of biological tissues," *Appl. Spectrosc. Rev.*, vol. 42, no. 5, pp. 493–541, 2007.

[184] J. E. Volanakis, "Human C-reactive protein: expression, structure, and function," *Mol. Immunol.*, vol. 38, no. 2, pp. 189–197, 2001.

[185] E. B. de Oliveira, C. Gotschlich, and T. Y. Liu, "Primary structure of human C-reactive protein.," *J. Biol. Chem.*, vol. 254, no. 2, pp. 489–502, 1979.

[186] S. Jarmelo, P. R. Carey, and R. Fausto, "The Raman spectra of serine and 3, 3-dideutero-serine in aqueous solution," *Vib. Spectrosc.*, vol. 43, no. 1, pp. 104–110, 2007.

[187] A. Dong, W. S. Caughey, and T. W. Du Clos, "Effects of calcium, magnesium, and phosphorylcholine on secondary structures of human C-reactive protein and serum amyloid P component observed by infrared spectroscopy.," *J. Biol. Chem.*, vol. 269, no. 9, pp. 6424–6430, 1994.

[188] G. Zhu, X. Zhu, Q. Fan, and X. Wan, "Raman spectra of amino acids and their aqueous solutions," *Spectrochim. Acta Part A Mol. Biomol. Spectrosc.*, vol. 78, no. 3, pp. 1187–1195, 2011.

[189] B. L. Silva, P. T. C. Freire, F. E. A. Melo, J. M. Filho, M. A. Pimenta, and M. S. S. Dantas, "High-pressure Raman spectra of L-threonine crystal," *J. Raman Spectrosc.*, vol. 31, no. 6, pp. 519–522, 2000.

[190] K. Machida, A. Kagayama, Y. Saito, Y. Kuroda, and T. Uno, "Vibrational spectra and intermolecular potential of the α-form crystal of glycine," *Spectrochim. Acta Part A Mol. Spectrosc.*, vol. 33, no. 5, pp. 569–574, 1977.

[191] N. B. C. Pfukwa, "Surface Enhanced Raman spectroscopy (SERS) of amino acids", MS Thesis, Stellenbosch: Stellenbosch University, Stellenbosch, South Africa, 2016.

Cited Literature (continued)

[192] F. M. Almeida, P. T. C. Freire, R. J. C. Lima, C. M. R. Remédios, J. Mendes Filho, and F. E. A. Melo, "Raman spectra of l-isoleucine crystals," *J. Raman Spectrosc. An Int. J. Orig. Work all Asp. Raman Spectrosc. Incl. High. Order Process. also Brillouin Rayleigh Scatt.*, vol. 37, no. 11, pp. 1296–1301, 2006.

[193] F. PF Filho, P. T. C. Freire, K. C. V Lima, F. E. A. Melo, and P. S. Pizani, "Raman spectra of L-leucine crystals", *arXiv preprint arXiv:0704.2792*, 2007.

[194] L. O. Narhi, J. S. Philo, T. Li, M. Zhang, B. Samal, and T. Arakawa, "Induction of α-helix in the β-sheet protein tumor necrosis factor-α: acid-induced denaturation," *Biochemistry*, vol. 35, no. 35, pp. 11454–11460, 1996.

[195] N. Kuhar, S. Sil, T. Verma, and S. Umapathy, "Challenges in application of Raman spectroscopy to biology and materials," *RSC Adv.*, vol. 8, pp. 25888–25908, 2018.

[196] C. M. Dubois, F. Blanchette, M.-H. Laprise, R. Leduc, F. Grondin, and N. G. Seidah, "Evidence that furin is an authentic transforming growth factor-β1-converting enzyme," *Am. J. Pathol.*, vol. 158, no. 1, pp. 305–316, 2001.

[197] G. Thomas, "Furin at the cutting edge: from protein traffic to embryogenesis and disease," *Nat. Rev. Mol. cell Biol.*, vol. 3, no. 10, p. 753, 2002.

[198] T. Komiyama, J. M. Coppola, M. J. Larsen, M. E. van Dort, B. D. Ross, R. Day, A. Rehemtulla, and R. S. Fuller, "Inhibition of furin/PC-catalyzed surface and intracellular processing by small molecules," *J. Biol. Chem.*, vol. 284, no. 23, pp. 15729–15738, 2009.

[199] S. Hallenberger, V. Bosch, H. Angliker, E. Shaw, H.-D. Klenk, and W. Garten, "Inhibition of furin-mediated cleavage activation of HIV-1 glycoprotein gpl60," *Nature*, vol. 360, no. 6402, p. 358, 1992.

[200] B. J. Robertson, J. M. Moehring, and T. J. Moehring, "Defective processing of the insulin receptor in an endoprotease-deficient Chinese hamster cell strain is corrected by expression of mouse furin.," *J. Biol. Chem.*, vol. 268, no. 32, pp. 24274–24277, 1993.

Cited Literature (continued)

[201] D. B. Constam and E. J. Robertson, "Regulation of bone morphogenetic protein activity by pro domains and proprotein convertases," *J. Cell Biol.*, vol. 144, no. 1, pp. 139–149, 1999.

[202] Y. Cui, F. Jean, G. Thomas, and J. L. Christian, "BMP-4 is proteolytically activated by furin and/or PC6 during vertebrate embryonic development," *EMBO J.*, vol. 17, no. 16, pp. 4735–4743, 1998.

[203] S. A. Fathy, F. F. Abdel Hamid, B. M. Zabut, A. F. Jamee, M. A. M. Ali, and A. M. Abu Mustafa, "Diagnostic utility of BNP, corin and furin as biomarkers for cardiovascular complications in type 2 diabetes mellitus patients," *Biomarkers*, vol. 20, no. 6–7, pp. 460–469, 2015.

[204] N. Ranta, H. Turpeinen, A. Oksanen, S. Hämäläinen, R. Huttunen, R. Uusitalo-Seppälä, E. Rintala, J. Aittoniemi, and M. Pesu, "The Plasma Level of Proprotein Convertase FURIN in Patients with Suspected Infection in the Emergency Room: A Prospective Cohort Study," *Scand. J. Immunol.*, vol. 82, no. 6, pp. 539–546, 2015.

[205] C. Guan, R. Dang ,Y. Cui, L. Liu, X. Chen, X. Wang, J. Zhu, D. Li, J. Li, and D. Wang, "Characterization of plasma metal profiles in Alzheimer's disease using multivariate statistical analysis," *PLoS One*, vol. 12, no. 7, p. e0178271, 2017.

[206] V. Agarwal, A. Kuchipudi, M. Fulde, K. Riesbeck, S. Bergmann, and A. M. Blom, "Streptococcus pneumoniae endopeptidase O (PepO) is a multifunctional plasminogen- and fibronectin-binding protein, facilitating evasion of innate immunity and invasion of host cells," *J. Biol. Chem.*, vol. 288, no. 10, pp. 6849–6863, 2013.

[207] L. Xue, B. Yan, Y. Li, Y. Tan, X. Luo, and M. Wang, "Surface-enhanced Raman spectroscopy of blood serum based on gold nanoparticles for tumor stages detection and histologic grades classification of oral squamous cell carcinoma," *Int. J. Nanomedicine*, vol. 13, pp. 4977, 2018.

[208] S. Kumar, "Vibrational study of aspartic acids," *AKGEC Int. J. Technol*, vol. 7, pp. 60–64, 2016.

Cited Literature (continued)

[209] Y. Numata, M. Otsuka, K. Yamagishi, and H. Tanaka, "Quantitative determination of glycine, alanine, aspartic acid, glutamic acid, phenylalanine, and tryptophan by Raman spectroscopy," *Anal. Lett.*, vol. 50, no. 4, pp. 651–662, 2017.

[210] Z. Q. Wen, L. Hecht, and L. D. Barron, "β-Sheet and associated turn signatures in vibrational Raman optical activity spectra of proteins," *Protein Sci.*, vol. 3, no. 3, pp. 435–439, 1994.

[211] F. J. Ramırez, I. Tunón, and E. Silla, "Amino acid chemistry in solution: structural properties and vibrational dynamics of serine using density functional theory and a continuum solvent model," *Chem. Phys.*, vol. 303, no. 1–2, pp. 85–96, 2004.

[212] N. K. Howell, G. Arteaga, S. Nakai, and E. C. Y. Li-Chan, "Raman spectral analysis in the C− H stretching region of proteins and amino acids for investigation of hydrophobic interactions," *J. Agric. Food Chem.*, vol. 47, no. 3, pp. 924–933, 1999.

[213] A. Roy, K. Chandra, S. Dolui, and N. C. Maiti, "Envisaging the Structural Elevation in the Early Event of Oligomerization of Disordered Amyloid β Peptide," *ACS Omega*, vol. 2, no. 8, pp. 4316–4327, 2017.

[214] S. Henrich, A. Cameron, G. P. Bourenkov, R. Kiefersauer, R. Huber, I. Lindberg, W. Bode, and M. E. Than, "The crystal structure of the proprotein processing proteinase furin explains its stringent specificity," *Nat. Struct. Mol. Biol.*, vol. 10, no. 7, p. 520, 2003.

[215] I. López-Peña, B. S. Leigh, D. E. Schlamadinger, and J. E. Kim, "Insights into protein structure and dynamics by ultraviolet and visible resonance Raman spectroscopy," *Biochemistry*, vol. 54, no. 31, pp. 4770–4783, 2015.

[216] I. Harada, T. Miura, and H. Takeuchi, "Origin of the doublet at 1360 and 1340 cm− 1 in the Raman spectra of tryptophan and related compounds," *Spectrochim. Acta Part A Mol. Spectrosc.*, vol. 42, no. 2–3, pp. 307–312, 1986.

[217] H. Takeuchi, "Raman structural markers of tryptophan and histidine side chains in proteins," *Biopolym. Orig. Res. Biomol.*, vol. 72, no. 5, pp. 305–317, 2003.

Cited Literature (continued)

[218] A. Rygula, K. Majzner, K. M. Marzec, A. Kaczor, M. Pilarczyk, and M. Baranska, "Raman spectroscopy of proteins: a review," *J. Raman Spectrosc.*, vol. 44, no. 8, pp. 1061–1076, 2013.

[219] B. Sjöberg, S. Foley, B. Cardey, and M. Enescu, "An experimental and theoretical study of the amino acid side chain Raman bands in proteins," *Spectrochim. Acta Part A Mol. Biomol. Spectrosc.*, vol. 128, pp. 300–311, 2014.

[220] S. Suzuki, T. Shimanouchi, and M. Tsuboi, "Normal vibrations of glycine and deuterated glycine molecules," *Spectrochim. Acta*, vol. 19, no. 7, pp. 1195–1208, 1963.

[221] I. Ashikawa and K. Itoh, "Raman spectra of polypeptides containing L-histidine residues and tautomerism of imidazole side chain," *Biopolym. Orig. Res. Biomol.*, vol. 18, no. 8, pp. 1859–1876, 1979.

[222] A. Pawlukojć, J. Leciejewicz, J. Tomkinson, and S. F. Parker, "Neutron scattering, infra red, Raman spectroscopy and ab initio study of L-threonine," *Spectrochim. Acta Part A Mol. Biomol. Spectrosc.*, vol. 57, no. 12, pp. 2513–2523, 2001.

[223] A. E. Aliaga, I. Osorio-Roman, C. Garrido, P. Leyton, J. Cárcamo, E. Clavijo, J. S. Gómez-Jeria, G. Díaz F., and M. M. Campos-Vallette, "Surface enhanced Raman scattering study of L-lysine," *Vib. Spectrosc.*, vol. 50, no. 1, pp. 131–135, 2009.

[224] P. T. C. Freire, F. M. Barboza, J. A. Lima, F. E. A. Melo, and J. Mendes Filho, "Raman Spectroscopy of Amino Acid Crystals," in *Raman Spectroscopy and Applications*, InTech, pp. 201, 2017.

[225] A. Sumayya, C. Y. Panicker, H. T. Varghese, and B. Harikumar, "Vibrational spectroscopic studies and ab initio calculations of L-glutamic acid 5-amide," *Rasayan J. Chem*, vol. 3, no. 1, pp. 548–555, 2008.

[226] R. A. Yadav, V. Dixit, M. Yogesh, and C. Santhosh, "Pharmaceutica Raman and IR Spectral and DFT Based Vibrational and Electronic Characterization of Isolated and Zwitterionic Forms of L-Tyrosine," *Pharm. Anal. Acta*, vol. 6, no. 10, p. 1000439, 2015.

Appendices

Appendix A

Chapter 2, Pages 7-24 have been reproduced from my own article published in *Nanotechnology*.

S. Ghosh, D. Datta, M. Cheema, M. Dutta, and M. A. Stroscio, "Aptasensor based optical detection of glycated albumin for diabetes mellitus diagnosis," *Nanotechnology*, vol. 28, no. 43, 2017.

Chapter 3. Pages 25-41 have been reproduced from my own article published in *IEEE Transactions on NanoBioscience.*

S. Ghosh, D. Datta, S. Chaudhry, M. Dutta, and M. A. Stroscio, "Rapid detection of Tumor Necrosis Factor-alpha using quantum dot based optical aptasensor," *IEEE Trans. Nanobioscience*, vol. 17, no. 4, pp. 417–423, 2018.

Chapter 4. Pages 42-53 have been reproduced from my own article presented in the 2019 IEEE EMBS International Conference on Biomedical & Health Informatics (BHI), May 19-22, 2019, University of Illinois at Chicago, Chicago, IL.

S. Ghosh, A. Metlushko, S. Chaudhry, M. Dutta, and M. Stroscio, "Detection of C-Reactive Protein using network – deployable DNA aptamer based optical nanosensor," in *IEEE-EMBS International Conference on Biomedical and Health Informatics*, Chicago, IL, USA, May 19-22, 2019.

Chapter 6. Pages 67-78 have been reproduced from my own article submitted to Nature Scientific Reports.

S. Ghosh, Y. Chen, J. Sebastian, A. George, M. Dutta, and M. A. Stroscio, "A study on the response of FRET based DNA aptasensors in intracellular environment," *Sci. Rep*, 2019. [Currently under review]

Appendix A (continued)

Chapter 8. Pages 100-101 have been reproduced from my own submitted to Nature Scientific Reports.

S. Ghosh, Y. Chen, J. Sebastian, A. George, M. Dutta, and M. A. Stroscio, "A study on the response of FRET based DNA aptasensors in intracellular environment," *Sci. Rep*, 2019. [Currently under review]

Appendix B

Institute of Physics Policy on Thesis and Dissertations

.

Assignment of copyright and publication agreement

IOP Publishing Limited ("IOP") agrees to publish:

Manuscript Title: Aptasensor based optical detection of glycated albumin for diabetes mellitus diagnosis (the "Article") written by

Names of all authors: Ghosh, Shreya; Datta, Debopam; Cheema, Mehar; Dutta, Mitra; Stroscio, Michael ("the Named Authors") in the following journal Nanotechnology ("the Journal")

Name of copyright owner(s) (if not the Named Author(s) – see Important Information above):
("the Copyright Owner")

IOP Ref: NANO-114822

Part 1 - Publication on a Subscription basis

1.1 In consideration for acceptance and publication of the Article, the Named Authors of the Article and/or the Copyright Owner hereby assign, where necessary by present assignment of future copyright, to IOP with full title guarantee the entire copyright in all original material published as part of the Article (which expression includes but is not limited to the text, abstract, tables, figures and graphs, related corrigenda or "comments" and multimedia content but excludes any other item referred to as supplementary material and/or any video abstract) throughout the world for the full term of copyright (including any extensions or renewals thereof) for all media and formats, whether known or unknown. Such assignment shall be effective only if the Article (or any resubmission of the Article) is accepted for publication. For the avoidance of doubt, copyright does not subsist in any fundamental data underlying the Article and nothing in this agreement is intended to limit access to or use of such data.

1.2 If the Article, or any part of it, is protected by Crown copyright, in consideration for acceptance and publication of the Article, the relevant Named Authors and the relevant originating department or agency hereby grant IOP a non-exclusive royalty-free worldwide freely-transferrable licence for the full term of copyright (including any extensions or renewals thereof) for all media and formats, whether known or unknown, to do in relation to the Article all acts restricted by copyright worldwide including, but not limited to, the right of action under section 101A of the Copyright Designs and Patents Act 1988. Such licence shall be effective only if the Article is accepted for publication.

1.3 If all the Named Authors are employees of the US Government, they represent and warrant to IOP that the Article was prepared as part of their official duties. In such circumstances, or where the Article was created as part of a work for hire, none of the original content within the Article is subject to copyright protection as it is in the public domain.

1.4 In consideration for acceptance and publication of the Article, the Named Authors and/or the Copyright Owner hereby grant IOP a royalty-free non-exclusive worldwide freely transferrable licence for the full term of copyright (including any extensions or renewals thereof) to do in relation to any supplementary material not deemed to be part of the Article and/or any video abstract all acts restricted by copyright worldwide. This shall include, but not be limited to, making the material available under any licence that IOP deems appropriate for purposes including, but not limited to, the maximisation of visibility and the long term preservation of the content.

1.5 Each of the Named Authors consents to all publication and processing of their personal data by IOP, as that data is displayed on the Article, including, but not limited to, the names and email addresses of the Named Authors. Accordingly, the Named Authors shall not object on data protection grounds to the use of their personal data on the Article wherever IOP chooses to display it, whether itself or via a third party.

Representations and warranties

2.1 The Copyright Owner and/or the Submitting Author on behalf of the Named Authors (as appropriate) represent and warrant that:

2.1.1 the Article is the original work of the Named Authors;

2.1.2 the Article has not been published previously in any form, other than as part of the Named Authors' research theses or dissertations (which fact has been notified to IOP in writing) or as a preprint on the arXiv.org or bioRxiv.org service (provided they did not select any form of open access licence when uploading it to arXiv.org or bioRxiv.org);

2.1.3 each of the Named Authors has made a material contribution to the conception and/or writing of the Article, has received the final version of the Article, has agreed to its submission on the terms contained herein and takes responsibility for it and submission has been approved as necessary by the authorities at the establishment where the research was carried out;

2.1.4 the Submitting Author completes and returns this agreement as authorised agent for and on

behalf of all the Named Authors and the Copyright Owner (as applicable) and has the full power to enter into this agreement and to make the grants and assignments it contains;

2.1.5 the Article has not been and shall not be submitted to another publisher prior to withdrawal or rejection by IOP;

2.1.6 the Article does not infringe any third party rights, it contains nothing libellous or unlawful, all factual statements are to the best of the Named Authors' knowledge true or based on valid research conducted according to accepted norms and all required permissions have been obtained in writing;

2.1.7 the Article expressly acknowledges any third party funding and/or potential conflicts of interest; and

2.1.8 any supplementary material or video abstract is the original work of the Named Authors, or is the property of the Copyright Owner, or permission has been obtained from its owner(s) for its publication by IOP and permission has been obtained for the inclusion of any third party content.
2.2 The Named Authors and/or the Copyright Owner (as appropriate) indemnify and will keep indemnified IOP against all costs and expenses suffered or incurred by IOP as a result of and/or arising out of any breach of the representations and/or warranties in this section 2.

The Named Authors' rights

3.1 IOP grants the Named Authors the rights specified in paragraphs 3.2 and 3.3. All such rights must be exercised solely for non-commercial purposes. Where possible, any use should display citation information and IOP's copyright notice, and, for electronic use, best efforts must be made to include a link to the online abstract in the Journal.

Exercise of the rights in paragraph 3.2 may use the peer reviewed, edited, formatted and typeset version of the Article including any tagging, indexing and other enhancements published by IOP and/or its licensors ("Final Published Version").

Exercise of the rights referred to in paragraph 3.3 must not use the Final Published Version and extend only to the version of the Article accepted for publication including all changes made as a result of the peer review process, and which may also include the addition to the article by IOP of a header, an article ID, a cover sheet and/or an 'Accepted Manuscript' watermark, but excluding any other editing, typesetting or other changes made by IOP and/or its licensors (the "Accepted Manuscript") and must be accompanied by the following statement of provenance:

'This is the Accepted Manuscript version of an article accepted for publication in Nanotechnology.
IOP Publishing Ltd is not responsible for any errors or omissions in this version of the manuscript or any version derived from it. The Version of Record is available online at [insert DOI].'

3.2 The rights are:

3.2.1 To make copies of the Final Published Version of the Article (all or part) for teaching purposes;

3.2.2 To include the Final Published Version of the Article (all or part) in a research thesis or dissertation provided it is not then published commercially;

3.2.3 To make oral presentation of the Final Published Version of the Article (all or part) and to include a summary and/or highlights of it in papers distributed at such presentations or in conference proceedings; and

3.2.4 To use original figures and text from the Final Published Version of the Article falling within the quota outlined in and subject to the STM Permissions Guidelines (http://www.stm-

assoc.org/permissions-guidelines/) at the relevant time in force.
For the avoidance of doubt, the Named Authors retain all proprietary rights in the Article other than copyright.

3.3 Additional rights of the Named Authors are to:

3.3.1 Use the Accepted Manuscript (all or part) without modification in personal compilations of the Named Authors' own works (provided not created by a third party publisher); and

3.3.2 Include the Accepted Manuscript (all or part) on the Named Authors' own Personal Website(s), institutional website(s), repositories, Scientific Social Networks and third party websites provided that this is fully in accordance with the Author Rights set out at the following url legal.ioppublishing.org/author-rights on the date of submission of the agreement.

Miscellaneous

4. To the extent that there are moral rights in the Article, all the Named Authors expressly reserve and assert their moral rights to be identified as the authors of the Article.

5. The Named Authors and/or the Copyright Owner shall execute such further documents, and take such actions and do such things, as may be requested by IOP at IOP's reasonable expense to give full effect to the terms of the agreement.

6. For the avoidance of doubt, the grants and assignment envisaged herein shall become effective only upon acceptance of the Article for publication. In the event that the Article is withdrawn prior to acceptance, or is rejected, this agreement shall have no effect and no party shall be bound by it.

7. The agreement shall be governed by English Law and subject to the non-exclusive jurisdiction of the English courts.

Confirmation

8. By selecting to publish on a subscription basis, the Submitting Author is responsible for ensuring that, where relevant, all Named Authors obtain a waiver for the Article from their institution or university's open access policy and retain such waiver as evidence of compliance. The Named Authors agree that they shall obtain such waivers and provide them to IOP if requested.

9. By typing the Submitting Author's name into the box at Part 3 below and clicking "Submit", the Named Authors agree to these terms. The Authorised Signatories of any third party Copyright Owner(s) and/or the Submitting Author agree, on behalf of such Copyright Owner(s), to these terms by typing the Copyright Owner's name into the "Copyright Owner" box at the top of the page.

Copyright Clearance Center Marketplace™

IOP Publishing, Ltd - License Terms and Conditions

Order Date	28-Oct-2019
Order license ID	1001038-1
ISSN	1361-6528
Type of Use	Republish in a thesis/dissertation
Publisher	IOP Publishing
Portion	Chapter/article

LICENSED CONTENT

Publication Title	Nanotechnology	Country	United Kingdom of Great Britain and Northern Ireland
Author/Editor	Institute of Physics (Great Britain)	Rightsholder	IOP Publishing, Ltd
Date	12/31/1995	Publication Type	e-Journal
Language	English	URL	http://www.iop.org/Journals/na

REQUEST DETAILS

Portion Type	Chapter/article	Rights Requested	Main product and any product related to main product
Page range(s)	435505	Distribution	Worldwide
Total number of pages	11	Translation	Original language of publication
Format (select all that apply)	Electronic	Copies for the disabled?	No
Who will republish the content?	Author of requested content	Minor editing privileges?	Yes
Duration of Use	Life of current and all future editions	Incidental promotional use?	No
Lifetime Unit Quantity	More than 2,000,000	Currency	USD

NEW WORK DETAILS

Title	Quantum Dot Based Aptasensors for the Detection of Biomolecules with Related Raman/SERS Spectral Analysis	Institution name	University of Illinois at Chicago
Instructor name	Shreya Ghosh	Expected presentation date	2019-11-08

ADDITIONAL DETAILS

Order reference number	N/A	The requesting person / organization to appear on the license	Shreya Ghosh

REUSE CONTENT DETAILS

Title, description or numeric reference of the portion(s)	Aptasensor based optical detection of glycated albumin for diabetes mellitus diagnosis	**Title of the article/chapter the portion is from**	Aptasensor based optical detection of glycated albumin for diabetes mellitus diagnosis
Editor of portion(s)	N/A	**Author of portion(s)**	Shreya Ghosh, Debopam Datta, Mehar Cheema, Mitra Dutta and Michael A Stroscio
Volume of serial or monograph	28		
Page or page range of portion	435505	**Issue, if republishing an article from a serial**	N/A
		Publication date of portion	2017-10-04

PUBLISHER TERMS AND CONDITIONS

These special terms and conditions are in addition to the standard terms and conditions for CCCâ€™s Republication Service and, together with those standard terms and conditions, govern the use of the Works. As the User you will make all reasonable efforts to contact the author(s) of the article which the Work is to be reused from, to seek consent for your intended use. Contacting one author who is acting expressly as authorised agent for their co-author(s) is acceptable. User will reproduce the following wording prominently alongside the Work: the source of the Work, including author, article title, title of journal, volume number, issue number (if relevant), page range (or first page if this is the only information available) and date of first publication. This information can be contained in a footnote or reference note; and a link back to the article (via DOI); and if practicable, and IN ALL CASES for new works published under any of the Creative Commons licences, the words â€œ© IOP Publishing. Reproduced with permission. All rights reservedâ€ Without the express permission of the author(s) and the Rightsholder of the article from which the Work is to be reused, User shall not use it in any way which, in the opinion of the Rightsholder, could: (i) distort or alter the author(s)â€™ original intention(s) and meaning; (ii) be prejudicial to the honour or reputation of the author(s); and/or (iii) imply endorsement by the author(s) and/or the Rightsholder. This licence does not apply to any article which is credited to another source and which does not have the copyright line â€˜© IOP Publishing Ltdâ€™. User must check the copyright line of the article from which the Work is to be reused to check that IOP Publishing Ltd has all the necessary rights to be able to grant permission. User is solely responsible for identifying and obtaining separate licences and permissions from the copyright owner for reuse of any such third party material/figures which the Rightsholder is not the copyright owner of. The Rightsholder shall not reimburse any fees which User pays for a republication license for such third party content. This licence does not apply to any material/figure which is credited to another source in the Rightsholderâ€™s publication or has been obtained from a third party. User must check the Version of Record of the article from which the Work is to be reused, to check whether any of the material in the Work is third party material. Third party citations and/or copyright notices and/or permissions statements may not be included in any other version of the article from which the Work is to be reused and so cannot be relied upon by the User. User is solely responsible for identifying and obtaining separate licences and permissions from the copyright owner for reuse of any such third party material/figures where the Rightsholder is not the copyright owner. The Rightsholder shall not reimburse any fees which User pays for a republication license for such third party content. User and CCC acknowledge that the Rightsholder may, from time to time, make changes or additions to these special terms and conditions without express notification, provided that these shall not apply to permissions already secured and paid for by User prior to such change or addition. User acknowledges that the Rightsholder (which includes companies within its group and third parties for whom it publishes its titles) may make use of personal data collected through the service in the course of their business. If User is the author of the Work, User may automatically have the right to reuse it under the rights granted back when User transferred the copyright in the article to the Rightsholder. User should check the copyright form and the relevant author rights policy to check whether permission is required. If User is the author of the Work and does require permission for proposed reuse of the Work, User should select â€˜Author of requested contentâ€™ as the Requestor Type. The Rightsholder shall not reimburse any fees which User pays for a republication license. If User is the author of the article which User wishes to reuse in Userâ€™s thesis or dissertation, the republication licence covers the right to include the Accepted Manuscript version (not the Version of Record) of the article. User must include citation details and, for online use, a link to the Version of Record of the article on the Rightsholderâ€™s website. User may need to obtain separate permission for any third party content included within the article. User must check this with the copyright owner of such third party content. User may not include the article in a thesis or dissertation which is published by ProQuest. Any other commercial use of Userâ€™s thesis or dissertation containing the article would also need to be expressly notified in writing to the Rightsholder at the time of request and would require separate written

permission from the Rightsholder. User does not need to request permission for Work which has been published under a CC BY licence. User must check the Version of Record of the CC BY article from which the Work is to be reused, to check whether any of the material in the Work is third party material and so not published under the CC BY licence. User is solely responsible for identifying and obtaining separate licences and permissions from the copyright owner for reuse of any such third party material/figures. The Rightsholder shall not reimburse any fees which User pays for such licences and permissions. As well as CCC, the Rightsholder shall have the right to bring any legal action that it deems necessary to enforce its rights should it consider that the Work infringes those rights in any way. For STM Signatories ONLY (as agreed as part of the STM Guidelines) Any licence granted for a particular edition of a Work will apply also to subsequent editions of it and for editions in other languages, provided such editions are for the Work as a whole in situ and do not involve the separate exploitation of the permitted illustrations or excerpts.

CCC Republication Terms and Conditions

1. Description of Service; Defined Terms. This Republication License enables the User to obtain licenses for republication of one or more copyrighted works as described in detail on the relevant Order Confirmation (the "Work(s)"). Copyright Clearance Center, Inc. ("CCC") grants licenses through the Service on behalf of the rightsholder identified on the Order Confirmation (the "Rightsholder"). "Republication", as used herein, generally means the inclusion of a Work, in whole or in part, in a new work or works, also as described on the Order Confirmation. "User", as used herein, means the person or entity making such republication.

2. The terms set forth in the relevant Order Confirmation, and any terms set by the Rightsholder with respect to a particular Work, govern the terms of use of Works in connection with the Service. By using the Service, the person transacting for a republication license on behalf of the User represents and warrants that he/she/it (a) has been duly authorized by the User to accept, and hereby does accept, all such terms and conditions on behalf of User, and (b) shall inform User of all such terms and conditions. In the event such person is a "freelancer" or other third party independent of User and CCC, such party shall be deemed jointly a "User" for purposes of these terms and conditions. In any event, User shall be deemed to have accepted and agreed to all such terms and conditions if User republishes the Work in any fashion.

3. Scope of License; Limitations and Obligations.

   3.1. All Works and all rights therein, including copyright rights, remain the sole and exclusive property of the Rightsholder. The license created by the exchange of an Order Confirmation (and/or any invoice) and payment by User of the full amount set forth on that document includes only those rights expressly set forth in the Order Confirmation and in these terms and conditions, and conveys no other rights in the Work(s) to User. All rights not expressly granted are hereby reserved.

   3.2. General Payment Terms: You may pay by credit card or through an account with us payable at the end of the month. If you and we agree that you may establish a standing account with CCC, then the following terms apply: Remit Payment to: Copyright Clearance Center, 29118 Network Place, Chicago, IL 60673-1291. Payments Due: Invoices are payable upon their delivery to you (or upon our notice to you that they are available to you for downloading). After 30 days, outstanding amounts will be subject to a service charge of 1-1/2% per month or, if less, the maximum rate allowed by applicable law. Unless otherwise specifically set forth in the Order Confirmation or in a separate written agreement signed by CCC, invoices are due and payable on "net 30" terms. While User may exercise the rights licensed immediately upon issuance of the Order Confirmation, the license is automatically revoked and is null and void, as if it had never been issued, if complete payment for the license is not received on a timely basis either from User directly or through a payment agent, such as a credit card company.

   3.3. Unless otherwise provided in the Order Confirmation, any grant of rights to User (i) is "one-time" (including the editions and product family specified in the license), (ii) is non-exclusive and non-transferable and (iii) is subject to any and all limitations and restrictions (such as, but not limited to, limitations on duration of use or circulation) included in the Order Confirmation or invoice and/or in these terms and conditions. Upon completion of the licensed use, User shall either secure a new permission for further use of the Work(s) or immediately cease any new use of the Work(s) and shall render inaccessible (such as by deleting or by removing or severing links or other locators) any further copies of the Work (except for copies printed on paper in accordance with this license and still in User's stock at the end of such period).

3.4. In the event that the material for which a republication license is sought includes third party materials (such as photographs, illustrations, graphs, inserts and similar materials) which are identified in such material as having been used by permission, User is responsible for identifying, and seeking separate licenses (under this Service or otherwise) for, any of such third party materials; without a separate license, such third party materials may not be used.

3.5. Use of proper copyright notice for a Work is required as a condition of any license granted under the Service. Unless otherwise provided in the Order Confirmation, a proper copyright notice will read substantially as follows: "Republished with permission of [Rightsholder's name], from [Work's title, author, volume, edition number and year of copyright]; permission conveyed through Copyright Clearance Center, Inc. " Such notice must be provided in a reasonably legible font size and must be placed either immediately adjacent to the Work as used (for example, as part of a by-line or footnote but not as a separate electronic link) or in the place where substantially all other credits or notices for the new work containing the republished Work are located. Failure to include the required notice results in loss to the Rightsholder and CCC, and the User shall be liable to pay liquidated damages for each such failure equal to twice the use fee specified in the Order Confirmation, in addition to the use fee itself and any other fees and charges specified.

3.6. User may only make alterations to the Work if and as expressly set forth in the Order Confirmation. No Work may be used in any way that is defamatory, violates the rights of third parties (including such third parties' rights of copyright, privacy, publicity, or other tangible or intangible property), or is otherwise illegal, sexually explicit or obscene. In addition, User may not conjoin a Work with any other material that may result in damage to the reputation of the Rightsholder. User agrees to inform CCC if it becomes aware of any infringement of any rights in a Work and to cooperate with any reasonable request of CCC or the Rightsholder in connection therewith.

4. Indemnity. User hereby indemnifies and agrees to defend the Rightsholder and CCC, and their respective employees and directors, against all claims, liability, damages, costs and expenses, including legal fees and expenses, arising out of any use of a Work beyond the scope of the rights granted herein, or any use of a Work which has been altered in any unauthorized way by User, including claims of defamation or infringement of rights of copyright, publicity, privacy or other tangible or intangible property.

5. Limitation of Liability. UNDER NO CIRCUMSTANCES WILL CCC OR THE RIGHTSHOLDER BE LIABLE FOR ANY DIRECT, INDIRECT, CONSEQUENTIAL OR INCIDENTAL DAMAGES (INCLUDING WITHOUT LIMITATION DAMAGES FOR LOSS OF BUSINESS PROFITS OR INFORMATION, OR FOR BUSINESS INTERRUPTION) ARISING OUT OF THE USE OR INABILITY TO USE A WORK, EVEN IF ONE OF THEM HAS BEEN ADVISED OF THE POSSIBILITY OF SUCH DAMAGES. In any event, the total liability of the Rightsholder and CCC (including their respective employees and directors) shall not exceed the total amount actually paid by User for this license. User assumes full liability for the actions and omissions of its principals, employees, agents, affiliates, successors and assigns.

6. Limited Warranties. THE WORK(S) AND RIGHT(S) ARE PROVIDED "AS IS". CCC HAS THE RIGHT TO GRANT TO USER THE RIGHTS GRANTED IN THE ORDER CONFIRMATION DOCUMENT. CCC AND THE RIGHTSHOLDER DISCLAIM ALL OTHER WARRANTIES RELATING TO THE WORK(S) AND RIGHT(S), EITHER EXPRESS OR IMPLIED, INCLUDING WITHOUT LIMITATION IMPLIED WARRANTIES OF MERCHANTABILITY OR FITNESS FOR A PARTICULAR PURPOSE. ADDITIONAL RIGHTS MAY BE REQUIRED TO USE ILLUSTRATIONS, GRAPHS, PHOTOGRAPHS, ABSTRACTS, INSERTS OR OTHER PORTIONS OF THE WORK (AS OPPOSED TO THE ENTIRE WORK) IN A MANNER CONTEMPLATED BY USER; USER UNDERSTANDS AND AGREES THAT NEITHER CCC NOR THE RIGHTSHOLDER MAY HAVE SUCH ADDITIONAL RIGHTS TO GRANT.

7. Effect of Breach. Any failure by User to pay any amount when due, or any use by User of a Work beyond the scope of the license set forth in the Order Confirmation and/or these terms and conditions, shall be a material breach of the license created by the Order Confirmation and these terms and conditions. Any breach not cured within 30 days of written notice thereof shall result in immediate termination of such license without further notice. Any unauthorized (but licensable) use of a Work that is terminated immediately upon notice thereof may be liquidated by payment of the Rightsholder's ordinary license price therefor; any unauthorized (and unlicensable) use that is

not terminated immediately for any reason (including, for example, because materials containing the Work cannot reasonably be recalled) will be subject to all remedies available at law or in equity, but in no event to a payment of less than three times the Rightsholder's ordinary license price for the most closely analogous licensable use plus Rightsholder's and/or CCC's costs and expenses incurred in collecting such payment.

8. Miscellaneous.

8.1. User acknowledges that CCC may, from time to time, make changes or additions to the Service or to these terms and conditions, and CCC reserves the right to send notice to the User by electronic mail or otherwise for the purposes of notifying User of such changes or additions; provided that any such changes or additions shall not apply to permissions already secured and paid for.

8.2. Use of User-related information collected through the Service is governed by CCC's privacy policy, available online here: https://marketplace.copyright.com/rs-ui-web/mp/privacy-policy

8.3. The licensing transaction described in the Order Confirmation is personal to User. Therefore, User may not assign or transfer to any other person (whether a natural person or an organization of any kind) the license created by the Order Confirmation and these terms and conditions or any rights granted hereunder; provided, however, that User may assign such license in its entirety on written notice to CCC in the event of a transfer of all or substantially all of User's rights in the new material which includes the Work(s) licensed under this Service.

8.4. No amendment or waiver of any terms is binding unless set forth in writing and signed by the parties. The Rightsholder and CCC hereby object to any terms contained in any writing prepared by the User or its principals, employees, agents or affiliates and purporting to govern or otherwise relate to the licensing transaction described in the Order Confirmation, which terms are in any way inconsistent with any terms set forth in the Order Confirmation and/or in these terms and conditions or CCC's standard operating procedures, whether such writing is prepared prior to, simultaneously with or subsequent to the Order Confirmation, and whether such writing appears on a copy of the Order Confirmation or in a separate instrument.

8.5. The licensing transaction described in the Order Confirmation document shall be governed by and construed under the law of the State of New York, USA, without regard to the principles thereof of conflicts of law. Any case, controversy, suit, action, or proceeding arising out of, in connection with, or related to such licensing transaction shall be brought, at CCC's sole discretion, in any federal or state court located in the County of New York, State of New York, USA, or in any federal or state court whose geographical jurisdiction covers the location of the Rightsholder set forth in the Order Confirmation. The parties expressly submit to the personal jurisdiction and venue of each such federal or state court.If you have any comments or questions about the Service or Copyright Clearance Center, please contact us at 978-750-8400 or send an e-mail to info@copyright.com.

v 1.1

Appendix C

Institute of Electrical and Electronics Engineers (IEEE) Policy on Thesis and Dissertations

Thesis / Dissertation Reuse

The IEEE does not require individuals working on a thesis to obtain a formal reuse license, however, you may print out this statement to be used as a permission grant:

Requirements to be followed when using any portion (e.g., figure, graph, table, or textual material) of an IEEE copyrighted paper in a thesis:

1) In the case of textual material (e.g., using short quotes or referring to the work within these papers) users must give full credit to the original source (author, paper, publication) followed by the IEEE copyright line © 2011 IEEE.
2) In the case of illustrations or tabular material, we require that the copyright line © [Year of original publication] IEEE appear prominently with each reprinted figure and/or table.
3) If a substantial portion of the original paper is to be used, and if you are not the senior author, also obtain the senior author's approval.

Requirements to be followed when using an entire IEEE copyrighted paper in a thesis:

1) The following IEEE copyright/ credit notice should be placed prominently in the references: © [year of original publication] IEEE. Reprinted, with permission, from [author names, paper title, IEEE publication title, and month/year of publication]
2) Only the accepted version of an IEEE copyrighted paper can be used when posting the paper or your thesis on-line.
3) In placing the thesis on the author's university website, please display the following message in a prominent place on the website: In reference to IEEE copyrighted material which is used with permission in this thesis, the IEEE does not endorse any of [university/educational entity's name goes here]'s products or services. Internal or personal use of this material is permitted. If interested in reprinting/republishing IEEE copyrighted material for advertising or promotional purposes or for creating new collective works for resale or redistribution, please go to http://www.ieee.org/publications_standards/publications/rights/rights_link.html to learn how to obtain a License from RightsLink.

If applicable, University Microfilms and/or ProQuest Library, or the Archives of Canada may supply single copies of the dissertation.

Vita

NAME	SHREYA GHOSH
EDUCATION	Ph.D., Bioengineering, University of Illinois at Chicago, Chicago, Illinois, USA, 2019
	M. E., Biomedical Engineering, Jadavpur University, Kolkata, West Bengal, India, 2014
	B. Tech., Biomedical Engineering, West Bengal University of Technology, Kolkata, West Bengal, India, 2012
EXPERIENCE	Research Assistant, Nanoengineering Research Laboratory, Departments of Bioengineering and Electrical and Computer Engineering, University of Illinois at Chicago, 2016-2019
	Teaching Assistant, Department of Bioengineering, University of Illinois at Chicago, 2016-2019
	Teaching Assistant, Department of Biological Sciences, University of Illinois at Chicago, 2017-2018
PUBLICATIONS	S. Ghosh, L. H. Bradley, J. Sebastian, Y. Zhao, J. Schwartz, A. Nicholls, M. Dutta, M. A. Stroscio, "Analysis of SERS spectrum of biomolecules using silver nanorod substrates", 2019 [manuscript in preparation]
	S. Ghosh, Y. Chen, A. George, M. Dutta, and M. A. Stroscio, "Fluorescence Resonant Energy Transfer based DNA aptamer probe for the detection of calcium ions," [manuscript in preparation]
	S. Ghosh, Y. Chen, J. Sebastian, A. George, M. Dutta, and M. A. Stroscio, "A study on the response of FRET based DNA aptasensors in intracellular environment," *Sci. Rep*, 2019. [under review]
	S. Ghosh, D. Datta, S. Chaudhry, M. Dutta, and M. A. Stroscio, "Rapid detection of Tumor Necrosis Factor-alpha using quantum dot based optical aptasensor," *IEEE Trans. Nanobioscience*, vol. 17, no. 4, pp. 417–423, 2018.
	A. Mohamed, S. Ghosh, M. Araque, D. Datta, M. Mazouchi, V. Rane, M. Dutta, and M. A. Stroscio, "Nanomechanical systems with normalized and coupled acoustic and electromagnetic modes in piezoelectric structures," *Solid*

State Commun., vol. 277, pp. 1-6, 2018.

S. Ghosh, D. Datta, M. Cheema, M. Dutta, and M. A. Stroscio, "Aptasensor based optical detection of glycated albumin for diabetes mellitus diagnosis," *Nanotechnology*, vol. 28, no. 43, pp. 435505, 2017.

D. Datta, A. Darbandi, S. Ghosh, M. A. Stroscio, and M. Dutta, "Quantization of acoustic-phonon modes in Siedel-White type waveguide nanostructures," *Solid State Commun.*, vol. 267, pp. 42-47, 2017.

V. Uskoković, S. Ghosh, and V. M. Wu, "Antimicrobial hydroxyapatite-gelatin-silica composite pastes with tunable setting properties," *J. Mater. Chem.* B, vol. 5, no. 30, pp. 6065-6080, 2017.

V. Uskoković and S. Ghosh, "Carriers for the tunable release of therapeutics: etymological classification and examples," *Expert Opin. Drug Deliv.*, vol. 13, no. 12, pp. 1729-1741, 2016.

S. Ghosh, V. Wu, S. Pernal, and V. Uskoković, "Self-Setting Calcium Phosphate Cements with Tunable Antibiotic Release Rates for Advanced Antimicrobial Applications," *ACS Appl. Mater. Interfaces*, vol. 8, no. 12, pp. 7691-7708, 2016.

M. A. Khan, V. M. Wu, S. Ghosh, and V. Uskoković, "Gene delivery using calcium phosphate nanoparticles: Optimization of the transfection process and the effects of citrate and poly(l-lysine) as additives," *J. Colloid Interface Sci.*, vol. 471, pp. 48-58, 2016.

PRESENTATIONS

S. Ghosh, A. Metlushko, S. Chaudhry, M. Dutta, and M. Stroscio, "Detection of C-Reactive Protein using network – deployable DNA aptamer based optical nanosensor," in *IEEE-EMBS International Conference on Biomedical and Health Informatics*, Chicago, IL, USA, May 19-22, 2019.

P. Chaudhuri, S. Ghosh, P. Basak, D. N. Tibarewala, and K. Bhattacharya, "Electrically Mediated In-Vitro Transdermal Drug Delivery By Means of Drug Loaded Nanocomposite Polymeric Membranes", *International Conference on Polymeric Biomaterials, Bioengineering and Biodiagnostics*, New Delhi, India, October 27, 2014.

S. Ghosh, P. Chaudhuri, P. Basak, and D. N. Tibarewala, "Synthesis and characterization of polyvinyl alcohol based gelatin membranes crosslinked by citric acid", *International Conference on Recent Advances in Analytical Science*, Varanasi, India, March 27-29, 2014.

S. Ghosh, P. Bera, P. Chaudhuri, P. Basak, and D. N. Tibarewala, "Hydroxyapatite-Polyvinyl Alcohol Nanocomposites as Drug Delivery Matrix. *25th Annual General Meeting, Materials Research Society of India*, Bangalore, India, February 13, 2014.

S. Saha, S. Ghosh, A. Konar, and A. K. Nagar, "Gesture Recognition From Indian Classical Dance Using Kinect Sensor", *2013 Fifth International Conference on Computational Intelligence, Communication Systems and Networks, IEEE,* Madrid, Spain, June 5-7, 2013.

S. Saha, S. Ghosh, A. Konar, and R. Janarthanan, "Identification of Odissi Dance Video Using Kinect Sensor," *2013 International Conference on Advances in Computing, Communications and Informatics, IEEE,* Mysore, India, August 22-25, 2013

S. Saha, S. Ghosh, A. Konar, R. Janarthanan, "A Study On Leg Posture Recognition From Indian Classical Dance Using Kinect Sensor", *International Conference on Human Computer Interactions, IEEE,* Chennai, India, August 23-24, 2013.